Development and Application of Quantitative Proteomics Method for S-Nitrosylation Analysis

Universität Duisburg-Essen

Fakultät für Chemie

A THESIS SUBMITTED IN FULFILMENT

OF THE REQUIREMENTS FOR THE ACADEMIC DEGREE

DOCTOR RERUM NATURALIUM

(Dr. rer. nat.)

by

M.Sc. Ruzanna Mnatsakanyan

from Yerevan, Armenia

Essen, 2020

The presented work was performed in the period from August 2015 to January 2019 at the Leibniz Institute for Analytical Sciences-ISAS-e.V., Dortmund, Germany and from February 2017 to March 2020 at the University of Duisburg-Essen, Faculty of Chemistry, Applied Analytical Chemistry under the supervision of Prof. Dr. Oliver J. Schmitz.

Date of the oral examination: 08.03.2021

Examination committee: Prof. Dr. Oliver J. Schmitz

Prof. Dr. Marcus Krüger

DOI: 10.17185/duepublico/74156
URN: urn:nbn:de:hbz:464-20210323-095216-0

Hereby I confirm that I performed the experiments and wrote the thesis independently. All supporting materials and sources used are specified.

The thesis contains excerpts and figures from:

Mnatsakanyan R, Markoutsa S, Walbrunn K, Roos A, Verhelst SHL, Zahedi RP. Proteome-wide detection of S-nitrosylation targets and motifs using bioorthogonal cleavable-linker-based enrichment and switch technique. Nature Communications. 2019;10(1):2195.

Mnatsakanyan R, Shema G, Basik M, Batist G, Borchers CH, Sickmann A, Zahedi RP. Detecting post-translational modification signatures as potential biomarkers in clinical mass spectrometry. Expert Review of Proteomics. 2018;15(6):515-35.

Acknowledgement

I offer my sincere gratitude to Prof. Dr. Oliver J. Schmitz for accepting me as a PhD student in his group, for his time and for valuable advice.

I am extremely thankful to my supervisor at Leibniz Institute for Analytical Sciences-ISAS-e.V Dr. René Zahedi for his continuous support, encouragement, thoughtful guidance and constructive critics.

I would like to thank Prof. Dr. Marcus Krüger for kindly agreeing to be in the committee of my PhD exam.

Many thanks to Dr. Stavroula Markoutsa for instructing me in the beginning of my thesis and for her contribution to the formulation of my scientific thinking.

I am kindly acknowledging Prof. Dr. Steven Verhelst for his advice, for inspiring me to work with bioorthogonal cleavable-linkers and for continuous support.

Many thanks to technical service bioanalytics at Leibniz Institute for Analytical Sciences-ISAS-e.V for providing technical support.

Thanks to all my colleagues for providing a friendly atmosphere and readiness to help.

And finally, thanks to my family and friends for their support and love.

Table of contents

List of abbreviations

AAA	Amino acid analysis
AC	Alternating current
ACN	Acetonitrile
ANOVA	Analysis of variance
asc	Sodium ascorbate
BST	Biotin switch technique
CAM	Carbamidomethylated
CE	Collision energy
cGMP	Guanylate cyclase monophosphate
CID	Collision induced dissociation
-cl	Cleaved form of the Diazo-biotin-azide linker
-cl+SO_3	Cleaved form of the Diazo-biotin-azide linker with added SO_3 group
cl-Dde	Cleaved form of the Dde-biotin-azide linker
CuAAC	Copper(I)-catalyzed alkyne-azide cycloaddition
Cys	Cysteine
Cys-BOOST	Cysteine analysis using bioorthogonal cleavable-linker and switch technique
DC	Direct current
DDA	Data dependent acquisition
Dde	1-(4,4-dimethyl-2,6-dioxocyclohex-1-ylidene)ethyl
DE	Dynamic exclusion
DMEM	Dulbecco's Modified Eagle Medium
DTT	Dithiothreitol
EDTA	Ethylenediaminetetraacetic acid
EIF	Eukaryotic translation initiation factor
ER	Endoplasmic reticulum
ESI	Electrospray ionization
FA	Formic acid
FASP	Filter-aided sample preparation
FBS	Fetal bovine serum
FDR	False discovery rate
FT	Flow through
GC	Gas chromatography
GO	Gene Ontology
GSH	Glutathione
GSNO	S-nitrosoglutathione
GuHCl	Guanidine hydrochloride
HAT	Histone acetyltransferase domain
HCD	Higher-energy collisional dissociation
HSP	Heat shock protein
IAA	Iodoacetamide
ICAT	Isotope-coded affinity tags
iodoTMT	Iodoacetyl tandem mass tags
IQR	Interquartile range

IT	Injection time
iTRAQ	Isobaric tags for relative and absolute quantification
IW	Isolation window
LC	Liquid chromatography
LIT	Linear ion trap
LOQ	Limit of quantification
m/z	Mass to charge ratio
MALDI	Matrix Assisted Laser Desorption/Ionization
MMTS	Methyl methanethiosulfonate
Mox	Oxidation of methionine
MS	Mass spectrometry
MWCO	Molecular Weight Cut-off
$NaIO_4$	Sodium periodate
NEM	N-ethylmaleimide
NHS	N-Hydroxysuccinimide
NO	Nitrogen monoxide
NO^+	Nitrosonium ion
NOS	Nitric oxide synthase
NSAF	Normalized spectral abundance factors
PBS	Phosphate buffered saline
PD	Proteome Discoverer
PEP	Posterior-error-probability
PPB	Potassium phosphate buffer
PPG	Polypropylene glycol
PSM	Peptide spectrum match
PTM	Post-translational modification
$R_{\%}$	Recovery
RAC	Resin-assisted capture
RF	Radio frequency
RNS	Reactive nitrogen species
ROS	Reactive oxygen species
RP	Reversed phase
RP-HPLC	Reversed Phase High Performance Liquid Chromatography
RSD	Relative standard deviation
$-S^-$	Thiolate anion
$-S^{\bullet}$	Thiyl radical
S/N	Signal/noise ratio
S-cys	S-cysteinylation
SD	Standard deviation
SDS	Sodium dodecyl sulfate
SILAC	Stable Isotope Labeling by Amino acids in Cell culture
SNAP	S-Nitroso-N-acetylpenicillamine
SNAP*	Soluble N-ethylmaleimide-sensitive Attachment Protein
SNO	S-nitrosylation
SOH	S-sulfenylation
SPE	Solid phase extraction

SPS	Synchronous precursor selection
S-S	Disulfide
SSG	S-glutathionylation
SSH	S-sulfhydration
ST	Switch technique
TC	Tissue culture
TCEP	Tris(2-carboxyethyl)phosphine hydrochloride
TEAB	Triethylamonium bicarbonate
TFA	Trifluoroacetic acid
THPTA	Tri(3 hydroxypropyltriazolylmethyl)amine
TIC	Total ion chromatogram
TMT	Tandem mass tags
TOF	Time-of-flight
UPR	Unfolded protein response
XIC	Extracted ion chromatograms

Abstract

Cysteine reversible post-translational modifications are emerging as important players in cellular signaling and redox homeostasis. Among them, S-nitrosylation has been shown to function as a redox-switch in several (patho)physiological events. However, investigation of S-nitrosylation, particularly on a proteome-wide level and in the native cellular environment remains challenging, due to the lack of the highly efficient analytical methods. In this work, a novel chemical proteomics strategy for quantitative analysis of reversibly modified cysteines using biorthogonal cleavable-linker and switch technique (Cys-BOOST) was developed. Direct comparison of Cys-BOOST with iodoTMT for analysis of total Cys from HeLa cell extracts demonstrated threefold higher sensitivity, considerably higher specificity and technical reproducibility for Cys-BOOST. The application of Cys-BOOST for the analysis of S-nitrosylation in S-nitrosoglutathione-treated and non-treated HeLa cell extracts identified an unprecedented number of S-nitrosylated proteins (3,632) and unique S-nitrosylation sites (8,304), covering a wide dynamic range of the HeLa proteome. Based on the quantitative data S-nitrosylation consensus motifs were deduced for S-nitrosylation sites with differential reactivity to S-nitrosoglutathione. These motifs prove the relevance of local hydrophobicity and acid-base catalysis for S-nitrosylation on proteome-wide scale and shed light on the exquisite target-selectivity of S-nitrosylation. *In-vivo* S-nitrosylation analysis in SH-SY5Y neuroblastoma cells revealed 2,158 unique S-nitrosylation sites on 1,443 proteins in basal condition and significantly changed S-nitrosylation levels in proteins involved in neuro(axono)genesis, glutamatergic synaptic transmission, cadherin binding, NADH metabolic process, protein folding, translation, and DNA replication as response to early nitrosative stress. Collectively, these findings establish Cys-BOOST as an efficient tool for proteome-wide quantitative S-nitrosylation analysis and suggest S-nitrosylation as a global regulator of protein function akin to phosphorylation and ubiquitination.

1. Introduction

1.1 Proteins

Proteins are the key functional components of every living cell, performing functions ranging from maintenance of the cellular structure, enzymatic catalysis, transporting ions and molecules, muscle contraction, immune response, protein synthesis and folding. Proteins are macromolecules synthesized through the polymerization of amino acids. In eukaryotes, there are 21 proteinogenic amino acids, 20 of which in the standard genetic code. The cellular translation machinery interconnects tens to thousands of amino acids by condensation reactions into a linear sequence that is encoded by a specific gene to form a specific protein. The linear amino acids chain is known as the primary protein structure. This specific sequence induces chemical forces and interactions, such as hydrogen bonds, disulfide bridges, hydrophobic and hydrophilic interactions as well as ionic interactions between charged residues, which together with cofactors and molecular chaperones cause the protein to fold. This leads to secondary structures such as the alpha helix and beta sheets. The same forces result in further tree-dimensional arrangements, giving rise to a tertiary protein structure. In case a protein contains more than one polypeptide chain, such as for instance Hemoglobin, the overall configuration of the multiple folded protein subunits forms the quaternary protein structure.

The human genome encodes for around 20,000 proteins [1]. In order to cope with the immense functional diversity, cells have developed additional mechanisms for versatile alteration of the protein's structure and function, giving rise to the formation of 'proteoforms'. Proteoforms are the different forms of a protein produced from the same gene with a variety of sequence variations, such as splice isoforms, and post-translational modifications (PTMs) [2].

1.1.1 Protein post-translational modifications

PTMs are one of the most energetically efficient, rapid and elegant ways to modulate functionality of a single gene product. PTM involves the attachment, removal, exchange, and rearrangement of functional groups to amino acid side chains and protein N-termini, but also the hydrolysis of peptide bonds (proteolysis). PTMs are involved in maintenance of the cellular homeostasis via modulation of (i) protein abundance levels, e.g., through altered expression, degradation, or both, (ii) protein localization, (iii) protein-protein interactions, (iv) protein function, and (v) protein activity. Specifically, reversible PTMs, such as phosphorylation and

cysteine (Cys) redox PTMs are key players in cellular signaling. Figure 1 is summarizing the most commonly occurring PTMs, their biological roles and analysis strategies [3].

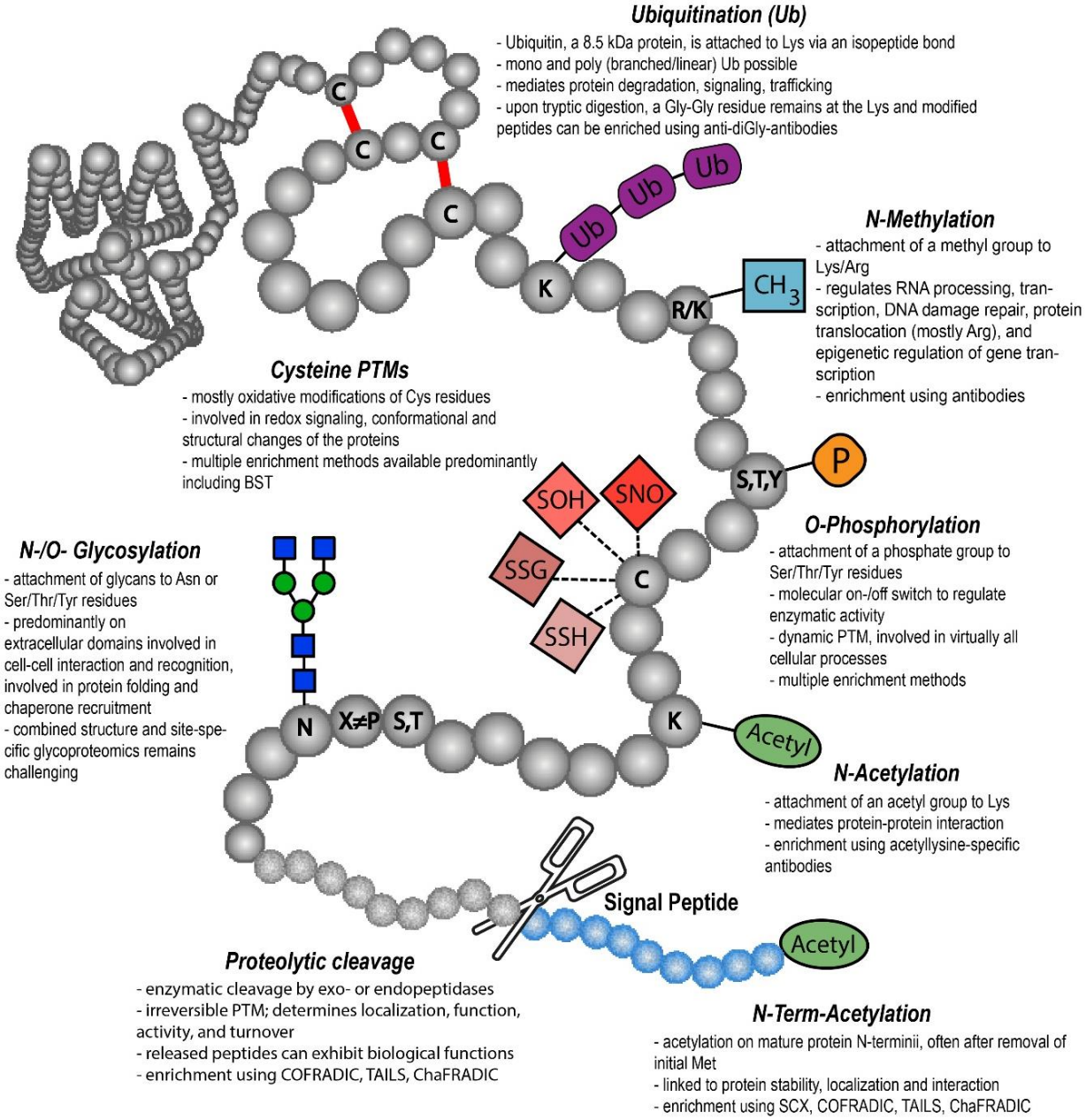

Figure 1.1 Some of the most frequent protein PTMs [3]. A single protein molecule can bear multiple PTMs at the same time, whereas individual protein molecules can differ in their PTM patterns, contributing to a large variety of proteoforms.

1.1.1.1 Cysteine post-translational modifications

Cys residues have a key involvement in modulation of the function, subcellular localization, enzymatic activity and interactions of proteins [4, 5], both in their unmodified and various PTM forms. A variety of Cys PTMs are formed as a result of direct or indirect interactions with reactive oxygen/nitrogen species (ROS/RNS) [5, 6]. Small reactive radical or non-radical ROS/RNS, such as superoxide ($O^{-\cdot 2}$) produced by the nicotinamide adenine dinucleotide phosphate (NADPH) oxidase family, and nitrogen monoxide (NO) produced by nitric oxide synthases (NOSs), are byproducts of cellular respiration [4] and primarily form redox modifications on Cys, due to the high reactivity of its thiol side chain [6, 7]. Reversible Cys redox PTMs include S-nitrosylation (SNO), S-sulfenylation (SOH), disulfide formation (S–S), S-glutathionylation (SSG), S-cysteinylation (S-Cys), and S-sulfhydration (SSH), while sulfinylation (SO_2H) and sulfonylation (SO_3H) are generally considered to be irreversible [5, 7] (Figure 1.2).

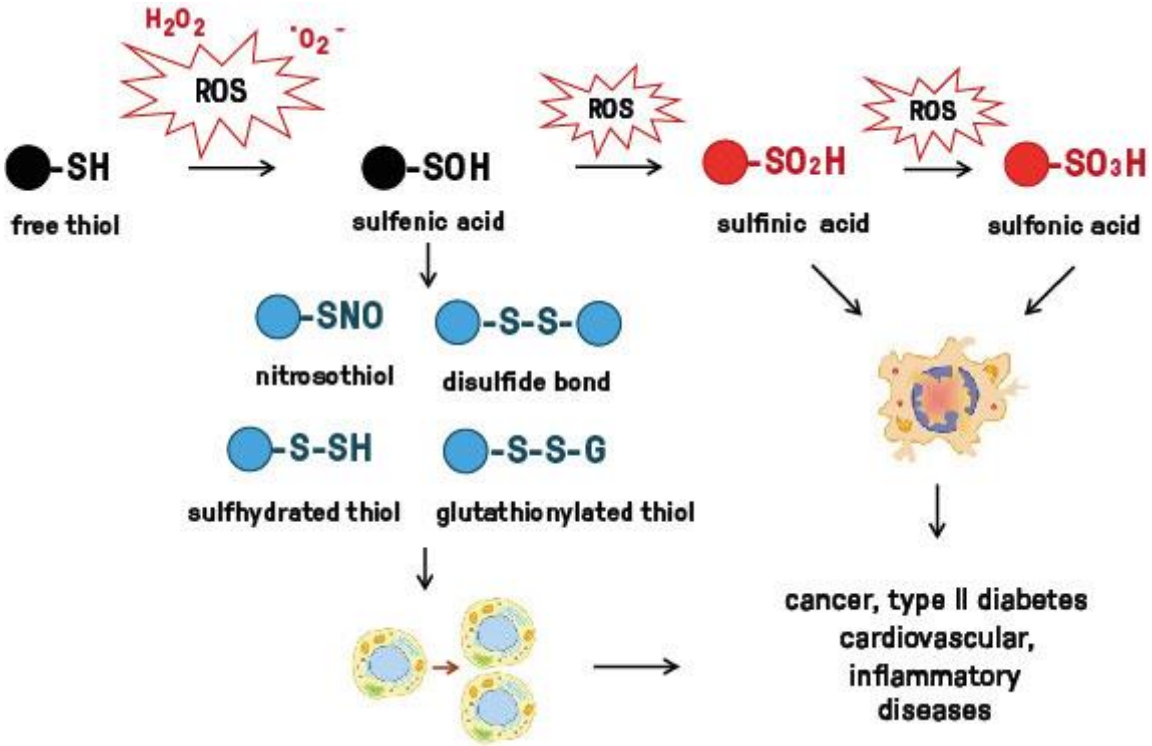

Figure 1.2 Diagram of the most commonly occurring Cys PTMs. Reversible/protective Cys PTMs are associated with cell proliferation, differentiation, and redox signaling, while irreversible PTMs such as sulfinylation (SO_2H) and sulfonylation (SO_3H) result in protein damage and are associated with cancer, cardiovascular, inflammatory and metabolic diseases.

Cys modifications are key regulators of cellular redox homeostasis [8]. At low ROS/RNS levels, reversible/protective PTMs are formed that are associated with cell proliferation, differentiation, and redox signaling, while increasing ROS/RNS levels result in irreversible or aberrant modifications and damage to proteins, known as oxidative/nitrosative stress, respectively [9, 10]. Importantly, specific redox-reactive Cys residues can be present in their reduced forms or may compete for different types of redox modifications, turning them into redox-switches which sense the redox microenvironment and allow reversible and, if necessary, irreversible fine tuning of biochemical processes [3, 5, 8]. ROS and RNS-mediated signaling is involved in many key biological processes, and affects a wide variety of upstream and downstream protein targets, thereby influencing the regulation of other PTMs such as phosphorylation, acetylation, and ubiquitination [11-13].

1.1.1.2 S-Nitrosylation

SNO occurs via oxidative modification of the Cys residue by NO. Initially, NO was recognized as a second messenger in signal transduction. It was shown that NO generated by endothelial cells binds to the Fe^{2+} in the heme group of guanylate cyclase, inducing cyclic guanosine monophosphate (cGMP)-mediated signaling, thus regulating vascular smooth muscle tone, immune response and neurotransmission [14]. In 1998 Furchgott, Ignarro, and Murad have been awarded the Nobel prize in Physiology/Medicine for biochemical characterization of NO as new signaling molecule and its implication in cardiovascular function [14]. Further studies revealed that the major target of NO in cells is the free thiol group of Cys, resulting in SNO. SNO-formation is indeed a way of stabilizing NO and preserving its biological activity [15, 16]. Furthermore, the reversible nature of SNO renders it as a redox-switch and a key player in redox signaling [17].

In cells NO is generated by specialized enzymes, NO synthetases (NOSs). Mammals have three district NOSs that generate NO from arginine (Arg) and O_2. Separate genes encode for neuronal NOS (nNOS or NOS1), endothelial NOS (eNOS or NOS3), both of which being constitutively expressed in specific tissues, and for cytokine-inducible NOS (iNOS or NOS2) mainly expressed in immune system cells [18]. Another source of cellular NO generation might include NOx species that originate exogenously (i.e., NO^{2-} from food or from bacterial flora or infecting agents) or endogenously (i.e., NO oxidation products, including N_2O_3). (Figure 1.3) [18, 19].

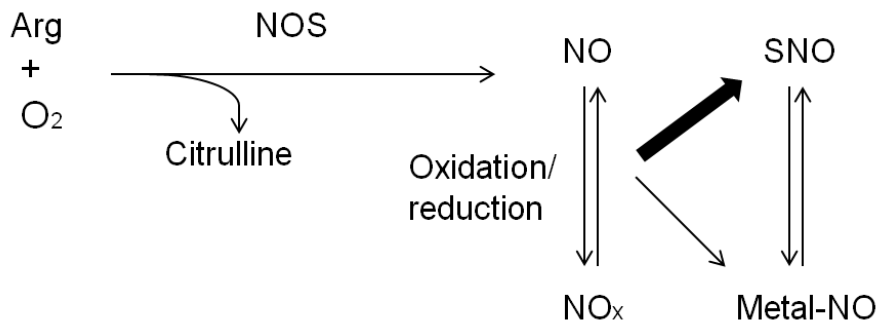

Figure 1.3 Cellular NO sources and targets. NO is generated enzymatically by NOS and via reduction of NO_X species.

Cys residues of both low molecular weight compounds (e.g. glutathione (GSH)) and proteins can undergo SNO. Three major mechanisms of SNO generation are known: 1) via radical formation, 2) via direct reaction of a Cys sulfhydryl group with NO or higher NO oxides, 3) via transfer of NO from one SNO molecule to another [18]. SNO formation via radical generation includes the reaction of $NO^{\bullet}$ with a thiyl radical ($-S^{\bullet}$), with the $-S^{\bullet}$ species derived from homolytic scission of a disulfide bond (-S-S-) or from -SH upon metal-catalyzed oxidation. However, as $-SH^{\bullet}$ is a chemically unstable species, a more widespread SNO generation mechanism plausibly involves Cys thiolate anion ($-S^{-}$), which can be formed by sulfur deprotonation even at physiological pH. Cys sulfhydryl (either as $-S^{-}$ or –SH) undergoes SNO by reacting directly with nitrosonium ion (NO^{+}, generated upon metal-catalyzed oxidation of $NO^{\bullet}$) or by reacting with N_2O_3 (generated via NO oxidation by O_2) [18, 20]. The transfer of NO^{+} from one SNO molecule (both protein and low molecular weight SNO) to free Cys represents the transnitrosylation mechanism of SNO generation in cells. For instance, S-nitrosoglutathione (GSNO), the nitrosylated tripeptide GSH, participates in protein SNO formation mainly through thiol-to-thiol NO^{+} transfer. A growing number of SNO proteins are recognized as transnitrosylases (NO donors), which transfer their NO^{+} to the free Cys of target proteins (NO acceptors) [21, 22]. These findings infer that transnitrosylation might be the dominat mechanism of NO action in cells.

The decompostion of SNO accurs by several mechanisims, such as the homolitic cleavge of S-NO bond in the presence of light and the decomposition by transition metal ions, such as Cu (I) [23]. Mercury (Hg^{+2}) reacts directly with SNO, displacing thiol-bound NO and forming a relatively stable covalent bond with the thiol, a process known as Saville reaction [24]. Additionally, enzymes called denitrosylases, such as the denitrosylase thioredoxin (Trx) system and specialized low molecular weight SNO (i.e. GSNO and SNO-coenzyme)

reductase systems are increasingly recognized as highly specific cellular SNO reduction mechanism regulating SNO-free thiol homeostasis in cells [22, 25].

SNO is considered a highly specific and selective PTM. In proteins with known SNO sites, SNO was shown to occur on selected Cys residues, even if the protein might contain multiple other Cys residues. Determinants of SNO specificity are assumed to be the microenvironment in which the reactive Cys is embedded, the presence of stabilizing/destabilizing groups (ionizing, aromatic and hydrophobic species) in the vicinity, allosteric regulators (i.e. Ca^{2+}, Mg^{2+} ions and O_2/redox groups) that can modulate thiol (solvent) accessibility or reactivity, as well as subcellular co-localization of SNO proteins with NOS isoforms. Furthermore, it was shown for a small subset of proteins that SNO of specific Cys is directed by highly conserved amino acid consensus motifs surrounding the Cys residue [16, 26]. Importantly, the enzymatic nature of SNO and denitrosylation is increasingly appreciated in target selectivity and specificity of SNO-mediated redox signaling.

The growing number of reported SNO substrates is in agreement with the ubiquity of SNO-mediated regulatory events [27, 28]. *In-vivo* and *in-vitro* studies report SNO to regulate the activity of a number of protein kinases and phosphatases, oxidoreductases, proteases, and metabolic enzymes, as well as respiratory proteins, receptor/ion channels and transporters, cytoskeletal and structural components, transcription factors, G proteins, and others [18, 27, 29, 30]. The functional diversity of SNO throughout its wide range of targets depends on its localization (e.g. active site or allosteric Cys), as well as its life span.

Today, SNO is established as a key player in NO-mediated signaling with vast (patho)physiological significance. The important role of SNO in cardiac function and neurotransmission has been suggested by multiple studies [9, 13, 31]. The cardioprotective potential of SNO has been attributed to its ability to shield thiol groups from irreversible oxidation [9, 12, 13]. nNOS produces NO in the brain resulting in SNO of neuronal proteins, which was first thought to have neurotoxic effect associated with neurodegenerative diseases. Recent studies, however, indicate also the protective function of SNO in neurotransmission and synaptic plasticity [31]. SNO has been shown to function as a redox-switch in several (patho)physiological events such as ischemia-reperfusion, cardioprotection, neurogenesis and synaptic transmission [31-36]. Aberrant SNO, as a result of a nitrosative stress, may lead to cellular damage, protein misfolding, synaptic damage, and apoptosis [10].

1.2 Analysis of S-Nitrosylation

The analysis of SNO in proteins is complicated by several factors [37, 38]. The weak S–N bond in nitrosothiols makes them sensitive to decomposition. Exposure to cellular reductants, transition metal ions and to direct light diminishes SNO. In addition, SNO proteins occur at substochiometric levels in biological samples. Thus, SNO analysis requires sensitive and specific methods for sample preparation and for detection, as well as the careful use of controls.

Several spectrometric assays can be used for assessment of the general SNO content in the sample [23]. Most of these assays involve decomposition of SNO in order to generate NO or nitrite which can be detected by chemiluminescence, using fluorescent probes or colorimetric assays. For instance NO can be photolytically cleaved from SNO, then reacted with ozone under reduced pressure to generate excited NO_2, which, upon returning to its ground state, releases a photon which can be detected [23, 39]. In another colorimetric assay NO^+ is displaced by Hg^{+2}, then the NO^+ is oxidized to nitrite and the nitrite is detected by characteristic red pink color upon the treatment of the sample with Griess reagent [40]. Alternatively, NO^+ derived from decomposed SNO can be detected via the reaction with fluorescent probes such as DAF-2, yielding a fluorescent triazolofluorescein (DAF-2T; excitation and emission, 485 and 520 nm) [41].

Immunodetection of SNO was made possible by generation of polyclonal and monoclonal antibodies against the SNO moiety. These antibodies are predominantly used for immunohistochemistry and Western blot detection of SNO-proteins [42]. Anti-SNO antibodies are rarely used for immunoprecipitation of SNO proteins as this approach suffers from low specificity and high costs.

Although spectrometric- and immuno- assays provide an information about the overall SNO content in the sample, they do not allow the identification of SNO modified proteins and the exact Cys residues on which SNO occurs. These challenges, however, can be addressed using mass spectrometry (MS)-based proteomics workflows for SNO analysis.

1.3 Mass spectrometry

MS analyses the mass to charge ratios (m/z) of ionized molecules in the gas phase. Mass spectrometers combine ion source and mass analyzer/detector units which are connected by diverse ion guide/ focusing elements [43].

1.3.1 Ionization methods

First step of the MS analysis is the generation of the gas-phase ions of the analyte. For this purpose, different ionization techniques can be applied [43]. The choice of the ionization technique largely depends on the matter (e.g. physical state and ionization energy) of analyte. Protein and peptide analysis have largely benefited from the development of the soft ionization techniques, such as electrospray ionization (ESI) [44, 45] and Matrix Assisted Laser Desorption/Ionization (MALDI) [46]. Nowadays, ESI is the most popular ionization technique used for proteomic analysis. ESI ionization is done at atmospheric pressure and involves ion-molecule reactions that produce adduct ions, such as $[M+H]^+$ generated via addition of a proton (H^+) to the analyte molecule (M). By applying a high voltage (~ 10^6 Vm^{-1}) between a metal capillary and the mass spectrometer's orifice at atmospheric pressure, the liquid on the tip of the capillary takes the shape of the Taylor cone, which emits small charged droplets. On their way into the MS, these droplets evaporate solvent, increasing their charge density. Once the charge repulsion surpasses the surface tension, "Coulomb explosions" occur, leading to smaller droplets. This process repeats and once the electric field on droplets' surface is significantly large, desorption of ions from the surface occurs and electrospray is created [43]. Commonly, ESI generates multiply charged ions, thus favoring the analysis of large molecules such as proteins. The charge of the ESI ion largely depends on the number of exposed ionizable groups on the molecule. Thus, ESI allows the analysis of the high molecular weight molecules using analyzers with a relatively small nominal mass limit and straightforward online coupling to LC systems [43].

1.3.2 Mass analyzers

There is a great variety of mass analyzers operating using different principals. The common characteristic of all of them is the use of static and/or dynamic electric and/or magnetic fields for separation of ions based on their m/z value. Principally all analyzers can be divided into two categories: scanning analyzers allowing transmission of selected m/z ions (e.g. quadrupole, ion traps) and analyzers allowing the simultaneous transmission of all ions (e.g. time-of-flight (TOF) and orbitrap) [43].

Quadrupole analyzers are constructed from four perfectly parallel rods of circular or hyperbolic shape. The positive direct current (DC) voltage is applied on two opposite rods, and the same value of the negative DC voltage is applied on the remaining two rods. The analyzer uses a combination of radio frequency (RF) alternating current (AC) and DC voltages to serve as a

mass filter. The AC is connected to all four rods. For a given pair of DC and RF voltages, only a narrow range of m/z values have stable trajectory and pass through the entire length of the quadrupole without colliding with quadrupole rods. Under this setting all other ions do not have a stable trajectory through the quadrupole and are neutralized by collisions with the quadrupole rods [47]. Quadrupoles are often used in combination with other analyzers as initial mass filters.

The Orbitrap [48] belongs to the second category of the analyzers allowing for simultaneous transmission of all ions. The Orbitrap comprises an outer barrel-like electrode and inner spindle-shaped electrode. An electrostatic voltage of several kilovolts is applied to the inner electrode, whereas the outer electrode is grounded. The ions are injected with a kinetic energy of few kiloelectronvolts (~ 1600 eV) subsequently rotate around and oscillate along the central electrode. This axial oscillation is only dependent on an analyte's m/z. The current induced by the oscillating ions is measured and converted by Fourier transformation to the individual frequencies and intensities, finally allowing to deduce m/z and generate a mass spectrum [43]. This non-impact acquisition is the main advantage of orbitrap analyzers, as prolonged scanning increases the resolution, enabling the acquisition of high resolution and high mass accuracy spectra at short transient times and at high sensitivity.

1.4 Chromatography

Chromatography is an analytical technique to separate a mixture of components based on differences in their interactions with a mobile and a stationary phase. The two major classes are gas and liquid chromatography (LC), mainly defined by the physical state of the mobile phase. Gas chromatography (GC) is primarily applied for separation of volatile compounds (e.g. pesticides), whereas the method of choice for protein and peptide separation is LC. In modern proteomics, reversed phase high performance LC (RP-HPLC) is commonly applied for protein/peptide separation in complex biological samples, such as cell and tissue extracts, and blood plasma. Other common LC techniques used in proteomics include size exclusion, ion exchange, affinity and hydrophilic interaction chromatography [49, 50].

1.4.1 Reversed phased high performance liquid chromatography

In proteomics applications the most common stationary phase for HPLC columns is a silica layer with covalently bound hydrocarbon chain (e.g. C18), so called reversed phase (RP). In RP-HPLC, the mobile phases are primarily more polar solvents such as water, methanol and

acetonitrile (ACN). The lower the polarity of the solvent, the higher its elution strength from RP material. Thus, the order of solvent strength is for instance: Water < ACN < isopropanol. For rough separation of peptide mixtures a linear gradient starting from high water content (e.g. 90%) and ending at high (close to 100%) ACN is applicable [50, 51], leading to the consecutive elution of increasingly hydrophobic peptides into the MS. Analytical depth of the proteomic analysis is highly reliant on the efficient LC separation. The elution of a peptide at a defined retention time and within a narrow retention time window yields an MS^1 precursor of maximum intensity, ideally above the background noise, thus allowing the peptide to be detected and selected for fragmentation. LC separation allows the comprehensive analysis of thousands of peptides and proteins within a single analysis, separating also near-isobaric analytes and therefore yielding substantially more information from complex samples matrices.

1.5 Tandem mass spectrometry

In order to enhance the accuracy of peptide precursor and fragment ion mass measurements and create more informative peptide fragment ions, several mass analyzers are combined in so called hybrid instruments. Commonly quadrupole and linear ion trap (LIT) are combined with TOF or orbitrap. Such setups allow for tandem MS experiments. The data dependent acquisition (DDA) on the Q-Exactive instrument equipped with quadrupole and orbitrap analyzers is a good example of such tandem MS experiment. Here, first the MS^1 scan is acquired in the orbitrap, representing all the ions present at a given chromatographic retention time. Next, the first analyzer (quadrupole) is used to isolate the most intense peptide precursor ion, which then undergoes higher-energy collisional dissociation (HCD), generating fragment ions which are acquired in a data-dependent scan in the orbitrap (MS/MS or MS^2). This procedure can be repeated for N number of most intense precursor ions. Generated fragment ion spectra are used to obtain peptide primary structure information. The HCD fragmentation is performed in a specialized HCD cell where a strong electric field accelerates the ions into a neutral gas (N_2), resulting in collisions between the ions and gas molecules. Part of the high kinetic energy of the ion is converted to internal energy, eventually breaking the peptide bonds on the peptide backbone, resulting in generation of fragment ions. Typically, each molecule fragments once and the most prevalent fragment ions formed by HCD are b-ions containing the N-terminus of a peptide and y-ions containing the C-terminus of a peptide.

1.6 Proteomics

Proteomics is the study of proteome: the entirety of all proteins expressed by an organism/cell/organelle at a given time point and under defined conditions [52]. Modern proteomics research primarily relies on MS-based methods. Two major classes of MS-based proteomics represent analysis of intact proteins (top–down) and analysis of peptides derived from enzymatically digested proteins (bottom–up) [53, 54]. In-depth and comprehensive analysis of complex proteomes requires LC separation techniques and high-resolution MS. Currently available commercial separation and MS analytical platforms are highly suited for bottom–up proteomics, whereas top-down proteomics demands further instrumental developments.

1.6.1 Bottom–up proteomics

The basic bottom-up proteomic workflow includes (i) cell or tissue lysis, (ii) reduction and alkylation of Cys residues, (iii) enzymatic digestion using a protease (most commonly trypsin, resulting in tryptic peptides), (iv) HPLC (most commonly RP C18 columns) separation of the generated peptides, (v) online-coupled MS detection [55]. In DDA mode, the mass spectrometer first acquires an MS^1 spectrum that represents the m/z and intensities of all analytes present at a given time point. When acquired with high-resolution and high mass accuracy instrumentation, the MS^1 spectrum allows to determine the molecular masses of the individual analytes with a mass accuracy of 10 ppm and higher. Next, usually the most intense analytes are isolated and fragmented successively to generate MS^2 spectra. Those MS^2 spectra contain fragment ions that allow to deduce a peptide's amino acid sequence, in HCD typically b- and y-ions. The experimental DDA data is then compared to *in-silico* data generated by specific search engines. Here, representative protein sequence databases (e.g. human or mouse Uniprot) are *in-silico* digested with the chosen enzyme (e.g. trypsin with a maximum of 1 missed cleavage). For each MS/MS spectrum the MS^1-derived molecular mass +/- the user-defined mass error (e.g. 10 ppm for Orbitrap instruments) is used to pre-filter the 100,000s of theoretical peptide sequences. The remaining sequences that fall within the defined mass window will then be *in-silico* fragmented and the generated theoretical MS/MS spectra matched with the experimental one, in order to determine the best matching sequence (peptide-spectrum-match, PSM) for which a posterior-error-probability (PEP) will be calculated. PSMs are then combined to peptides which are then used to infer proteins in the sample. Since a PSM can also be a random event, potentially leading to the false-positive identification of a protein, false discovery rates (FDR) are determined on the PSM, peptide

and protein level. This is typically achieved through searching the data not only against the canonical (forward) protein database, but in addition against a reversed (or randomized) version of it. The rationale is that each reverse PSM reflects the potential occurrence of a false-positive hit in the forward database at the same PEP or search engine score. Commonly used search engines comprise e.g. Sequest [56] (Thermo Scientific), Mascot (Matrix Science) [57] or Andromeda [58], which are then used in combination with more sophisticated software tools such as Proteome Discoverer (Thermo Scientific) or MaxQuant [59].

1.6.2 Quantitative proteomics

MS-based quantitative proteomics is accomplished either by stable isotope labeling or label-free approaches [55]. The choice of the quantification method depends on the type (i.e. cell culture or clinical samples), the number of samples, costs, the analytical question, and the availability of appropriate MS instrumentation.

1.6.2.1 Label-free quantification

For label-free quantification samples are measured individually. Typically, for each peptide the MS^1 precursor intensity over time is used to calculate an area in a particular LC-MS run. For a given peptide, this area can be compared across multiple runs, allowing a relative quantification. Alternatively, in “spectral counting” the number of PSM belonging to a protein is considered as an indicator for its respective amount in each MS measurement (sample). In general, proteins are relatively quantified in each sample based on the abundance of at least one unique peptide per protein [60].

1.6.2.2 Stable Isotope labeling-based quantification

Stable isotope labeling approaches involve labeling of the samples with differentially stable-isotope coded tags. These approaches allow the pooling (multiplexing) of multiple samples at different experimental stages, depending on the type of the label. Quantitative information on relative protein or peptide abundance across samples can be obtained by acquiring the intensities of different isotope coded peaks by MS. Multiplexed quantification makes comparisons more straightforward, robust and can reduce instrument time. Importantly, once samples are multiplexed they can be further fractionated or processed without inducing further variation, which allows conducting even complex workflows, for instance to enrich for specific

PTMs. There are two major strategies in stable isotope-based quantification: one uses isotopic tags enabling the relative quantification of peptide precursor ions in MS^1 scans (i.e. Stable Isotope Labeling with Amino acids in Cell culture (SILAC)); another, makes use of isobaric tags that are quantified in MS^2 scans and are discussed below (i.e. tandem mass tags (TMT) and isobaric tags for relative and absolute quantification (iTRAQ)) [61].

1.6.2.2.1 Tandem mass tags

TMT-10plex represents a set of 10 amine-reactive stable isotope labeled isobaric reagents. The tag contains a mass reporter region, an HCD cleavable-linker, a mass normalizer region and an amine-reactive N-Hydroxysuccinimide (NHS) group (Figure 1.4).

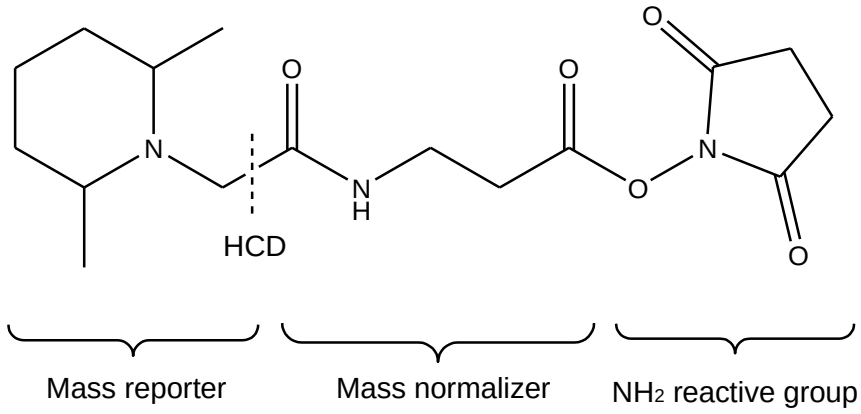

Figure 1.4 Structure of the amine-reactive TMT.

TMT-10plex tags are designed in a way, that they have 10 different mass reporter regions (126.127726 m/z, 127.124761 m/z, 127.131081 m/z, 128.128116 m/z, 128.134436 m/z, 129.131471 m/z, 129.13779 m/z, 130.134825 m/z, 130.141145 m/z, 131.13818 m/z) and corresponding mass normalizer regions to ensure the overall mass of all 10 TMT tags is the same. After labeling of 10 different samples with the respective 10 TMT labels on the peptide level, samples are typically pooled (multiplexing) and processed as one. In LC-MS/MS, the 10 differentially labeled forms of a peptide co-elute, appear as a single isotope pattern in MS^1 and are co-isolated for fragmentation where the different mass reporters are released. The intensities of the 10 reporter ions, detected in the low mass region of the MS^2 spectrum, represent the relative abundance of the peptide in the 10 samples.

Recently, TMT labeling enables the quantification of up to 16 samples in a single analysis, without increasing the complexity of the MS^1 scan. Complex, e.g. PTM-centric workflows and

fractionation schemes can be conducted to significantly increase the depth of the proteome analysis. One limitation of TMT is the co-isolation of co-eluting peptides with similar m/z resulting in poor quantification accuracy, also termed “ratio compression” [62]. This can be partially addressed through extensive fractionation, very narrow isolation windows (IW) for MS^2, and/or inclusion of the additional fragmentation event (MS^3 scan) [55, 60] in order to obtain more accurate ratios.

1.7 Proteomics strategies for S-Nitrosylation analysis

The investigation of proteome-wide SNO targets is hindered by the analytical challenges related to the lability (potential loss and reshuffling during sample preparation/analysis) and low abundance of the SNO. In contrast to another reversible PTM, protein phosphorylation, which is sufficiently stable during sample processing and MS measurement, SNO can be reduced during the sample preparation via exposure to ambient light and even ESI and MALDI might induce dissociation of the S-N bond. These challenges are addressed via derivatization of SNO accompanied by the inclusion of the thorough controls. In order to study the SNO in complex biological samples several proteomics strategies involving enrichment of SNO proteins/peptides followed by MS detection were developed [38]. These strategies allow the identification of the SNO proteins and sites, and often also enable relative quantification of SNO levels at a specific site. Commonly applied proteomics strategies include SNO derivatization using reagents which directly react with SNO to form stable adducts (direct methods of SNO detection) [20] or application of variations of the biotin switch technique (BST), involving selective reduction of SNO followed by derivatization of the liberated thiol (indirect methods of SNO detection) [38, 63].

1.7.1 Direct methods of S-Nitrosylation analysis

Ischiropoulos et al. made use of the organomercury complexes in their proteomic strategy of SNO analysis [64]. Their method comprises three steps: 1) free thiols are blocked with methyl methanethiosulfonate (MMTS), 2) SNO proteins are captured by phenylmercury moiety conjugated to agarose beads or a biotin tag, 3) after tryptic digestion and enrichment, SNO peptides are subjected to LC-MS/MS analysis. This mercury-based method was used to identify 1011 SNO sites in 647 proteins in various mouse tissues [64]. The phenylmercury reagents seem to preferentially react with SNO and not with other oxidized thiols (i.e. mixed

disulfides), however, they can react with free thiols and therefore SH should be blocked in the first step of the assay. Careful controls of SH blocking completeness are required.

Zhang et al. [65] made use of the highly specific reaction of SNO and triaryl-substituted phosphine substrates, in which SNOs are converted to disulfides via reductive ligation under mild conditions. Importantly, triaryl-substituted phosphine reagents do not react with free thiols or any other oxidized form of Cys. The authors developed a biotin-linked phosphine substrate for enrichment of SNO proteins from cell extracts. The first step of the assay includes blocking of the free thiols with N-ethylmaleimide (NEM). In this method the blocking step is required in order to avoid transnitrosylation (SNO exchange) reactions after cell lysis, thus the original cellular SNO is preserved. In the next step, the SNO proteins are labeled with biotin-linked phosphine substrate. The labeled SNO proteins are then detected by Western blot by incubation with NeutrAvidin-HRP, a deglycosylated form of avidin that provides highly specific, low-background binding of biotinylated substrates. [65]. The limitation of the method is the poor compatibility with bottom-up proteomics workflows, as SNO is exchanged with a disulfide bond, thus prohibiting usual reduction and alkylation before tryptic digestion, eventually reducing the digest efficiency resulting in poor proteome coverage.

1.7.2 Indirect methods of S-Nitrosylation analysis

The most widely applied methods of SNO analysis include BST or its derivative switch techniques (ST), such as isotope-coded affinity tags (ICAT) [66], iodoacetyl tandem mass tags (iodoTMT) [67] and resin-assisted capture (RAC) [68]. These assays include:1) blocking of the free thiols, 2) selective reduction of SNO with sodium ascorbate, 3) introduction of functional groups enabling stable-adduct formation, enrichment, and (preferably) also quantitation of the switched SNO [63].

Here, it is crucial that the ascorbate reduction exclusively targets SNO, but no other oxidized Cys. The specificity is demonstrated by the distinct mechanism of SNO-specific reduction. Ascorbate reduction relies on a transnitrosylation reaction, yielding the semidehydroascorbate radical and NO, which is not possible for any other oxidized Cys [37]. Additionally, incomplete blocking of free thiols in the first step of the BST might result in false positive identifications, thus careful controls (i.e. skipping the addition of ascorbate will detect the non-completely blocked Cys) are required.

1.7.2.1 Isotope-coded affinity tags

ICAT represents a pair of isotopically labeled (heavy and light) Cys-reactive tags. ICAT was first used for differential quantification of two protein samples [69]. The quantification is based on the Cys peptides. ICAT was designed to contain a biotin group allowing selective purification of Cys peptides using avidin or streptavidin beads. After LC-MS/MS measurement the differential expression of proteins can be determined based on the heavy/light ratio of Cys peptide intensities. Later, ICAT reagents were incorporated in a BST assay for SNO analysis, the method was termed SNOxICAT [35]. In the cell lysates the free Cys are labeled (blocked) with light version of ICAT, in the next step the SNO is reduced with ascorbate and labeled with heavy version of ICAT. The samples are combined and digested with trypsin, followed by enrichment of the Cys peptides via binding of the biotin group of the ICAT to avidin affinity cartridge. After elution, the samples are analyzed by LC-MS/MS. Using SNOxICAT the relative site occupancy (SNO/free Cys ratio) was defined for ~1000 Cys residues in ischemic mouse hearts with or without NO_2 exposure [35]. The disadvantage of ICAT reagents is the bulky nature of the biotinylated tag, which might interfere with the ionization of the peptides and complicate the MS/MS spectra, thus the peptide assignment.

1.7.2.2 Iodoacetyl tandem mass tags

The iodoTMT represent a set of six isobaric Cys reactive reagents (iodoTMT™-6plex). The reagent is an analogue of the conventional TMT tag, however, using a thiol reactive iodoacetyl group for covalent labeling of the Cys, rather than an NHS-group. Six isobaric iodoTMT tags are used for relative MS/MS-based quantification of iodoTMT labeled peptides (analogous to amine-reactive TMT). An anti-TMT monoclonal antibody allows the purification of TMT labeled peptides after immunoprecipitation. IodoTMT-based SNO ST is performed by complete blocking of free Cys, specific reduction of SNO by ascorbate followed by iodoTMT labeling of reduced SNO proteins. Next, the maximum of six protein samples labeled with six isobaric tags are pooled and digested. The iodoTMT labeled peptides are enriched using anti-TMT antibody resin, followed by LC-MS/MS analysis. Using a IodoTMT switch assay Pan et al. identified 169 SNO proteins and 266 SNO sites in hypoxic cardiomyocytes [70]. This was the first method to be tested in the course of this thesis, but even after extensive optimization of the protocol it turned out that the main limitation of the assay is the poor specificity of anti-TMT antibody-based enrichment.

1.7.2.3 Resin-assisted capture

RAC is a modified BST where the SNO switch is performed using thiol-reactive (thiopropyl-sepharose) resin instead of thiol-reactive biotin, thus combing the labeling and pulldown steps of the ST. Free Cys are blocked with MMTS, ascorbate converts SNOs to free thiols which are covalently bound to thiopropyl-sepharose resin via formation of disulfide bond, the background proteins are depleted and SNO proteins are trypsinized on-resin and common disulfide reductants (i.e dithiothreitol (DTT)) are used to elute the switched SNO peptides. The procedure also enables on-resin isobaric reagent (i.e. iTRAQ) labeling for further LC-MS/MS based quantitative analysis. The RAC showed high specificity ~ 95 % and superior sensitivity for proteins higher than 100 kDa compared to BST [68, 71]. Using another RAC approach in combination with iTRAQ labeling, Forrester et al. demonstrated the progressive decay of SNO signal over time as a result of Cys-NO treatment of HEK293 cells. Roughly 300 negatively-regulated SNO sites were quantified [71]. Limitations of disulfide-exchange based RAC are possible reshuffling of reduced Cys during binding to thiopropyl-sepharose resin and inefficient on-bead digestion, because the usual reduction and alkylation of protein disulfides before tryptic digestion is prohibited here.

2. Objectives

Transient and target-selective nature of SNO makes it a redox-switch, which plays an essential role in NO-mediated signaling. SNO has been shown to be involved in several (patho)physiological events such as neurogenesis/neurodegeneration and cardioprotection [9, 30, 72-74]. The growing number of SNO substrates reported across protein classes suggests the significance of SNO-mediated cellular regulatory events. However, the investigation of proteome-wide SNO targets is hindered by the analytical challenges related to the transient nature (potential loss and reshuffling during sample preparation/analysis [20]) and low abundance of the SNO. The application of proteomics strategies revealed a great potential for the analysis of SNO in complex biological samples, enabling the identification of hundreds of SNO proteins and SNO sites [75]. Numerous MS-based analytical strategies have been development for SNO analysis [35, 37, 76]. Nevertheless, all of them suffer from certain limitations impeding the advancement in SNO research. The objectives of the thesis were: 1) to develop a highly sensitive, reproducible and robust proteomics strategy for in-depth, proteome-wide quantitative analysis of SNO -- and importantly endogenous -- SNO, 2) to apply the method on a (patho)physiologically relevant model system in order to discover novel SNO targets and thus broaden our knowledge on the mechanisms of SNO formation and the biological processes regulated by SNO, 3) to perform combined quantitative analysis of SNO, global protein expression and other PTMs.

3. Results and discussion

3.1 S-Nitrosylation analysis using iodoTMT

First, SNO was analyzed in HeLa lysates (N=3) *in-vitro* nitrosylated with 200 µM GSNO using ST with sodium ascorbate and commercially available iodoTMT assay, followed by anti-TMT antibody slurry-based enrichment. The eluates from 50 µg protein starting amount (enriched digests) and 1 µg of the iodoTMT-labeled total digests were measured by nano-LC-MS/MS using 120 min gradient. As a result, on average an only 2.8-fold increase in the number of iodoTMT-switched SNO peptides was detected after the iodo-TMT-based enrichment (on average N=120) compared to the direct measurement of 1 µg total digest (on average N=43), even though 50 x higher starting protein amount was used for the enrichment compared to the measurement of the total digest. In conclusion, this result demonstrates a surprisingly weak gain from conducting the complex and costly iodo-TMT-based enrichment under these conditions.

3.1.2 Anti-TMT enrichment recovery test

In order to assess the recovery of the anti-TMT enrichment, TMT labeled synthetic peptides were required as standards and had to be generated first. Due to the reshuffling properties of the thiol group, the generation of iodoTMT labeled standard Cys peptides represents a significant challenge. To overcome this limitation, synthetic peptides (N=3) containing a single primary amine group at the N-terminus (i.e. containing no Lysine) were labeled with two different channels (TMT1 and TMT2) of amine-reactive TMT, instead of using iodoTMT. The generated standard peptides can be used for testing the recovery of anti-TMT enrichment. The fact that the anti-TMT antibody is recognizing the reporter region of the TMT tag, which is the same of iodoTMT and amine-reactive TMT, allows to assume similar recoveries for iodoTMT and amine-reactive TMT labeled peptides. It should be considered that the localization of the TMT tag on the peptide N-terminus as opposed to within the sequence for Cys residues, might slightly affect the binding properties. A known amount of the TMT1-labeled peptides was spiked to HeLa or bovine serum albumin (BSA) digests before the anti-TMT enrichment, whereas the same amount of the peptides labeled with TMT2 was spiked to the eluates after the enrichment and the eluate was measured by LC-MS/MS. In advance, the TMT1 and TMT2 peptides were mixed and measured by LC-MS/MS in order to confirm the equal concentrations of the stocks based on the TMT reporter intensities. The recovery ($R_{\%}$)

of anti-TMT enrichment was calculated for each peptide based on the TMT reporter intensities ($R_{\%}$= Int_{TMT2} x 100/ Int_{TMT1}), where Int represents the intensity of the TMT reporter ion. As shown in Figure 3.1, the maximum recovery was ~ 25% for the peptide dGNGFLSAAELR, where the N-terminus of the aspartic acid (d) is labeled with TMT. Experiments with HeLa and BSA backgrounds showed similar recoveries, indicating the independence of the results from the background proteome. Both this recovery test and the later conducted iodoTMT-based SNO analysis indicate the poor recovery and the low efficiency of anti-TMT enrichment.

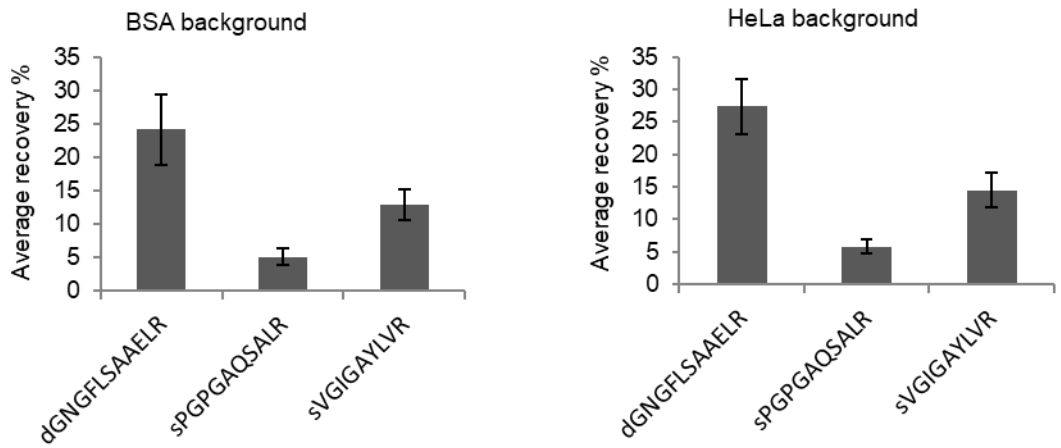

Figure 3.1 Average of N=3 technical replicates recovery (%) of anti-TMT enrichment shown for each of the 3 standard peptides used for recovery assessment both with BSA and HeLa background matrixes. Error bars indicate the standard deviation.

3.2 Development of the bioorthogonal cleavable-linker-based enrichment of cysteine peptides

The low abundance of SNO demands a highly efficient enrichment strategy. Application of biotinylated thiol-reactive probes allows for enrichment using immobilized streptavidin, which was proven to be efficient even for highly diluted and low abundant targets. Nevertheless, there are crucial limitations in application of biotinylated thiol-reactive probes (i.e. ICAT), including: 1) harsh, denaturing conditions needed to disrupt the biotin–streptavidin interaction, resulting in contamination of eluate with avidin monomers, 2) the bulky nature of the biotin containing tag, resulting in compromised ionization of the peptides and enhanced complexity of MS/MS spectra. The incorporation of a cleavable functional group between the biotin tag and the labeled Cys residue enables specific elution of the Cys peptides via the chemical cleavage of the biotin-containing part of the linker. Recently, several biotin-azide cleavable-

linkers have been reported, such as Diazo-biotin-azide with diazo cleavable group, Diol-biotin-azide with diol cleavable group and 1-(4,4-dimethyl-2,6-dioxocyclohex-1-ylidene)ethyl (Dde)-biotin-azide with Dde cleavable group [77, 78]. These linkers contain a bioorthogonal azide functional group which can be selectively conjugated to an alkyne functional group via copper(I)-catalyzed alkyne-azide cycloaddition (CuAAC) click chemistry [79], a biotin group for biotin-streptavidin interaction and a chemically cleavable group for elution of the probe labeled proteins/peptides. Availability of the thiol reactive alkyne-derivatized iodoacetamide reagent (IAA-alkyne) allows to design a bioorthogonal cleavable-linker-based enrichment strategy for Cys peptides. Taking into the account the poor performance of the iodoTMT-based enrichment, in this thesis a novel method for Cys peptide enrichment from complex biological sample (proteome digest) based on the use of bioorthogonal cleavable-linker and CuAAC click chemistry was developed. Briefly**,** the method includes: 1) labeling of the Cys peptides with IAA-alkyne, 2) conjugation of the biotin-azide cleavable-linker to alkyne-labeled peptides via CuAAC, 3) affinity binding of the Cys peptides to streptavidin beads via the biotin group of the linker, 4) depletion of background peptides, 5) chemical release of the Cys peptides via cleavage of the linker, 6) on-tip pH 10 fractionation of the eluate (optional), 7) nano-LC-MS/MS analysis. In the following, the optimization of the individual steps is summarized.

3.2.1 Iodoacetamide alkyne labeling of synthetic cysteine peptides

The first step of the bioorthogonal cleavable-linker-based enrichment is the IAA-alkyne labeling of the Cys peptides (Figure 3.2).

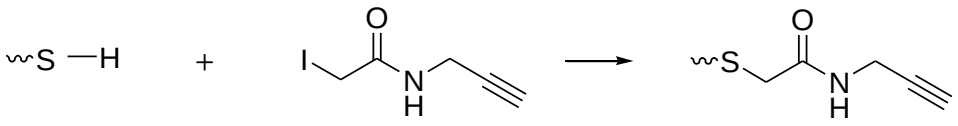

Cys peptide *IAA-alkyne* *Peptide-alkyne*

Figure 3.2 Reaction of the Cys peptide with IAA-alkyne.

Four synthetic Cys-containing peptides (Table 3.1) were used to confirm the efficiency of Cys labeling with IAA-alkyne. An equimolar mix of the four synthetic Cys peptides (total amount 0.55 nmol per peptide) was reduced with Tris(2-carboxyethyl)phosphine hydrochloride (TCEP) and incubated with IAA-alkyne. After nano-LC-MS/MS measurement, a Mascot search with IAA-alkyne set as a variable modification identified only 1 PSM for the unlabeled Cys peptide, but >100 PSM for the alkyne-labeled forms (Table 3.1). As the number of PSMs correlates

also with the abundance of a peptide, this result demonstrates the high efficiency of the labeling with IAA-alkyne.

Table 3.1 PSMs of IAA-alkyne labeled and unlabeled Cys peptides.

Peptide	***Peptide-alkyne PSMs***	***Unlabeled PSMs***
ETCVVVYTGYGNR	15	0
CSDIISYTFK	27	0
GEHGFIGCR	34	1
YLAADKDGNVTCER	58	0

3.2.2 Best reaction conditions for click chemistry-based peptide bioconjugation

The second step of the bioorthogonal cleavable-linker-based enrichment is the conjugation of the biotin-azide cleavable-linker to IAA-alkyne labeled peptides via CuAAC.
The first cleavable-linker tested was Diazo-biotin-azide (Figure 3.3).

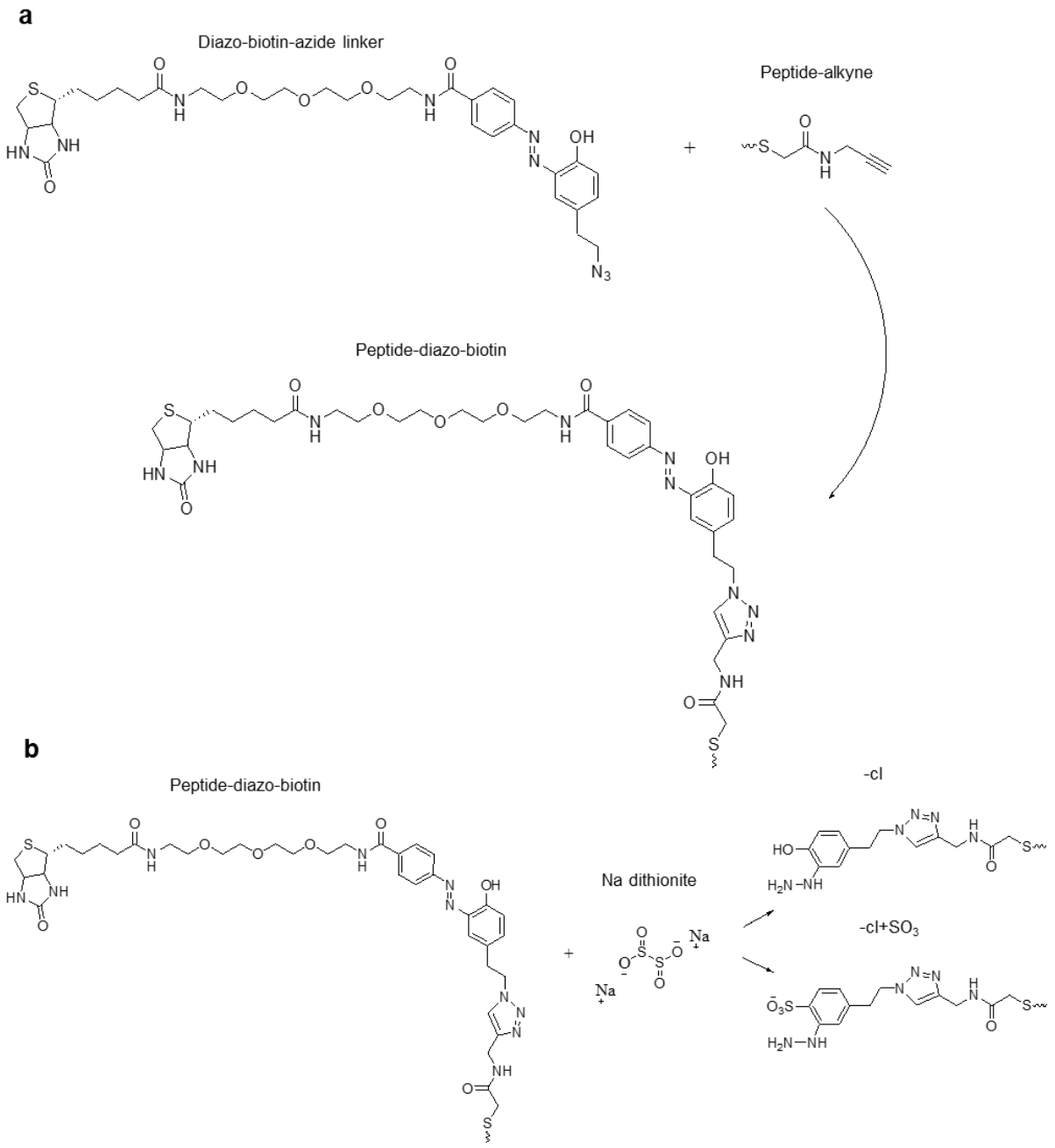

Figure 3.3 The structure and the reactions of the Diazo-biotin-azide linker. (a) Reaction of the Diazo-biotin-azide linker with peptide-alkyne. (b) Cleavage of the Diazo-biotin-azide linker with sodium dithionite resulting in two different forms of the cleaved linker (-cl: cleaved form of the Diazo-biotin-azide linker, cl+SO_3 (-cl+79.95): cleaved form of the Diazo-biotin-azide linker with added SO_3 group).

In order to define the best reaction conditions for CuAAC-based conjugation, peptide-alkynes were reacted with Diazo-biotin-azide linker (Figure 3.3a) using three different protocols (P1 [79], P2 [77] and P3 [80]; Table 3.2). The basic CuAAC process requires only Cu^+ ions, which is usually provided by a mixture of a Cu(II) salt ($CuSO_4$) and a reducing agent (sodium ascorbate or TCEP). The addition of Tri(3 hydroxypropyltriazolylmethyl)amine (THPTA) serves the dual purpose of acting as Cu^+ stabilizing ligand, and sacrificially intercepting the radicals and/or peroxides derived from O_2/Cu/ascorbate that oxidize histidine and other residues. Aminoguanidine is recommended for suppression of the reactions between dehydroascorbate and protein side chains (principally Arg) [79]. The three protocols tested here use the same amount of peptide-alkyne and Diazo-biotin-azide linker, but different concentrations of $CuSO_4$, ascorbate and THPTA, besides P3 is using TCEP as a reducing agent, and P1 is using aminoguanidine hydrochloride as a sacrificial agent (Table 3.2). The reactions were performed in parallel with the same incubation times and the reaction volumes.

Table 3.2 Comparison of the CuAAC protocols (P1, P2 and P3).

Reagents	***P1***	***P2***	***P3***
Peptide-alkyne	25 µM	25 µM	25 µM
$CuSO_4$	0.25 mM	2 mM	1 mM
THPTA	1.25 mM	0.1 mM	0.1 mM
Ascorbate	5 mM	2 mM	x
TCEP	x	x	1 mM
Aminoguanidine hydrochloride	5 mM	x	x
Biotin-azide linker	150 µM	150 µM	150 µM

First, the peptide mixture was measured directly after the CuAAC and the precursor intensities of the Diazo-biotin-azide labeled peptides (peptide-diazo-biotin, Figure 3.3) were compared. The extracted ion chromatograms (XICs) of the two peptides ETCVVVYTGYGNR and CSDIISYTFK (Figure 3.4) show that the highest signal intensities of peptide-diazo-biotin were obtained by P1, which is using the smallest amount of $CuSO_4$ and aminoguanidine for suppression of the side reactions. This result indicates that Cu-driven side reactions are

significantly affecting the yield of the CuAAC for peptide bioconjugation. P2, which is using 2 mM CuSO4, showed significantly lower intensities when compared to P1 (Figure 3.4). P3, which is using TCEP as a reducing agent, showed the poorest performance (Figure 3.4), thus was not tested further.

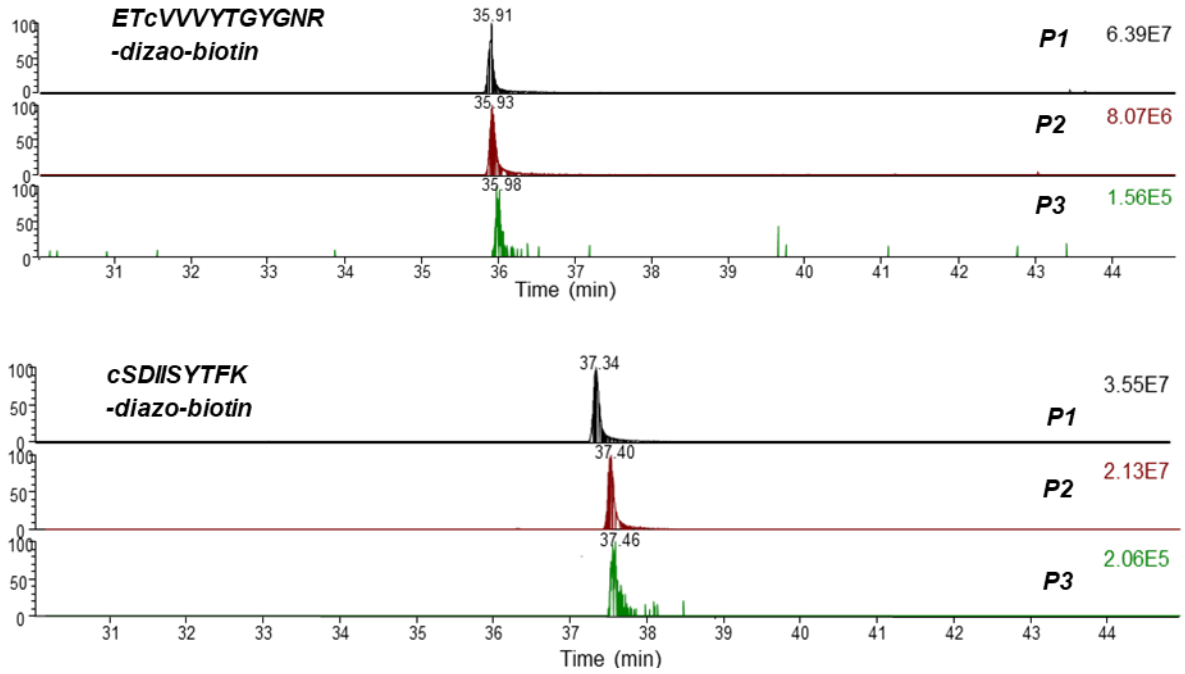

Figure 3.4 XICs of Diazo-biotin-azide labeled ETCVVVYTGYGNR and CSDIISYTFK comparing the efficiency of P1, P2 and P3 CuAAC protocols.

In the next experiment the precursor intensities of the Cys peptides were compared after the cleavage of the Diazo-biotin-azide labeled peptides with Na dithionite (Figure 3.3b). The P1 was compared to P2 and to P4, which uses 0.5 mM $CuSO_4$ (2-fold higher compared to P1, but 4-fold lower compared to P2). As shown in Table 3.3, the number of PSMs of the Cys peptides with cleaved form of the linker (cl: cleaved form of the Diazo-biotin-azide linker, cl+SO_3: cleaved form of the Diazo-biotin-azide linker with added SO_3 group; Figure 3.3b) is higher for P1 compared to P2 and P4. These results indicate that the P1 protocol using 0.25 mM $CuSO_4$ has the best CuAAC conditions for peptide-alkyne bioconjugation. The negligible number of the PSMs of non-reacted form of the peptides (peptide-alkyne) indicates close to complete conversion, thus the high efficiency of the CuAAC reaction (Table 3.3).

3.2.3 Choice of the bioorthogonal cleavable-linker

Three different bioorthogonal cleavable-linkers: Diazo-biotin-azide, Diol-biotin-azide and Dde-biotin-azide were tested for suitability and performance.

3.2.3.1 Diazo-biotin-azide linker

As mentioned above the Diazo-biotin-azide linker (Figure 3.3) was the first cleavable linker tested. It is cleaved in the presence of the 50 mM Na dithionite, for the best results the cleavage reaction is repeated N=3 times. In the experiment using synthetic Cys peptides (see 3.2.2) it was observed the cleavage reaction leads to the formation of two different form of the cleaved linker (cl and cl+SO_3 (cl+79.95); Figure 3.3b) detected for each peptide (Table 3.3). The presence of cl+SO_3 could be explained by the sulfonation reaction of the dithionite anion (S_2O4^{2-}) with the hydroxyl group of the Diazo-biotin-linker, which results in the formation of the sulfonated form (cl+SO_3) of the cleaved linker.

Table 3.3 PSMs of all the peptide forms (cl: cleaved form of the Diazo-biotin-azide linker, cl+SO_3: cleaved form of the Diazo-biotin-azide linker with added SO_3 group) detected after direct cleavage of Diazo-biotin linker labeled Cys peptide mixture with Na dithionite.

Peptide	***P1***	***P2***	***P4***
YLAADKDGNVTcER_alkyne	0	0	3
YLAADKDGNVTcER_cl	29	3	10
YLAADKDGNVtcER_cl+SO_3	79	13	51
GEHGFIGcR_alkyne	0	0	0
GEHGFIGcR_cl	3	4	1
GEHGFIGcR_cl+SO_3	23	5	16
ETcVVVYTGYGNR-alkyne	2	1	2
ETcVVVYTGYGNR_cl	13	5	10
ETcVVVYTGYGNR_cl+SO_3	15	8	13
cSDIISYTFK_alkyne	2	1	4
cSDIISYTFK_cl	26	9	18
cSDIISYTFK_cl+SO_3	63	16	74

As shown in the Table 3.3, cl+SO_3 is even more dominant than the cl, as higher number of PSMs were detected for the cl+SO_3 than for the -cl in all analyzed peptide sequences. The fact that the cleavage of the Diazo-biotin-azide linker does not lead to the formation of a single product might significantly reduce the sensitivity of the enrichment, as peptide precursor intensities will be split across two different forms.

Another issue observed for the Diazo-biotin-azide linker-based enrichment was the contamination of the Na dithionite reagent with polypropylene glycol (PPG). The direct measurement of a trace amount of the Na dithionite by LC-MS proved the presence of PPG in Na dithionite stocks from four different vendors, thus indicating that the PPG contamination comes from the production process of Na dithionite. PPGs of ~ 400-800 m/z detected in Na dithionite (Supplementary Figure 1) can bind to the C18 RP chromatographic material, used for the desalting and also during LC-MS, thus compromising the binding of the peptides, leading to major interfering signals and background, and making the procedure non-compatible with bottom-up proteomics.

Taking into the account the above-mentioned limitations and the need for the multistep (N=3 repetitions) cleavage procedure, as well as possible side reactions of the dithionite anion (S_2O4^{2-}) with the hydroxyl group on the side chains of serine and threonine, the Diazo-biotin-azide linker was not used in the further experiments.

3.2.3.2 Diol-biotin-azide cleavable-linker

Next, Diol-biotin-azide was used as a bioorthogonal cleavable-linker (Figure 3.5a). In order to test the performance of the linker, IAA-alkyne labeled Cys synthetic peptides were conjugated with Diol-biotin-azide via CuAAC. The peptides were bound to the streptavidin beads and released by the oxidative cleavage of the vicinal diol with sodium periodate ($NaIO_4$). For the optimal cleavage the reaction is repeated N=3 times. The main cleavage product is expected to be cl-aldehyde, nevertheless the cl-acetal and cl-oxime forms (Figure 3.5b) were also observed in stoichiometric amounts (Table 3.4). Thus, for this linker the issue of splitting the peptide's precursor intensity in multiple forms occurs as well.

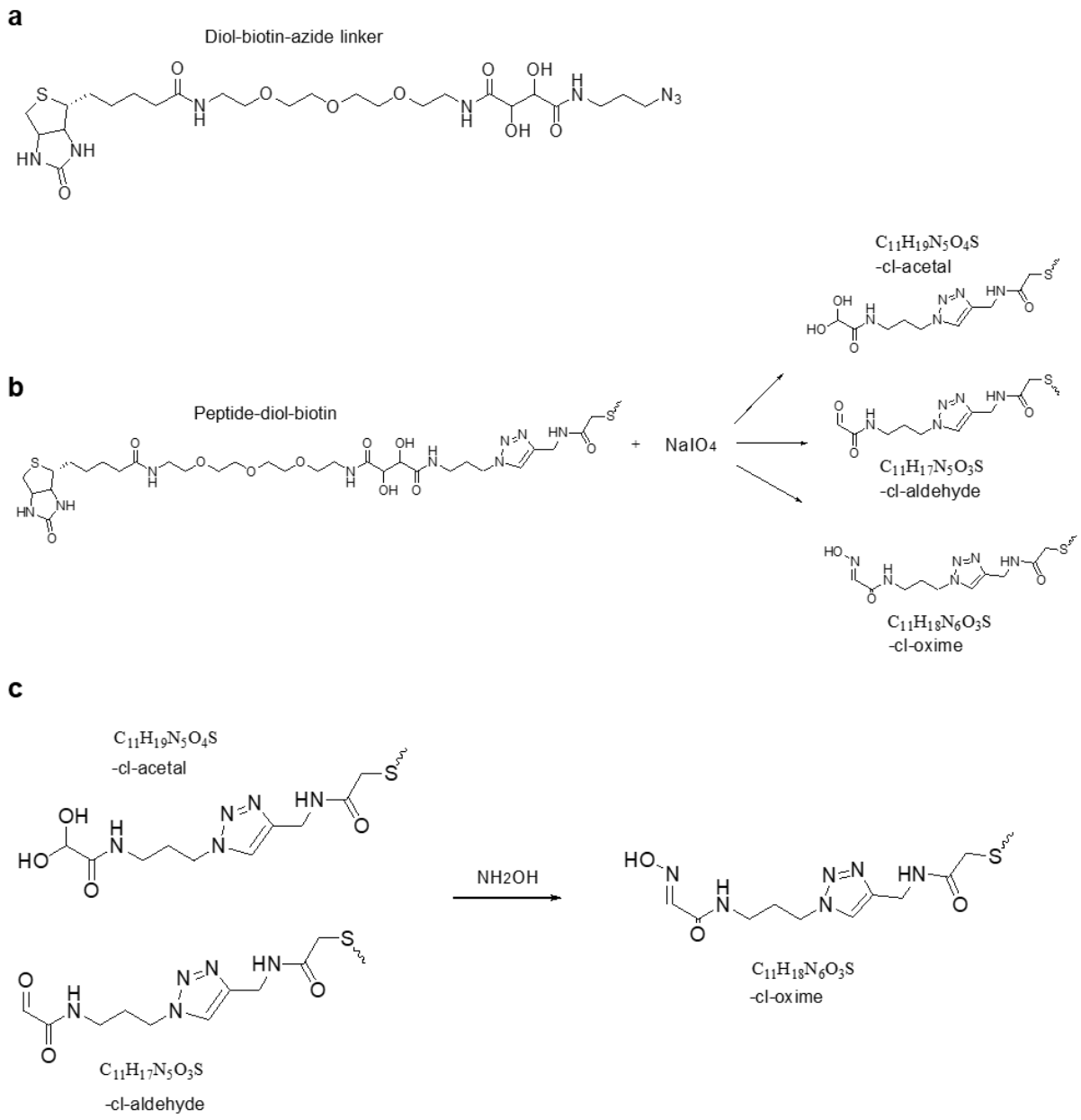

Figure 3.5 The structure and the cleavage products of the Diol-biotin-azide linker. (a) The structure of Diol-biotin-azide, (b) cleavage of the vicinal diol group of the linker leading to cl-acetal, cl-aldehyde and cl-oxime forms, (c) conversion of the both cleaved forms to cl-oxime using 5% hydroxylamine.

Another consideration for the use of the Diol-biotin-azide linker is the strong oxidative nature of the cleaving reagent $NaIO_4$. Thus, to define the appropriate concentration of $NaIO_4$ for efficient cleavage, concentrations of 1 mM and 10 mM were compared using synthetic Cys peptides. As shown in Table 3.4, the use of the 10 mM did not increase the intensity of the cleaved products, in contrary, in some cases it decreased the intensity of the cleaved products.

This can be explained by the oxidative side reactions of $NaIO_4$ on the side chains of several amino acids. Thus, quenching of the $NaIO_4$ is required after the cleavage reaction. First, diol-containing DTT was used for this purpose, which efficiently quenched the $NaIO_4$, nevertheless polymer formation as a result of the oxidation of the thiol groups of the DDT to disulfides was observed. This polymer interferes with the LC-MS analysis in a similar way described above for the PEG. The issue was resolved by replacement of the DDT with threitol, which contains the sacrificial diol for $NaIO_4$ quenching, but does not contain thiol groups.

Table 3.4 Comparison of the MS precursor intensities for the all three cleavage products of Diol-biotin-azide labeled synthetic Cys peptides with 1 mM (light form of the peptide indicated by uppercase last amino acid) vs 10 mM (heavy form of the peptide indicated by lowercase last amino acid) $NaIO_4$.

Sequence	1 mM $NaIO_4$			10 mM $NaIO_4$		
	cl-aldehyde	cl-acetal	cl-oxime	cl-aldehyde	cl-acetal	cl-oxime
FECQPGYR/r	2.47E+08	1.91E+09	8.19E+09	1.46E+08	1.31E+09	9.68E+09
LCFDNSFSTISEK/k	3.24E+08	1.68E+10	6.51E+09	2.82E+08	1.95E+10	6.51E+09
VNLSCGGVSHPIR/r	1.04E+09	7.14E+07	1.82E+09	4.68E+08	8.92E+06	7.26E+08

Interestingly, cl-aldehyde and cl-acetal can be converted to cl-oxime by the reaction with 5% hydroxylamine (Figure 3.5c), thus this reaction was tested to yield a single form of the cleaved peptide. As demonstrated in Table 3.5, the reaction with hydroxylamine results in the formation of the cl-oxime as the dominant form (inferred from the precursor intensities), although the other two forms are still detectable with lower intensities. Additionally, the efficiency of the conversion to cl-oxime via the application of 5% hydroxylamine was tested on a complex sample. The treatment of the eluate of the enrichment of total Cys peptides from HeLa lysate with 5% hydroxylamine shifted the equilibrium from cl-aldehyde:cl-acetal:cl-oxime from 21.9:76.2:1.9 to 0.6:3.3:96.1, while increasing the total number of identified peptides concurrently by a factor of 4 (2363 vs 8086), thus showing highly efficient conversion of cl-acetal and cl-aldehyde to cl-oxime form.

Table 3.5 Comparison of the MS precursor intensities for the all three cleavage products of Diol-biotin-azide labeled synthetic Cys peptides with and without 5% NH_2OH reaction after the cleavage. Light form (5% NH_2OH) of the peptide indicated by uppercase and the heavy form (Control) of the peptide indicated by lowercase last amino acid.

Sequence	5% NH_2OH			Control		
	cl-aldehyde	cl-acetal	cl-oxime	cl-aldehyde	cl-acetal	cl-oxime
FECQPGYR/r	5.96E+06	2.95E+08	3.31E+09	2.10E+07	7.79E+08	2.00E+08
LCFDNSFSTISEK/k	1.58E+07	1.19E+09	9.19E+09	1.01E+08	6.77E+09	2.89E+09
VNLSCGGVSHPIR/r	7.25E+08	1.48E+07	3.71E+09	2.81E+08	4.38E+06	5.51E+07

In conclusion, significant optimization of the cleavage and quenching conditions lead to the improved results for Diol-biotin-azide, thus making it a suitable candidate of a cleavable-linker. Although certain limitations still remain, such as the multistep (N=3 repetitions) cleavage procedure, the need for $NaIO_4$ quenching, and the need to perform the hydroxylamine reaction immediately before the LC-MS measurement.

3.2.3.3 Dde-biotin-azide cleavable-linker

Next, the Dde-biotin-azide cleavable-linker (Figure 3.6a) was tested. Here, the Dde group is cleaved by a single step, mild chemical cleavage with 2% hydrazine (Figure 3.6b).

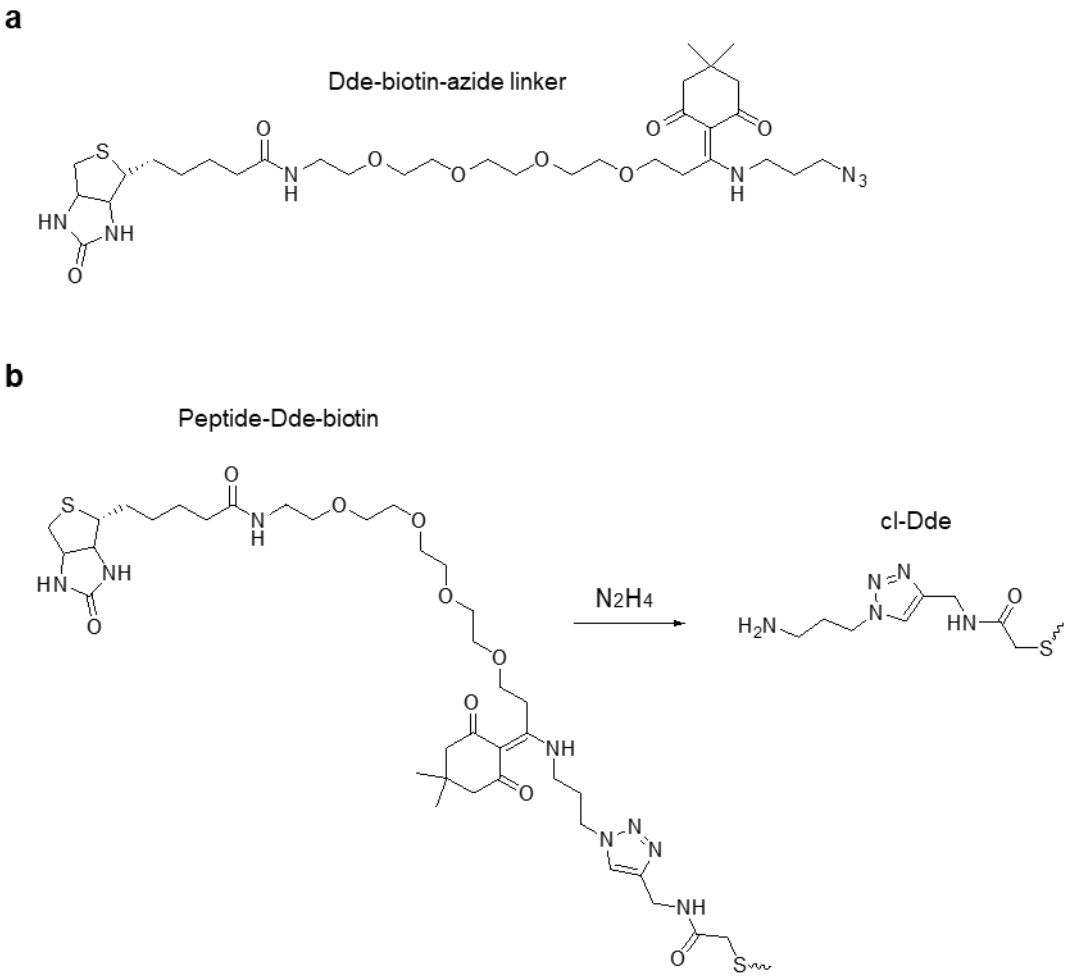

Figure 3.6 The structure and the cleavage of the Dde-biotin-azide linker. (a) The structure of the Dde-biotin-azide, (b) cleavage of the Dde group of the linker with hydrazine leading to the formation of the single cleaved form cl-Dde.

To test the performance of the linker the Dde-biotin-azide was conjugated via CuAAC to IAA-alkyne-labeled Cys synthetic peptides (the same stock of the IAA-alkyne labeled peptide mixture as used for the Diol-biotin-azide linker test) followed by the incubation with streptavidin beads and single step elution with 2% hydrazine. After nano-LC-MS/MS measurement of the eluate (0.5 pmol per peptide, estimated from the initial peptide amount) all three peptides were detected with a single cleaved form of the Dde-biotin-azide linker (cl-Dde), with high number of PSMs and with good reproducibility in all 4 replicates, as shown in Figure 3.7.

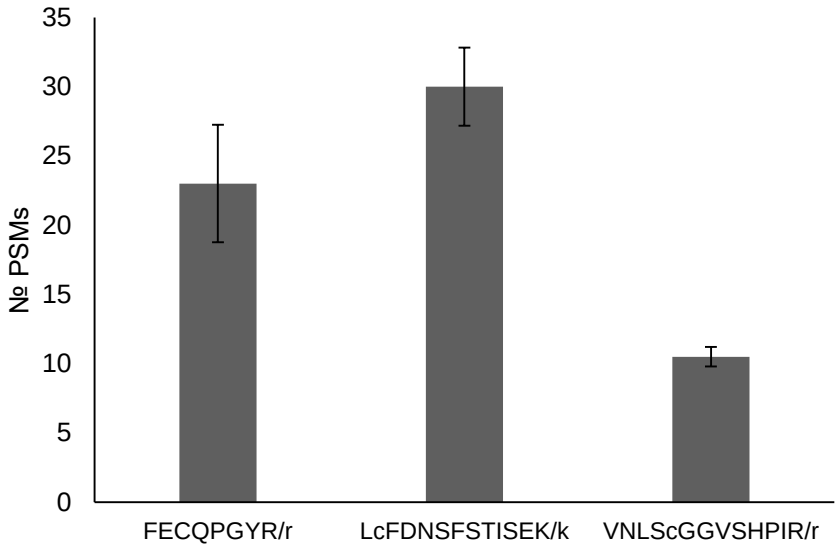

Figure 3.7 Number of PSMs of cl-Dde peptides in the eluate of the Dde-boitin-azide linker-based enrichment of the synthetic Cys peptides. Light form of the peptide indicated by uppercase and the heavy form of the peptide indicated by lowercase last amino acid. Error bars represent the standard deviation (SD) of 4 replicates.

Additionally, the cl-Dde modified peptide demonstrate good characteristics for MS/MS-based identification, as exemplified for the cl-Dde modified VNLSCGGVSHPIR, where almost complete coverage of the y^{+} fragment ions was achieved, with the y^{9+}-y^{11+} and b^{10+} fragment ions containing the cl-Dde modification (Figure 3.8).

In conclusion, the use of the Dde-biotin-azide allows for single step mild chemical cleavage that results in a single cleavage product, without the need for any additional quenching or byproduct conversion reactions. Additionally, the cl-Dde peptides show good fragmentation behavior and favor MS/MS-based identification. The only drawback is the high toxicity of the cleaving reagent hydrazine, which should be handled with extreme precaution.

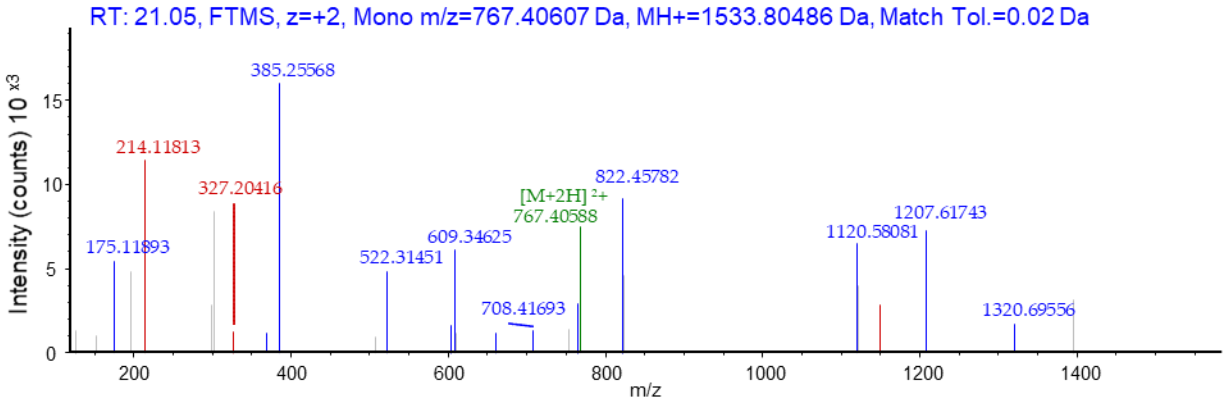

#1	Immonium	b⁺	b²⁺	Seq.	y⁺	y²⁺	#2
1	72.08078	100.07570	50.54149	V			13
2	87.05529	214.11863	107.56295	N	1434.73833	717.87280	12
3	86.09643	327.20270	164.10499	L	1320.69540	660.85134	11
4	60.04439	414.23473	207.62100	S	1207.61133	604.30930	10
5	76.02155	712.35593	356.68160	C-cl-Dde	1120.57930	560.79329	9
6	30.03383	769.37740	385.19234	G	822.45810	411.73269	8
7	30.03383	826.39887	413.70307	G	765.43663	383.22195	7
8	72.08078	925.46729	463.23728	V	708.41516	354.71122	6
9	60.04439	1012.49932	506.75330	S	609.34674	305.17701	5
10	110.07127	1149.55823	575.28275	H	522.31471	261.66099	4
11	70.06513	1246.61100	623.80914	P	385.25580	193.13154	3
12	86.09643	1359.69507	680.35117	I	288.20303	144.60515	2
13				R	175.11896	88.06312	1

Figure 3.8 HCD MS/MS spectrum of the Dde-cleaved-peptide VNLScGGVSHPIR2+. Assigned b/y-ions are labeled in red and blue, respectively.

3.2.3.4 Comparison of the Dde-biotin-azide and Diol-biotin-azide cleavable-linkers

The performance of Dde-biotin-azide and Diol-biotin-azide linkers was compared by the enrichment of total Cys peptides from HeLa lysate. The Cys in HeLa lysate were reduced, labeled with IAA-alkyne, the sample was digested with trypsin and divided into N=4 aliquots. N=2 aliquots were conjugated with Dde-biotin-azide and the other N=2 with Diol-biotin-azide. The peptides were bound to streptavidin beads, the background peptides were washed off and Cys peptides were eluted via the linker-specific chemical cleavage (for Diol-biotin-azide the final, optimized protocol was used). As a result, Dde-biotin-azide linker-based enrichment identified ~ 20 % more Cys peptides (9852 (± 304) vs 7832 (± 223)) compared to Diol-biotin-azide linker-based enrichment. Both methods show high specificity with only ~ 1% background

peptides (non-Cys-containing; 73 (± 5) and 123 (± 9) for Dde-biotin-azide and Diol-biotin-azide linker-based enrichments, respectively) present, proving the effectiveness of the applied washing steps.

Around 61% of the Cys peptides identified in the eluates of the Dde linker-based enrichment were also identified in the eluates of the Diol linker-based enrichment, showing a slight selectivity, which on the one hand may be explainable through different ionization, fragmentation and chromatographic characteristics for both methods (Figure 3.9a), but on the other hand for 2 replicates of the Dde linker-based enrichment an overlap of 75% was detected (Figure 3.9b).

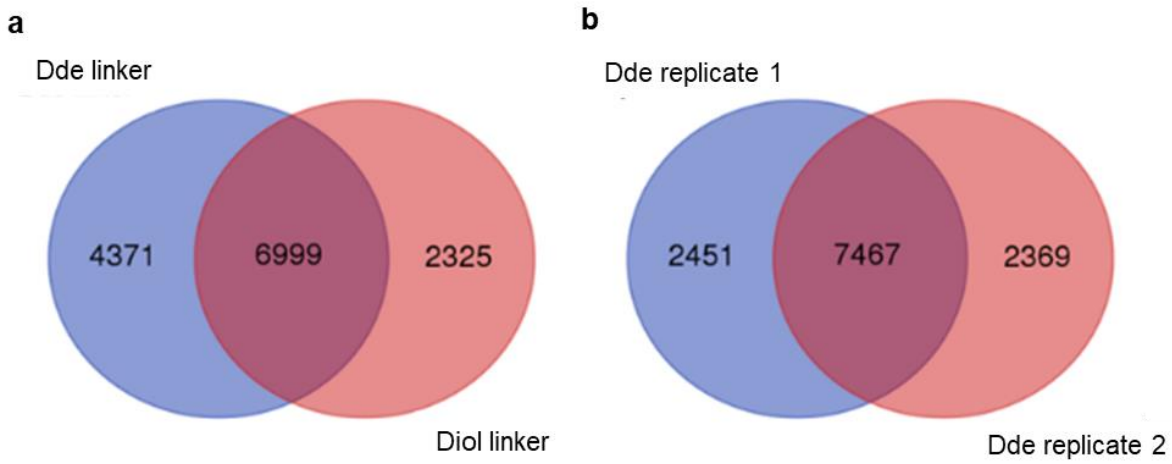

Figure 3.9 Venn diagrams of enriched Cys peptides. (a) Overlap of all the Cys peptides (identified in N=2 replicates) detected in the eluates of the Dde-biotin-azide or Diol-biotin-azide linker-based enrichments. (b) Overlap of the Cys peptides in the replicates of the Dde-biotin-azide linker-based enrichment.

Taking into the account the superior performance and the simpler workflow, the Dde-biotin-azide linker was selected for the use in the further experiments.

3.3 On-tip high pH fractionation of enriched cysteine peptides

Due to the presence of ten thousands of Cys peptides in the proteome, even after efficient depletion of background peptides the sample is still highly complex. Thus, fractionation of the enriched peptides prior to LC-MS is needed to increase the number of identified (and quantified) peptides, and thus the depth of the analysis. One possibility is to use high pH RP

fractionation, which has been shown to be orthogonal to RP-LC performed under acidic pH, commonly used for peptide mixture separation [81]. One of the important factors influencing peptide retention in RP-LC is the net charge of a peptide. This is defined by the charge states of all ionizable groups (e.g. amine and acid carboxyl groups) and their pKa values. Consequently, using extreme pH values for LC solvents, such as < pH 2 for acidic and > pH 8 for high pH RP-LC results in orthogonal retention for the peptides. High pH RP-LC using analytical columns is a widely applied in proteomics. Although such a setup was available in our laboratory, it was not suitable for the fractionation of the enriched eluates, as it requires considerably higher amount of starting material (~ 30-50 µg of peptide). Thus, on-tip high pH fractionation technique suitable for fractionation of less than 10 µg of total digest or eluates was established using pipette tips (200 µL) packed with 2 mm of C18 3M Empore solid phase extraction (SPE) extraction material and 500 µg of Oligo R3 RP Resin. Samples were stepwise eluted with increasing concentrations of ACN in ammonium formate, at pH 10. First, stepwise fractionation of 10 µg HeLa digest was performed according to the Chen et al. [81]. As shown by the number of PSMs identified in each fraction (Table 3.6) an unfavorable, highly heterogeneous distribution between the fractions was observed.

Table 3.6 On-tip pH 10 peptide fractionation. Number of PSMs identified by LC-MS from each fraction of a 10 µg total HeLa digest, using elution conditions according to Chen et al.

Fraction	***PSMs***
3% ACN	1655
6% ACN	5422
9% ACN	8925
15% ACN	18538
80% ACN	21678

Thus, the individual elution steps were optimized to obtain a more homogenous distribution of the proteome across the fractions in order to increase the depth of the analysis. As a result, the optimized setting using 12 %, 16 %, 20 %, 24 %, 28 % and 80 % ACN for stepwise fractionation was applied for the total Cys peptides enriched from 200 µg of HeLa digest (~ 10 – 20 µg of peptides on cartridge). As a result, the fractions 20 %, 24 %, 28 % and 80 % ACN show even distribution and have ~ 5500 PSMs each, whereas 12 % and 16 % had in sum ~

5500 PSMs (Table 3.7). Thus, it was concluded to combine the 12 % and 16 % fractions and use 16 %, 20 %, 24 %, 28 % and 80 % ACN in ammonium formate, pH 10, for stepwise on-tip high pH fractionation in the future experiments.

Table 3.7 Number of PSMs identified in each fraction after on-tip high pH fractionation of the total Cys eluate from 200 µg HeLa digest using the optimized elution conditions.

Fraction	***PSMs***
12% ACN	2064
16% ACN	3487
20% ACN	5383
24% ACN	6372
28% ACN	6024
80% ACN	5636

3.4 Tandem mass tag-based quantitative analysis

TMT-10plex was selected as quantification strategy in order to enable the relative quantification of Cys peptides and the global proteome changes under different conditions (e.g. treatment, stimulation or clinical samples). High labeling efficiency (> 90%), demonstrated by the share of labeled TMT peptides compared to all peptides, was observed in multiple experiments including the experiments (HeLa digest) described in 3.2.3.4 and 3.3.

3.4.1 MS/MS vs synchronous precursor selection for tandem mass tag-based quantification

Besides the labeling efficiency, accurate ratio determination is highly important in TMT-based relative quantification. The isobaric nature of TMT reagents allows multiplexed analysis, thus the digests of different conditions and/or replicates (with the chemicals used in this work up to N=10 samples) can be combined after labeling and the further sample preparation (e.g. enrichment and fractionation) as well as measurement procedures can be performed for a

single sample, without adding further technical variation. In general, multiplexing offers reduced total analysis time, increased robustness and reproducibility of the analysis, and importantly generally avoids the issue of missing values in quantitative datasets, as for each peptide quantitative values will be obtained for all used channels [82]. However, it was demonstrated that the accuracy of quantitative analysis from such experiments is diminished as contaminating near isobaric precursor ions are co-isolated and co-fragmented together with the target ions, thus affecting reporter ion intensities [60, 83]. In complex peptide mixtures, where only a small fraction of the peptides shows significant changes, the interference effect causes an underestimation of these changes (also called ratio compression), thus shifting the ratios towards the more abundant peptides with stable ratios, i.e. towards a ratio of 1.0. The analytical approaches applied for the solutions of this issue are mostly prefractionation to reduce sample complexity, the application of a narrow IW (e.g. 0.4 *m/z*) for MS/MS, and/or inclusion of an additional fragmentation event (MS^3 scan) [60, 83]. Here MS^3 analysis in synchronous precursor selection (SPS) mode was tested in comparison to MS/MS (IW 0.4 *m/z*) on an Orbitrap Fusion Lumos for relative quantification of Cys peptides in a complex matrix of background proteome. A sample with significantly downregulated free Cys was generated by treatment of the HeLa lysate with oxidizing agent (H_2O_2) and comparing the levels of free Cys to untreated controls. For comparison of MS/MS and SPS the relative quantification of carbamidomethylated (CAM) free Cys peptides was preferred to oxidized Cys, as the Cys oxidation products are diverse complicating their quantitative analysis. Exactly the same sample (from a single vial) was measured by MS/MS and SPS with N=3 measurement replicates, each. As shown in Table 3.8, the number of identified proteins, total peptides, and CAM peptides were higher after MS/MS measurement, whereas the number of significantly downregulated CAM peptides was higher by SPS. This result demonstrates that although MS/MS is more sensitive and can identify higher number of peptides, less regulated peptides are detected by MS/MS due to ratio compression. Even though SPS identified less CAM peptides (1520 vs 2094) more of them were significantly downregulated (203 vs 77). After normalizing the number of downregulated CAM peptides to the number of total CAM peptides detected by each method, SPS outperforms MS/MS by ~ 3-fold (Table 3.8).

Table 3.8 Average (N=3 measurements) numbers of proteins, peptides, CAM peptides and significantly downregulated (≥ 2-fold, analysis of variance (ANOVA) p-value ≤ 0.05) CAM peptides identified by SPS or MS/MS.

Method	***Proteins***	***Peptides***	***CAM peptides***	***Downregulated CAM peptides***	***Downregulated CAM peptides/total CAM peptides***
SPS	1937 (± 135)	11243 (± 780)	1520 (± 105)	203 (± 14)	0.13 (± 0.009)
MS/MS	2637 (± 184)	16137 (± 1112)	2094 (± 125)	77 (± 6)	0.04 (± 0.0028)

Additionally, the pairwise comparison of the fold changes of significanly downregulated (Figure 3.10) CAM peptides quantified by both MS/MS and SPS demonstrates that, besides the higher number of regulated peptides detected by SPS, the ratios are improved as well.

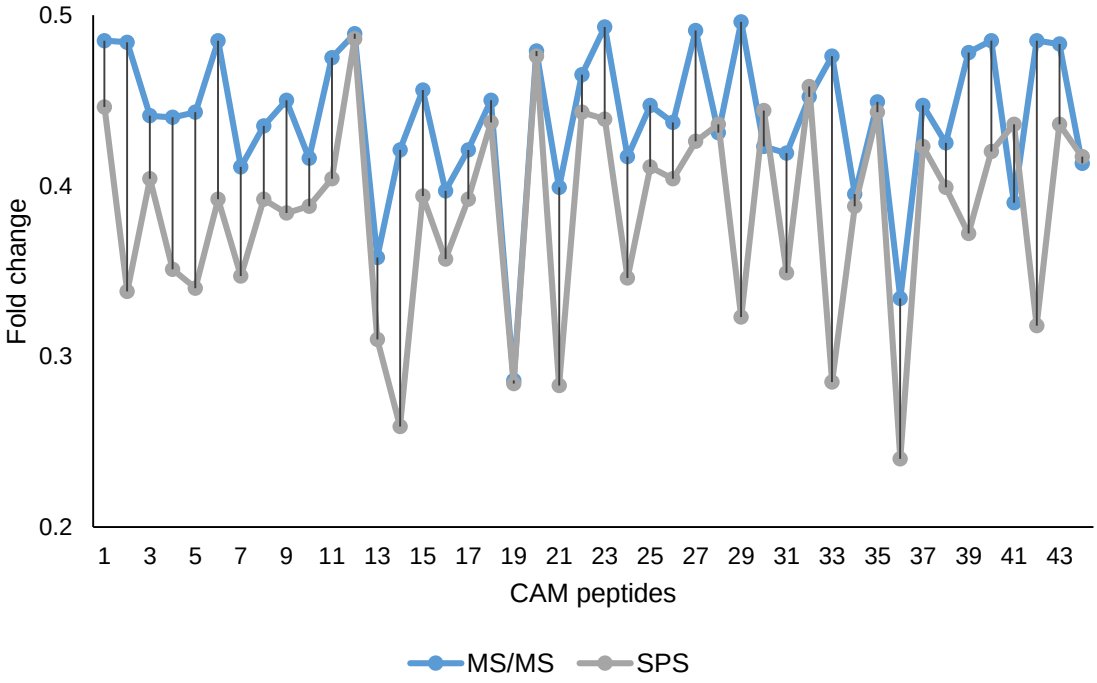

Figure 3.10 The pairwise comparison of the fold changes of significanly downregulated (≥ 2-fold, p-value ≤ 0.05) CAM peptides quantified by both MS/MS and SPS.

Conclusively, SPS results in more accurate TMT-based quantification, thus is more suited for the TMT-based analysis of endogenous PTM levels that generally are of low abundance and

may show only minor changes after short term stimulation of cells (e.g. in this thesis, the 5 min NO-donor treatment of SH-SY5Y cells).

3.5 Optimization of the S-Nitrosylation switch technique

ST is a non-direct method for SNO detection, where the modified Cys is reversed to its free form before the analysis. In this context ensuring complete blocking of all free Cys in the initial step of the ST is imperative to exclude the presence of free Cys prior to sodium ascorbate reduction [37, 63, 84], leading to false positive identification of SNO sites. In order to assure the completeness of free Cys blocking, the minimum amount of the blocking reagent required for total free Cys labeling in HeLa lysate was defined by applying increasing concentrations (5 mM, 25 mM, 50 mM or 100 mM) of IAA-alkyne, followed by SDS-PAGE and fluorescence detection (Figure 3.11a). The flourescence signal was normalized to protein abundance (Coomassie staining, Supplementary Figure 2) in each lane. Weak signals are detected in the lanes where 5 mM IAA-alkyne blocking was applied. The signals become more saturated as the concentration of IAA-alkyne increases and an only 4.6 % increase in signal is detected in the 100 mM compared to 50 mM IAA-alkyne labeled samples, indicating saturation of labeling at 100 mM (Figure 3.11b). This result demonstrates that 100 mM of blocking reagent is sufficient for total free Cys labeling.

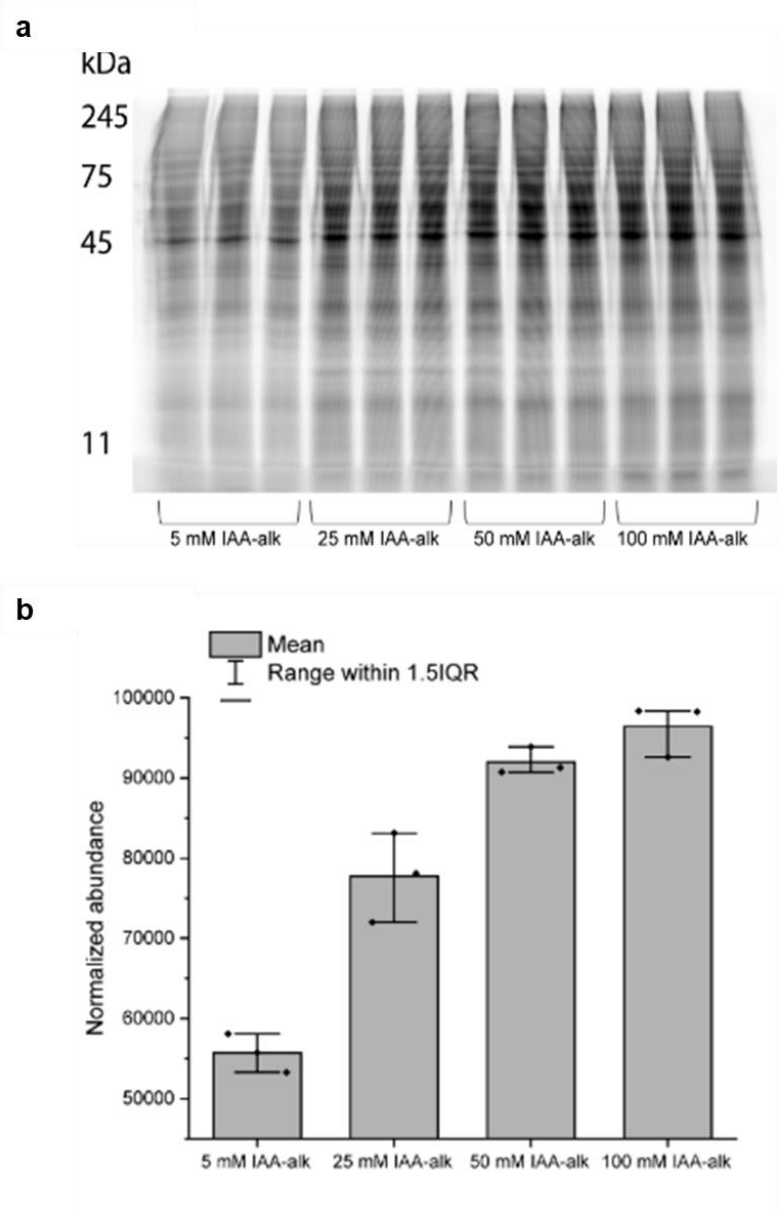

Figure 3.11 Total free Cys labeling with increasing concentrations of IAA-alkyne. (a) Fluorescence detection of the HeLa lysates separated by SDS-PAGE. (b) The fluorescence signal (normalized to protein abundance (Coomassie staining)) shows on average a 4.6 % increase in 100 mM compared to 50 mM IAA-alkyne labeled samples. Error bars represent the data range within 1.5 the interquartile range (IQR) [27].*

Another commonly used strategy to demonstrate the specificity of the ST is using the control without the addition of sodium ascorbate (-asc). After the blocking of free Cys with 100 mM iodoacetamide (IAA) SNO reduction conditions: 1) +asc, 2) exposure to UV, and 3) -asc (control), were tested in GSNO-treated HeLa lysates. After the reduction the SNO peptides were labeled with IAA-alkyne and enriched using the Dde-biotin-azide linker. The amount of

switched SNO peptides was relatively quantified in each sample based on the TMT reporter ion intensity signal/noise ratio (S/N). Boxplots (Figure 3.12) of S/N of 7575 SNO PSMs considered for quantification (average reporter S/N threshold ≥ 10, without CAM on Cys and oxidation on Met) show comparable S/N for +asc and UV reduction. The mean S/N of the -asc samples (N=3) is 2.6, the median is 0.56 (center line), with an average of 7.2 % of PSMs having S/N ≥ 10. Accordingly, the -asc control indicates the near completeness of the first blocking step using 100 mM IAA. The weak remaining signals in the -asc samples, mostly below the limit of quantification (LOQ S/N ≥ 10), can be most likely attributed to the SNO reduction by negligible exposure to light.

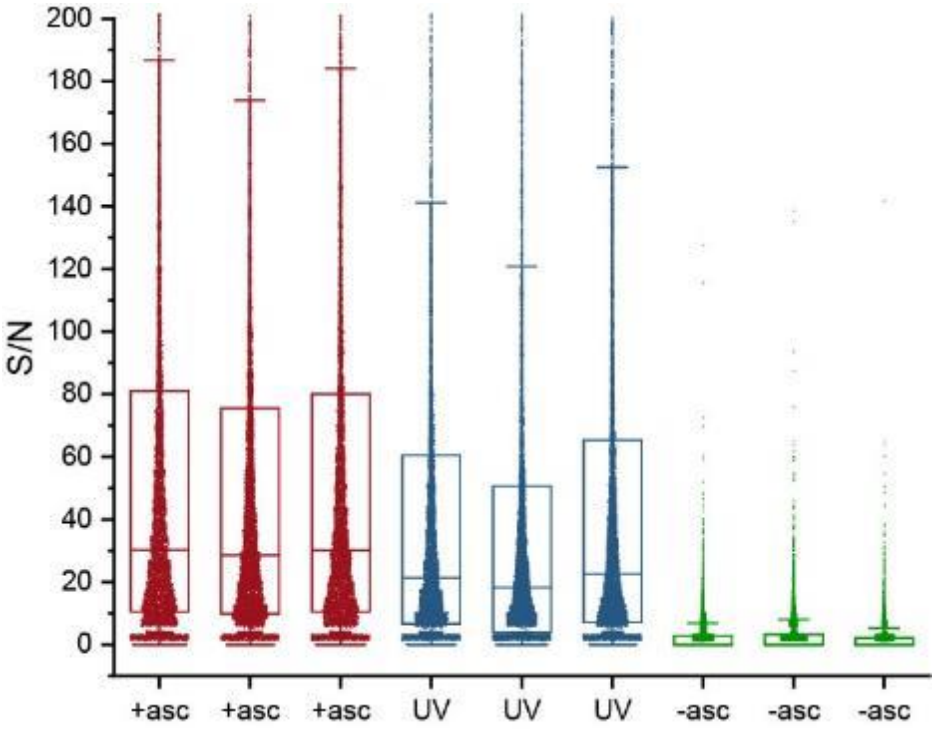

*Figure 3.12 ST specificity test. Relative quantification of the enriched SNO peptides applying ST with +asc, UV and -asc (control) for SNO reduction in GSNO-treated HeLa lysates after the blocking of free Cys with 100 mM IAA. Box limits are the 75 and 25% percentiles, i.e. the IQR; the whiskers correspond to the highest or lowest respective value or if the lowest or highest value is an outlier (greater than 1.5 * IQR from the bounds of the boxes) it is exactly 1.5 * IQR [27].*

In order to overcome the drawback of the possible reduction of SNO by exposure to ambient light when -asc is used as control for evaluating ST specificity, an alternative control experiment was applied. Thus, after the initial blocking step of free Cys with 25 mM, 50 mM, or 100 mM IAA, the excess of the IAA was removed, and a second labeling step with IAA-

alkyne was applied in SH-SY5Y cell lysates. The IAA-alkyne labeled peptides (Cys peptides remaining free after the blocking) were enriched using the Dde-biotin-azide linker. The amount of the remaining free Cys after IAA blocking was relatively quantified in each sample based on the TMT reporter ion intensities (S/N). Boxplots (Figure 3.13) of S/N of 2521 PSMs considered for quantification (average reporter S/N threshold ≥ 10, without CAM on Cys and oxidation on Met) show drastic reduction of remaining free Cys after 50 mM and 100 mM IAA blocking compared to 25 mM. The mean S/N is 6.3 and 0.4, the median (center line) is 0.9 and 0, with on average 15 % and 1% of PSMs having S/N ≥ 10 in 50 mM and 100 mM IAA blocked samples respectively. Hence, confirming the completeness of the free Cys blocking with100 mM IAA.

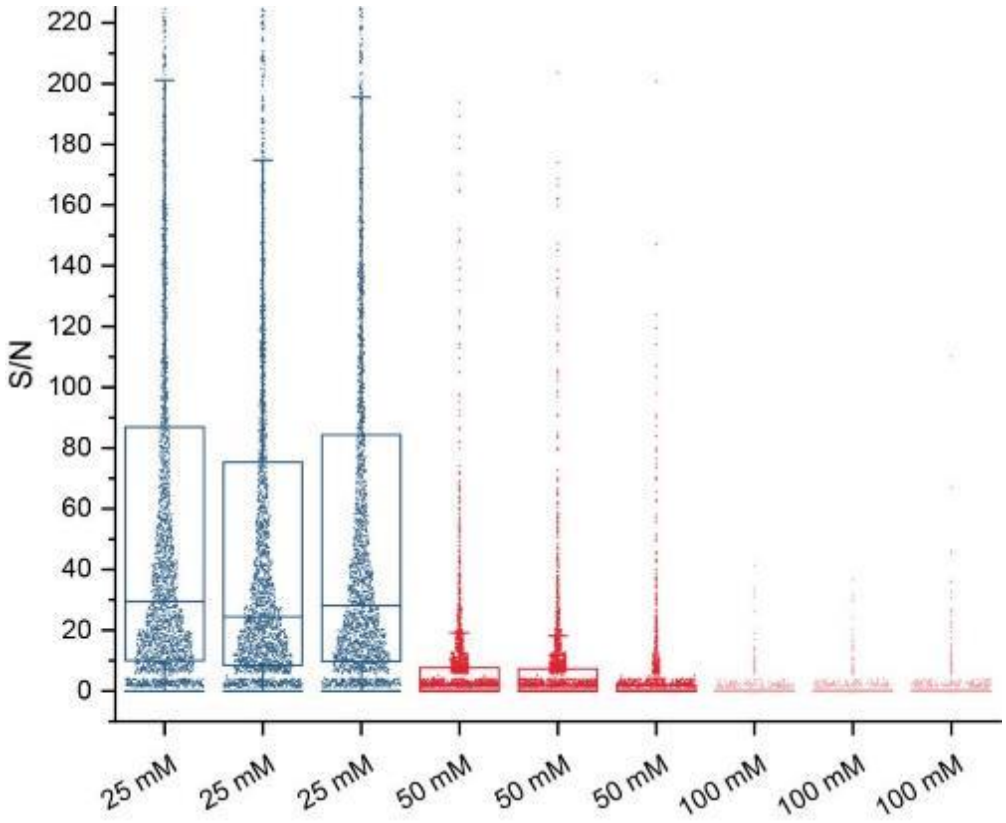

*Figure 3.13 Analysis of completeness of IAA blocking of free Cys in the initial step of the ST. In SH-SY5Y cell lysates the amounts of the remaining free Cys after 25 mM, 50 mM and 100 mM IAA blocking were relatively quantified. Box limits are the 75 and 25% percentiles, i.e. the IQR; the whiskers correspond to the highest or lowest respective value or if the lowest or highest value is an outlier (greater than 1.5 * IQR from the bounds of the boxes) it is exactly 1.5 * IQR [27].*

In conclusion, three independent experiments performed using orthogonal strategies (-asc as a control and increasing concentration of a blocking reagent) for two different cell lines (HeLa and SH-SY5Y) show the completeness of free Cys blocking in the initial step of the ST with 100 mM IAA or IAA-alkyne.

3.6 S-nitrosylation analysis using Cys-BOOST

After the development of biorthogonal cleavable-linker-based enrichment of Cys peptides it was combined with ST and TMT labeling for quantitative analysis of SNO. The method was termed analysis of nitrosylated Cys using bioorthogonal cleavable-linker and switch technique, short Cys-BOOST. It incorporates the following steps: 1) irreversible blocking of all free thiols with IAA, 2) specific reduction of SNO by sodium ascorbate and labeling with IAA-alkyne, 3) reduction and alkylation of the remaining oxidized Cys (e.g. mixed disulfides), 4) protein digestion with trypsin, 5) TMT labeling for multiplexed quantitative analysis, 6) conjugation of the Dde-biotin-azide linker to IAA-alkyne labeled peptides via CuAAC, 7) affinity binding of the Cys peptides to streptavidin beads via the biotin group of the Dde-biotin-azide linker, 8) release of the target peptides with 2 % hydrazine by single step, mild chemical cleavage of the Dde bond, 9) on-tip pH 10 fractionation of the eluate before 10) LC-MS/MS analysis. The workflow is summarized as schematic in Figure 3.14 for SNO analysis in untreated and GSNO-treated HeLa lysates.

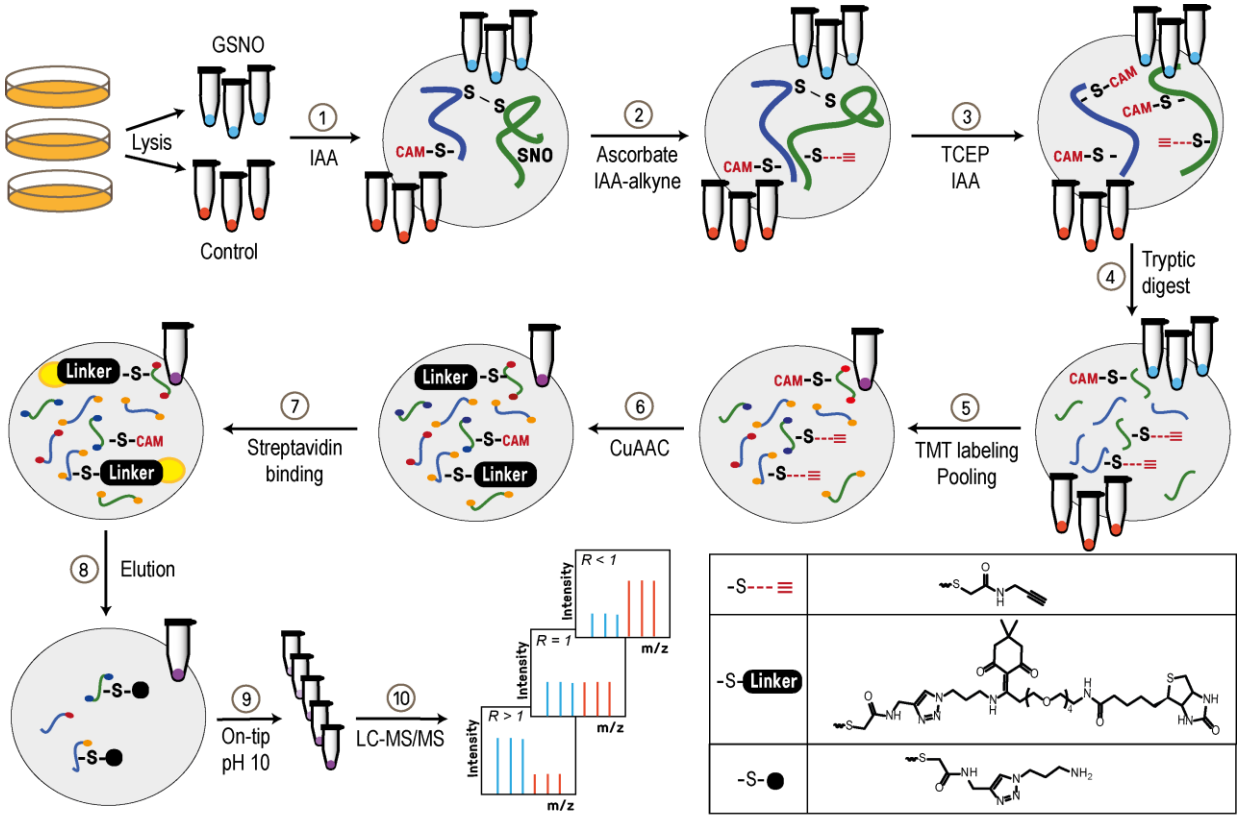

Figure 3.14 Schematic representation of Cys-BOOST workflow exemplified for SNO analysis of untreated (N=3) and GSNO-treated (N=3) HeLa cell extracts [27].

In addition to the given example, Cys-BOOST can also be applied for the analysis of other oxidative Cys PTMs or general Cys oxidation, by using different reducing agents (e.g. sodium arsenite for Cys-sulfenylation or TCEP for general Cys oxidation) at step 2 of the workflow.

3.7 Comparison of Cys-BOOST and iodoTMT

Before applying Cys-BOOST for SNO analysis, its specificity, sensitivity and technical reproducibility were tested in comparison to iodoTMT-based enrichment in order to demonstrate the improvements obtained by the workflow developed in this thesis in comparison to one of the gold standards in the field. For this purpose, the total Cys peptides captured from HeLa cell lysate by both methods were analyzed (Figure 3.15). Thus, all oxidized Cys were reduced with TCEP, the lysate was divided into 6 aliquots, and all free Cys (freshly reduced and initially free) were alkylated by IAA-alkyne (N=3) and iodoTMT (N=3), respectively. Next, proteins were digested with trypsin. For Cys-BOOST, peptides from the three IAA-alkyne aliquots were labeled with three different TMT-10plex labels, to enable

quantification based on the TMT reporter ion intensities. This is intrinsically possible for iodoTMT. In the Cys-BOOST protocol the Cys peptides were enriched using the Dde-biotin-azide linker followed by chemical elution via cleavage of the Dde bond. IodoTMT labeled peptides were enriched via the anti-TMT antibody, followed by elution at acidic pH. Importantly, both the Cys-BOOST and the iodoTMT aliquots were only multiplexed after the enrichment, thus allowing the assessment of the technical variation for both workflows. The mutliplexed Cys-BOOST and iodoTMT samples were then fractionated by on-tip pH 10 RP SPE, to reduce the complexity prior to LC-MS/MS (Figure 3.15a). Using iodoTMT-based enrichment 9966 Cys peptides and 3446 background peptides were identified, corresponding to an enrichment specificity of 74% (Figure 3.15b). In contrast, using Cys-BOOST with the same samples, we identified 25,019 Cys peptides and only 581 background peptides, which corresponds to a specificity of 98% and a concurrent 2.5-fold increase in the number of Cys peptides (Figure 3.15c). Notably, the technical reproducibility of the enrichment for both methods was assessed by comparing TMT reporter ion intensities across the triplicates, thus obtaining RSDs of 9 % and 36 % for Cys-BOOST and iodoTMT, respectively. Although the number of quantified peptides is 2.5 × higher for Cys-BOOST, the boxplots of the scaled TMT reporter intensities (abundances) of all quantified Cys containing peptides show a much narrower distribution and more reproducible mean values for Cys-BOOST than for iodoTMT (Figure 3.15d). In general, Cys-BOOST displays excellent technical reproducibility, which opens the possibility to use it for complex studies by combining multiple TMT sets with a common normalizer-channel present in each set. The average scaled TMT reporter intensities (sum of all TMT reporter intensities of Cys containing PSMs/number of Cys containing PSMs) was compared for of all Cys containing PSMs quantified by either Cys-BOOST or iodoTMT (Figure 3.15e). Despite the higher number of Cys peptides for Cys-BOOST which may come along with the identification of many low abundant peptides, the average scaled TMT intensity observed for Cys-BOOST was around 4 times higher. This indicates a considerably higher recovery, which comes along with more precise quantification. Consequently, even with the very stringent criteria (FDR ≤ 1%, reporter ion co-isolation threshold ≤ 20, average reporter S/N ≥ 10) applied for data analysis, Cys-BOOST allowed the quantification of 60 Cys peptides per µg of HeLa lysate (compared to 24 for iodoTMT) which makes it the most sensitive method for analyzing Cys peptides to date (Figure 3.15f). In conclusion, these results demonstrate the superior performance of Cys-BOOST compared to iodoTMT and reinforce Cys-BOOST as an effective analytical strategy for Cys peptide analysis.

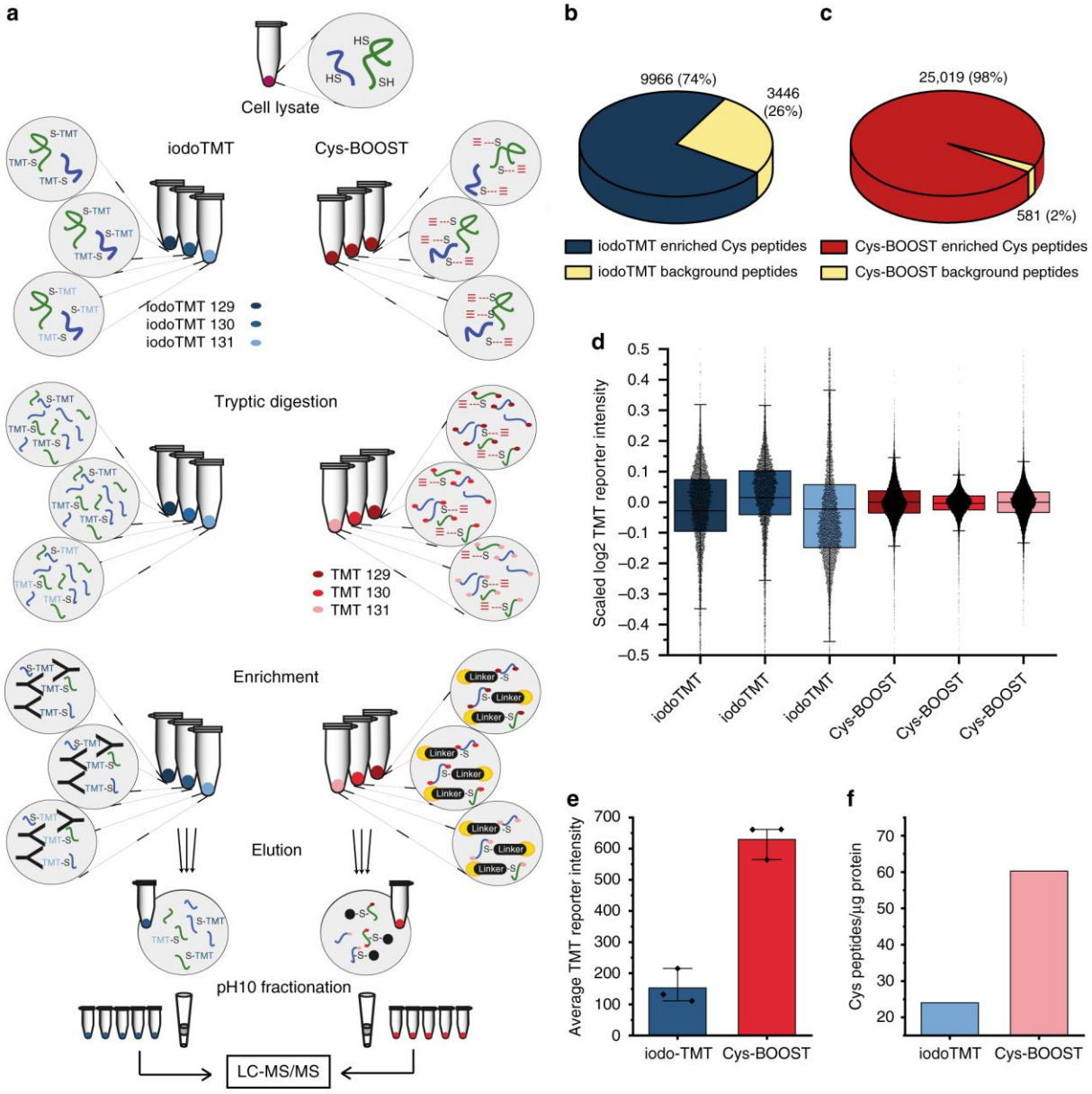

Figure 3.15 Total Cys analysis by iodoTMT and Cys-BOOST. (a) Comparison of iodoTMT and Cys-BOOST workflows for total Cys peptides analysis from 100 µg of HeLa lysate per replicate. (b, c) Pie charts showing the share of the target (Cys containing) and background peptides for iodoTMT and Cys-BOOST. (d) Boxplots of scaled log_2 TMT reporter intensities of all quantified Cys containing peptides display a substantially more accurate and precise quantification for Cys-BOOST as compared to iodoTMT (center line: mean; box limits: upper and lower quartiles; whiskers: correspond to the highest or lowest respective value or if the lowest or highest value is an outlier it is 1.5 IQR). (e) Average TMT reporter intensities of Cys containing PSMs (error bars show the minimum and maximum of N=3 replicates) indicate a higher recovery for Cys-BOOST. (f) Number of Cys containing peptides quantified per µg of HeLa lysate [27].*

3.8 S-Nitrosylation analysis in GSNO-treated and control HeLa extracts

After demonstrating that Cys-BOOST allows highly efficient qualitative and quantitative analysis of total Cys peptides, it was applied for the analysis of one of the more challenging Cys PTMs: SNO. Considering the vast biological significance of SNO [17, 37, 85] and its well-established specific reduction by ascorbate [63, 84], the analysis of SNO was chosen as a prominent example to demonstrate the potential of Cys-BOOST for the proteome-wide quantitative analysis of Cys oxidative PTMs with high sensitivity and high precision. SNO analysis was performed for untreated (N=3) and *in-vitro* GSNO-stimulated (N=3) HeLa cell extracts. SNO peptides were reduced by sodium ascorbate and switched with IAA-alkyne. The following steps were performed according to the Cys-BOOST workflow (Figure 3.14). After TMT labeling the untreated and GSNO-treated samples were pooled, and the enrichment was performed for a single multiplexed sample. The eluate was then fractionated by on-tip RP at pH 10, and analyzed by LC-MS/MS.

As a result, Cys-BOOST enabled the proteome-wide discovery of SNO targets and consensus motifs. 3632 SNO proteins with 9314 SNO peptides and 8304 unique SNO sites were identified, out of which 6247 SNO peptides were confidently quantified (FDR ≤ 1%, ptmRS SNO site localization probabilities ≥ 99%, reporter ion co-isolation threshold ≤ 20, average reporter S/N ≥ 10). Mapping the identified SNO proteins to the HeLa proteome based on the normalized abundance factors (NSAF) [86], showed that the SNO proteome covers the whole dynamic range of the HeLa proteome (Figure 3.16).

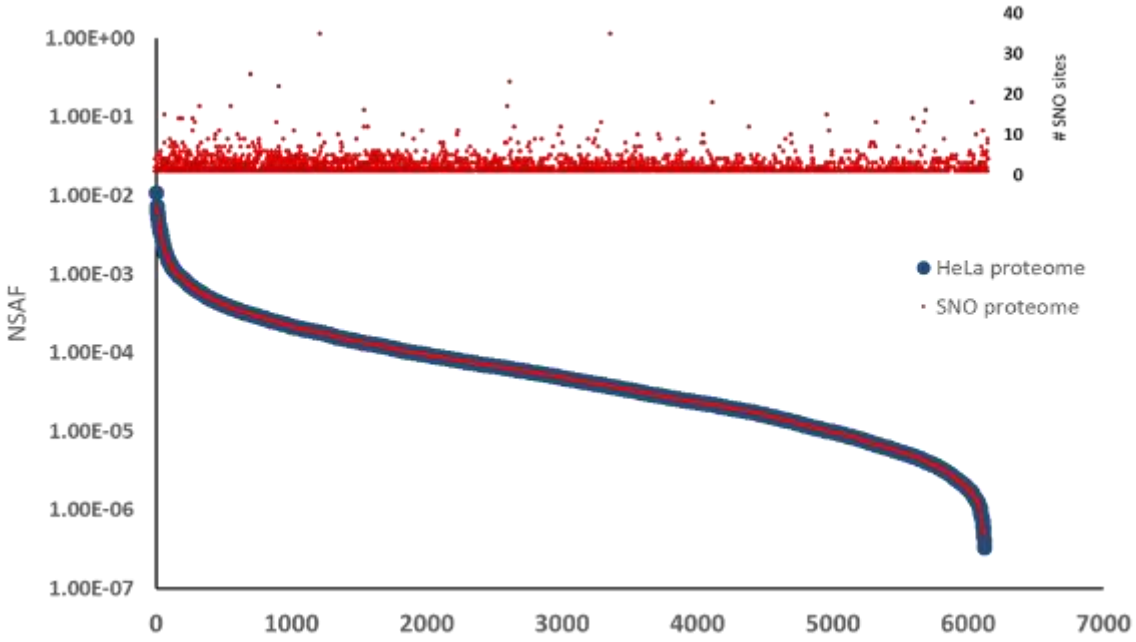

Figure 3.16 Good coverage of the HeLa SNO proteome. Proteome dynamic range represented by NSAF values (blue): Only proteins with at least 1 unique peptide (1% protein false discovery rate) were considered and ordered in descending abundance, as represented by descending NSAF values, corresponding to 6120 HeLa proteins. SNO proteome (red): The NSAF values for proteins with quantified high confidence SNO sites are shown as red dots, corresponding to 3007 HeLa SNO proteins. Top: for each of the identified SNO proteins the number of detected SNO sites is given, indicating that even for proteins of low abundance multiple SNO sites could be identified [27].

Next, consensus motifs for Cys sites having differential reactivity to GSNO were identified for three distinct groups defined by their $R_{[GSNO]:[Control]}$ ratios (Figure 3.17, Supplementary Table 1). SNO sites showing downregulation and no significant changes after GSNO treatment ($R \leq 1.5$) were considered as GSNO non-reactive and they correspond to endogenous SNO. The decreased SNO levels might be explained by reduction or exchange of endogenous SNO for instance by free glutathione, after its NO was transferred to another Cys. SNO sites with $1.5 < R < 6$ (p-value ≤ 0.05) were considered as GSNO mild-reactive. SNO sites with $R \geq 6$ (p-value ≤ 0.05) were considered as GSNO hyper-reactive (p-values defined by ANOVA). From 480 mappable GSNO non-reactive sites 362 (75 %) were matched by motif-x [87] to one of the motifs in Figure 3.17a. The high percentage of SNO sites matching to the motifs demonstrates that the motifs are highly representative for the GSNO non-reactive group. These motifs are dominated by the presence of hydrophobic amino acids leucine (Leu; L), isoleucine (Ile; I), valine (Val; V) and aromatic phenylalanine (Phe; F), particularly the position

– 4 (4 amino acids N-terminal of the Cys) proves to be significant. From 1894 mappable GSNO mild-reactive sites, 283 (15 %) were matched to two motifs, both containing lysine (Lys; K) either at the position + 6 or - 6 from the SNO site (Figure 3.17b). From 3446 mappable GSNO hyper-reactive sites, 2826 (82 %) were matched to one of the motifs presented in Figure 3.17c. Again, these motifs are highly representative for GSNO hyper-reactive group. Interestingly, 19 of 20 motifs defined for hyper-GSNO reactive SNO sites contain at least one of the two acidic amino acids, aspartate (Asp; D) and glutamate (Glu; E). Moreover, at the positions ± 3 and ± 4 both Asp and Glu containing versions of the motifs were individually found by motif-x (Figure 3.17c).

The presence of the flanking acidic amino acids in the majority of motifs defined for GSNO hyper-reactive sites might be explained by indirect acid-base catalysis, based on the favorable positioning of the NO group via hydrogen bonding between γ-glutamyl amine of GSNO and the γ-carboxylate of Glu or β-carboxylate of Asp, as illustrated for Cys 199 of OxyR [18]. The occurrence of the Asp at the position + 3 from the active Cys 199 allows positioning of the NO group of GSNO within ~ 4 Å of the Cys 199 free thiol, thus assisting the NO^+ transfer [18]. In this thesis, the prominent motifs with Asp or Glu at ± 3 and ± 4 positions from the hyper-reactive SNO sites suggest proteome-wide occurrence of this principle. Occurrence of Asp or Glu in 3 or 4 amino acids distance from SNO sites is in agreement with former studies of SNO motifs based on smaller subset of proteins [26, 88, 89]. For the motifs with Asp or Glu at positions ± 1 and ± 2 the influence might be explained by direct acid–base catalysis of nitrosylation/denitrosylation [17, 90-92]. Under physiological pH the deprotonated carboxyl group of Glu or Asp within ~ 6 Å (~ 2 amino acids) from the free Cys might act as a base, withdrawing the proton of the thiol and facilitating nucleophilic thiolate formation. Alternatively, the presence of the carboxyl group of Glu or Asp in the intermediate vicinity of the nitrosyaltion target free Cys might facilitate the protonation of GSNO and consequently promote the donation of its NO group, as demonstrated for methionine adenosyltransferase by Perez-Mato *et al.* [90]. Next, two motifs for GSNO mild-reactive SNO sites were identified, both possessing Lys at ± 6 position from the SNO site. These Lys motifs were recently identified also by Smith *et al*. in SNO analysis of nuclear extracts from rat cortical neurons [93]. The presence of the basic amino acid Lys within ~ 6 Å will enhance the nucleophilicity of the thiol group, thus making the Cys more susceptible to nitrosylation and oxidation in general. However, this mechanism would be possible only within a framework of certain structural conformations that position the Lys closer to the Cys, whereas the theoretical linear distance (calculated using 3.5 Å as amino acid average length) of the ± 6 Lys would be ~ 20 Å.

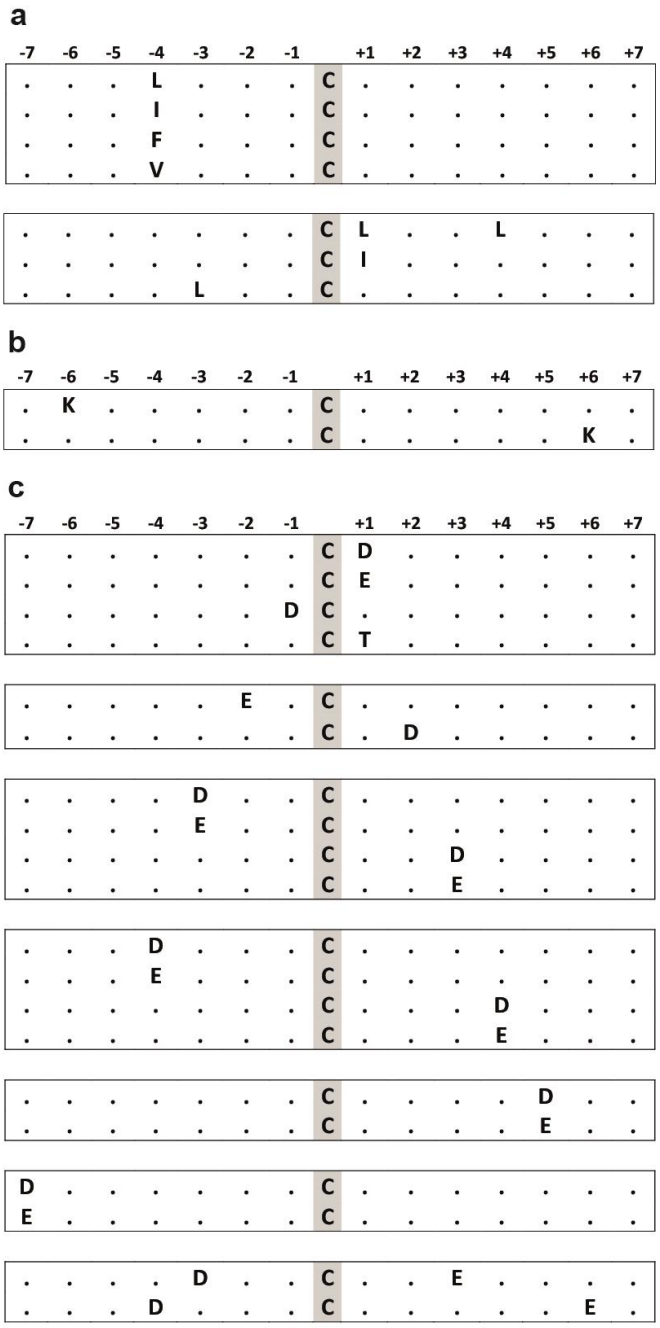

Figure 3.17 SNO consensus motifs identified by motif-x v1.2. Significance < 1 × 10^{-6}, fold increase ≥ 1.59. (a) Motifs for GSNO non-reactive (R ≤ 1.5), (b) GSNO mild-reactive (1.5 < R < 6; ANOVA p-value ≤ 0.05), and (c) GSNO hyper-reactive (R ≥ 6; ANOVA p-value ≤ 0.05) SNO sites [27].

The combined knowledge of SNO motifs containing characteristic acidic amino acid or basic Lys allows the discussion of the model of nitrosylation via indirect acid-base catalysis not only for GSNO, but also for transnitrosylases. Here, the indirect acid-base catalysis could be

accomplished by favorable positioning of the SNO group of the NO^+ donor protein and the free thiol of the acceptor protein. By assistance of hydrogen bonding between the side chain ε-amino group of ± 6 Lys and the side chain carboxylate of the ± 3, ± 4, + 5 or - 7 acidic amino acid, the SNO could be placed in an appropriate distance (~ 4 Å) for transnitrosylation. It should be noticed that the proteins having one of these motifs could act both as NO donor and acceptor, in agreement with the dual function of transnitrosylases. SNO sites with the ± 6 Lys motif might be putative targets of transnitrosylation rather than being directly nitrosylated by GSNO, which could explain their presence in the GSNO mild-reactive group.

Apparently, the mechanism of the acid-base assisted nitrosylation/transnitrosylation/de-nitrosylation is dependent on the proximity and structural arrangement of the flanking acidic and basic amino acids to target thiol. On the one hand the acidic/basic residues located in direct proximity (~ 6 Å) of the Cys might increase its nucleophilicty or facilitate the NO release from GSNO or transnitrosylases; on the other hand, the acidic/basic residues located ~ 7 - 20 Å away from the Cys might catalyze the SNO formation indirectly, via favorable positioning of the NO group of either GSNO or transnitrosylases.

The GSNO non-reactive sites identified by Cys-BOOST should represent the more stable naturally occurring SNO. As evidenced by the consensus motifs of this group, the SNO is shielded by flanking hydrophobic amino acids. The enrichment of hydrophobic amino acids in the motifs of GSNO non-reactive sites might indicate SNO formation by NO directly or by auto-oxidation products of NO (e.g. NO_2, N_2O_3). Several arguments support the relevance of the protein local hydrophobicity for endogenous SNO and SNO formed by NO directly [17, 18, 74, 94]. Primarily the restricted access of hydrophilic reductants and low molecular weight thiols in hydrophobic milieu inhibits the de-nitrosylation [18]. Next, the hydrolysis of NO auto-oxidation products is inhibited and the intermediate radical species (e.g. $NO^{\bullet}$, $RSNO^{\bullet -}$) are stabilized in the presence of hydrophobic residues [18, 95]. The statement is also supported by endogenous SNO sites found in the juxtamembrane region [72, 96]. The decrease of SNO levels of certain Cys in this group might be a consequence of NO transfer to free glutathione or other free thiols.

The identification of distinct sequence motifs for these three classes demonstrates the appropriateness of the initial grouping. Nevertheless, when discussing SNO motifs the transient nature of SNO should be taken into the account. Indeed, SNO formed via *in-vitro* treatment with GSNO might be exchanged with free thiols and other Cys PTMs. In addition, SNO proteins may act as transnitrosylases and nitrosylate Cys targets that are not susceptible to nitrosylation by GSNO.

A STRING network analysis of the proteins possessing either significantly downregulated (Figure 3.18) or the 500 strongest upregulated (Figure 3.19) SNO sites illustrates the association of SNO to stress response, ubiquitin mediated proteolysis, translation, splicing, DNA replication, GTPase mediated signaling and vesicle mediated transport pathways.

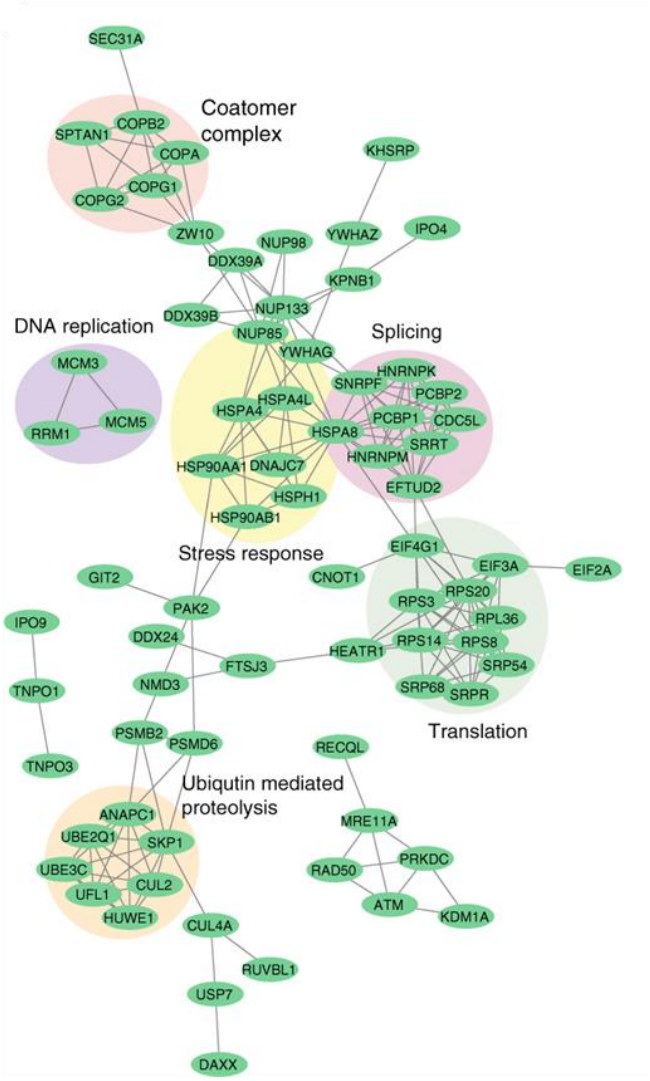

Figure 3.18 The STRING network of proteins with significantly downregulated SNO sites after GSNO treatment of HeLa extracts. The network indicates the role of SNO in splicing, translation, ubiquitin mediated proteolysis, DNA replication, cellular response to heat stress, vesicle mediated transport (coatomer complex) [27].

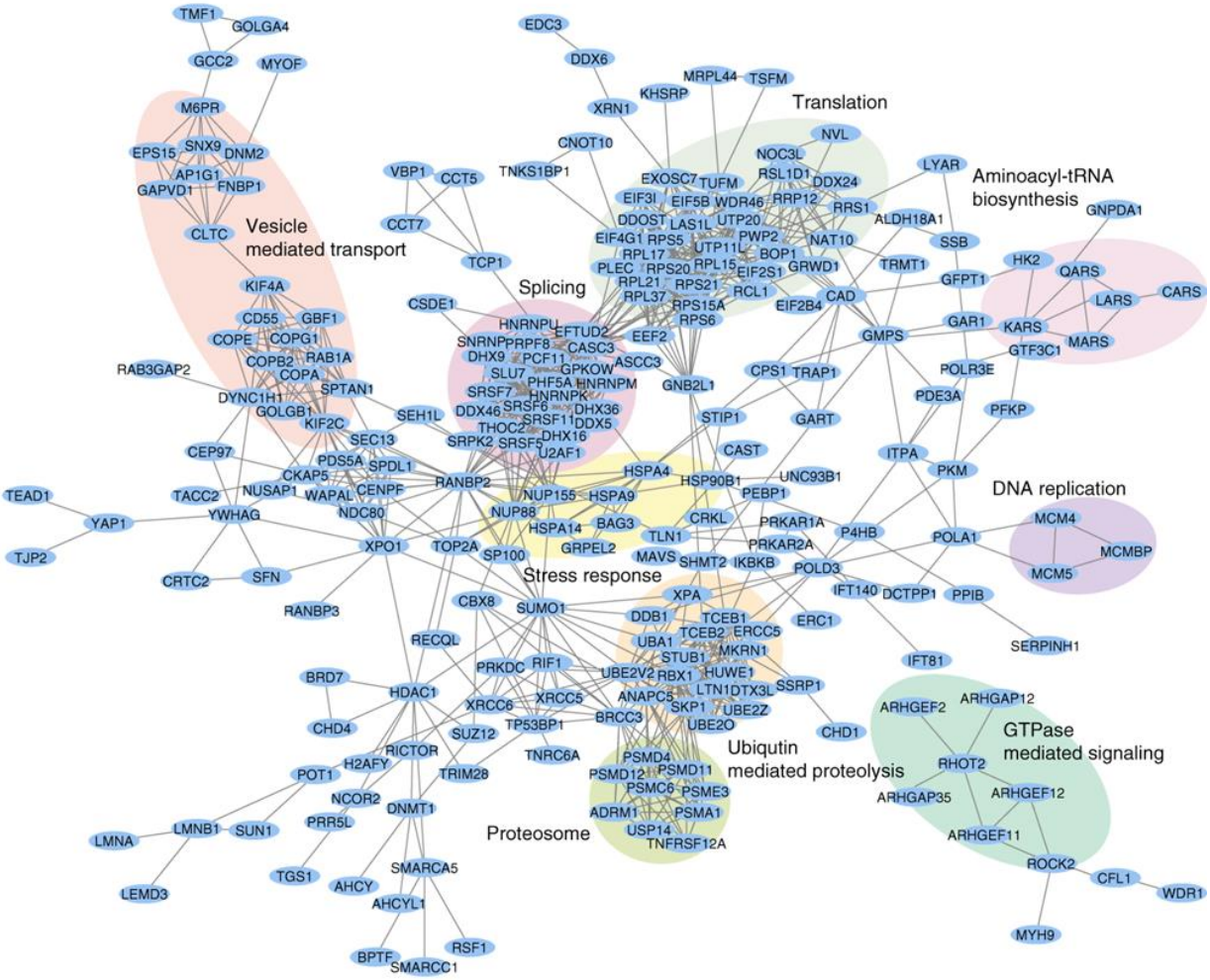

Figure 3.19 The STRING network of the 500 proteins with the strongest upregulated SNO sites after GSNO treatment of HeLa extracts. The network indicates the role of SNO in splicing, translation, ubiquitin mediated proteolysis, DNA replication, cellular response to heat stress, vesicle mediated transport, GTPase mediated signaling and aminoacyl-tRNA biosynthesis pathways [27].

Heat shock proteins HSP90-alpha, HSP90-beta, HSPA8, HSPA4, HSPA4L, HSPA14, HSPH1, mitochondrial HSPD1 and HSPA9 were identified with multiple SNO sites. Remarkably, different (even adjacent) Cys sites of the same protein had highly varying levels of SNO, as depicted for of HSP90-alpha (Figure 3.20a), which is known for its NOS regulatory activity [97]. Here, the SNO level of Cys 420 was 5-fold decreased while the SNO level of Cys 374 was 14-fold increased. Furthermore Cys 597 and Cys 589 from the C-terminal domains of HSP90-alpha and HSP90-beta, respectively, were identified as endogenously nitrosylated (GSNO non-reactive), whereas the adjacent Cys were detected as free in agreement with former studies [97, 98]. Besides, 4 novel SNO sites on HSP90-alpha and 3 novel sites on

HSP90-beta were identified. The SNO level of Cys 310, which is located in a structurally similar region of HSPA4, HSPA4L and HSPH1 was significantly decreased in all three proteins (Figure 3.20a).

SNO seems to make a considerable contribution to the regulation of the ubiquitin–proteasome system. In total, 44 E3 ubiquitin-protein ligases, as well as multiple proteasome subunits were identified as SNO targets. SNO sites on the Cys proteases: caspase 1 (Cys 136), 2 (Cys 343), 3 (Cys 170) and 4 (Cys 109), were found in the vicinity of the active sites, but active site Cys themselves were not identified as nitrosylated, pointing to SNO mediated allosteric regulation. Only caspase 8 was detected with multiple SNO sites (Cys 164, 203, 360, 426) including the active site Cys 360. Allosteric regulation could also explain the SNO sites on 86 phosphatases and phosphatase subunits detected by Cys-BOOST.

Nucleic acid binding is one of the most prominent molecular functions matched by STRING for the SNO proteins, indicating the important role of SNO in transcription and translation. Indeed, 43 RNA and 4 DNA helicases were found to be nitrosylated. Taking into the account that the human genome encodes for only 64 non-redundant RNA helicases there is a substantial enrichment. SNO levels of Cys 198 of spliceosome RNA helicase DDX39B ($HFILDEC_{198}DKMLEQ$) and Cys 197 of ATP-dependent RNA helicase DDX39A ($HFVLDEC_{197}DKMLEQ$) located at structurally similar regions, inside the conserved DECD motif, were found significantly decreased in both proteins (R = 0.2 and R = 0.3 respectively).

Interestingly, STRING networks of proteins with both significantly downregulated and upregulated SNO levels show an enrichment of coatomer protein complex subunits and other proteins involved in vesicle mediated transport (more pronounced for upregulated sites), which is in agreement with formerly detected regulation of exocytosis by SNO [99, 100].

From proteins involved in DNA replication, minichromosome maintenance proteins (MCMs) appear to be more susceptible to SNO. Three of the four Cys present in the MCM domains of MCM2, MCM3, MCM5 and all four of MCM7 were detected as nitrosylated, with varying $R_{[GSNO]:[Control]}$.

Cys-BOOST detected multiple SNO proteins involved in redox regulation including thioredoxin, peroxiredoxin and glutaredoxin family proteins. Cys 62 and 69 of thioredoxin were identified as SNO, which is in agreement with X-ray crystallography analysis of the GSNO-treated protein [101]. Nitrosylated Cys 343 and 312 of another redox sensitive protein, protein disulfide-isomerase (PDIA1), are located in a noticeable distance from active sites Cys 53 and 56 which were not detected as nitrosylated themselves, again inferring a potential allosteric

regulation via SNO. Moreover, both Cys 342 and 312 are located in immediate structural proximity but display extremely varying SNO levels (Figure 3.20a).

Although the cells were not exposed to hypoxia, SNO sites were detected on several important hypoxia players. Two novel SNO sites were detected on hypoxia upregulated protein 1 (HYOU1). Cys 352 and 805 are surface exposed and are found in the small disordered regions between two alpha-helixes (Figure 3.20a). Both sites show no significant change after GSNO treatment, thus represent possible endogenous SNO targets. Additionally, Cys-BOOST identified SNO sites on hypoxia responsive transcriptional activators: Cys 404 of CREB binding protein (CBP), which is located at the CH1 domain, Cys 1621 and 1247 of p300, from which Cys1621 is located at the histone acetyltransferase domain (HAT). Another interesting target of nitrosylation represents Cys 169 of Cbp/p300-interacting transactivator 4 (CITED4) which has a C-terminal localization similar to Cys 800 of hypoxia inducible factor 1-alfa (HIF1α), a known SNO target (Figure 3.20b) [102]. All nine Cys of NOS-interacting protein (NOSIP) were identified, five of which as nitrosylated and the other four as free Cys (Figure 3.20c).

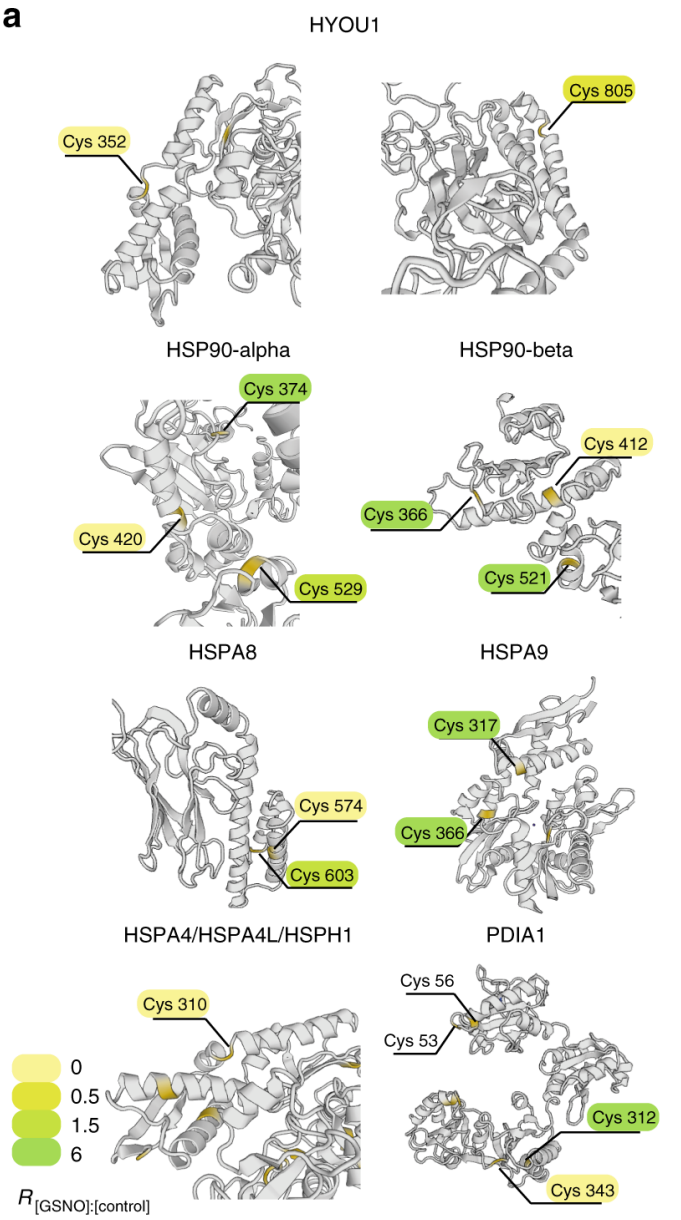

Figure 3.20 SNO proteins relevant in heat shock response and hypoxia. (a) Structures of HYOU1, heat shock proteins (HSP) and PDIA1 with highlighted SNO sites. The color gradient

of the highlighted background of Cys symbolizes the R $_{[GSNO]:[Control]}$ ratio. The yellow highlights on the protein structure correspond to the position of the Cys. Protein structures are obtained from SWISS-MODEL (https://swissmodel.expasy.org/). (b) SNO sites (red) of CITED4 (novel site detected by Cys-BOOST) and HIF1α (detected formerly) both located at C-terminals and putatively involved in activation of hypoxia-responsive genes. Cys 184 of CITED4 was detected as free. (c) All 9 Cys of NOSIP were identified from which 4 were free Cys (green) and 5 were nitrosylated (red)[27].

The protein network analyses underline the importance of SNO in cellular stress response. The role of SNO is recognized in several cellular stress events, particularly nitrosative and oxygen shock–related stress (hypoxia and oxidative stress) [103-105]. In this thesis an enrichment of regulated SNO sites was observed for translation, splicing, proteolytic degradation and vesicle mediated transport pathways, which are in line with the rapid adaption of the proteome through PTMs [106], while new mRNA is transcribed and processed [107]. The detected regulation of SNO sites on proteins involved in RNA binding might have several implications. The presence of SNO at the active site of proteins involved in translation (e.g. eukaryotic translation initiation factors (EIFs), ribosomal subunit proteins) may rapidly inactivate them, thus reducing the levels of global protein synthesis as a common result of a stress response. For instance, it is known that during hypoxia translational regulation is more widespread than transcriptional control [107]. Concurrently, the transcriptional modulation of selected proteins opposing the induced stress might be activated by nitrosylation/transnitrosylation of target transcription factors or coactivators. Examples of such regulatory targets might be represented by the novel SNO sites detected in this thesis on hypoxia relevant CBP (Cys 404), P300 (Cys 1247 and 1621) and CITED4 (Cys 169) transcriptional coactivators. The interaction of HIF1α C-terminal transactivation domain with the CH1 domain of p300 and/or CBP is required for the activation of hypoxia-responsive genes [108, 109]. It is also known that HIF1α and CITED4 compete for binding to p300/CBP [110]. The C-terminal Cys 800 of HIF1α was detected by Yasinska *et al.* as SNO target and was shown to activate its interaction with p300 [102]. In this thesis, a novel SNO site was detected on the C-terminal part of CITED4 (Cys 169), which presumably has a similar function as SNO Cys 800 of HIF1α. As CITED4, unlike HIF1α, is stable at normoxic conditions, the involvement of SNO Cys 169 in activation of hypoxia-responsive genes during temporary or physiological hypoxia can be hypothesized.

Another interesting phenomenon that might be explained by protein-protein interaction regulated by transnitrosylation is the ‘hit-and-run’ catalysis of histone acetylation proposed by Liu *et al.* [111]. A novel SNO site on Cys 1621, located at the second highly electronegative

pocket of p300 HAT domain, was detected by Cys-BOOST. The transnitrosylation of histone protein by SNO Cys 1621 will cause transient protein-protein interaction which may bring the acetyl group of p300 closer to the acetylation target, thus resulting in 'hit-and-run' catalysis.

Besides the signaling through nitrosylation/transnitrosylation and direct inactivation/activation of active Cys by SNO, the interplay of SNO and other PTMs may as well contribute to stress induced proteome modulation. In this context protein phosphorylation and ubquitinylation are the most studied PTMs [17, 30, 103, 112-114]. Many parallels could be drawn between protein phosphorylation and nitrosylation, such as the reversible nature of both PTMs, involvement in stimulus-dependent signaling and PTM formation by consensus motif recognition. The identification of SNO sites on 86 phosphatase subunits in this thesis implies the common nature of SNO and phosphorylation crosstalk, which was formerly demonstrated for a few phosphatases [103, 112, 115, 116]. For instance nitrosylation of Cys 259, one of two SNO sites of STAT3 detected in the current study as well, was shown by Kim *et al.* to abolish the phosphorylation of STAT3 Tyr705, thus regulating the inflammatory response [103].

STRING networks for both highly upregulated and downregulated SNO sites show an enrichment of the proteins involved in ubiquitin-mediated proteolysis. Interestingly, the regulation of ubiquitinylaton activity directly by SNO was formerly shown for at least one E3 ubiquitin-protein ligase, PARKIN [30]. More than 40 E3 ubiquitin-protein ligases were identified as SNO targets in this study, suggesting that the regulation of ubiquitinylaton activity by SNO might be a common regulatory mechanism.

The 200 µM *in-vitro* GSNO treatment results in widespread SNO formation. 57 % of the proteins were detected with multiple SNO sites. Nevertheless, the detected SNO proteome covers the whole dynamic range of the HeLa proteome emphasizing the selectivity of SNO targets and the high sensitivity of Cys-BOOST. Interestingly, the SNO levels of multiple sites detected on individual proteins diverge significantly, once more reinforcing the high specificity of SNO targets. The occurrence of SNO on a range of protein classes is in agreement with numerous regulatory functions attributed to SNO [74]. Although, all 8304 unique SNO sites detected here are unlikely to occur in endogenous conditions simultaneously, each of them represents a potential *in-vivo* SNO target, which may occur individually at the given circumstances.

3.9 Combined S-Nitrosylation and protein phosphorylation analysis in SNAP-treated and control SH-SY5Y cells

Next, it was evaluated whether Cys-BOOST can be combined with other enrichment techniques to conduct multi-PTM studies. Therefore, SNO and protein phosphorylation were analyzed together in untreated and S-Nitroso-N-acetylpenicillamine (SNAP)-treated SH-SY5Y cells. The neuroblastoma SH-SY5Y cell line is widely used as neuronal *in vitro* system [117], for instance in Parkinson's disease and Alzheimer's disease research. To study the effects of short-term nitrosative stress on SNO and protein phosphorylation mediated signaling, SH-SY5Y cells were treated for 5 min with cell permeable NO donor SNAP (N=4) or incubated with PBS (N=4) as controls (i.e. basal conditions). SNO analysis were performed using the Cys-BOOST workflow. Additionally, the flow through (FT) of the Cys-BOOST enrichment was collected, desalted, partially used for TiO_2-based enrichment of phosphorylated peptides and partially for global proteome quantification (Figure 3.21). Thus enabling the combined quantitative analysis of SNO, protein phosphorylation and global protein expression.

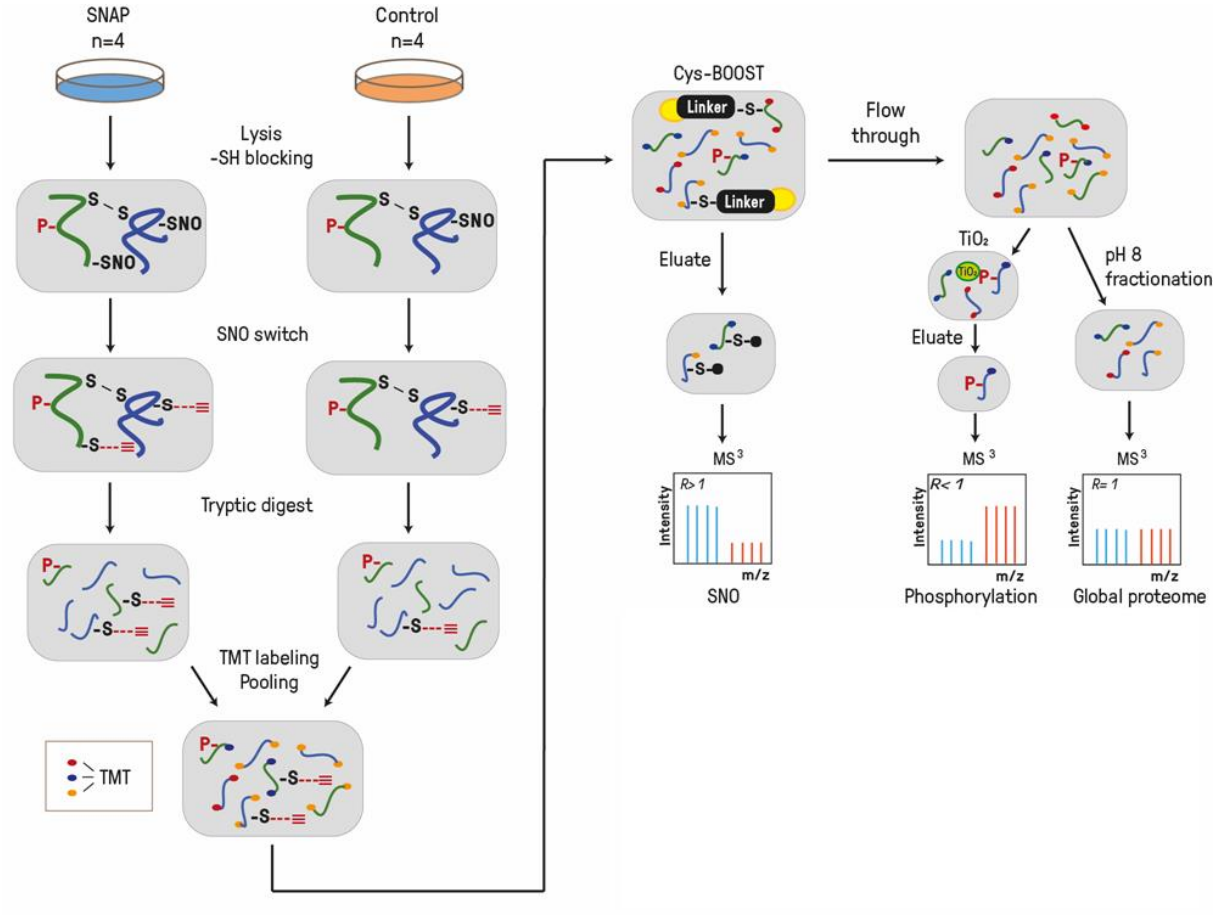

Figure 3.21 Workflow for the combined quantitative analysis of protein SNO, phosphorylation and expression in SNAP-treated and non-treated SH-SY5Y cells. Cys-BOOST was used for SNO analysis. The FT of Cys-BOOST was used for TiO_2 enrichment (25% of the FT) of phosphorylated peptides and global proteome analysis (5% of the FT) after RP fractionation at pH 8.

The rationales of preforming SNO analysis in neuronal *in vitro* system are that *(i)* in neurons physiological levels of SNO notoriously regulate neurogenesis, neural development, synaptic plasticity and neurotransmitter release [36], and *(ii)* increased SNO has been linked to activation of neuroprotective properties of proteins [118], whereas *(iii)* excessive (pathophysiological) levels of SNO, known as nitrosative stress, have been related to neuronal damage and the etiology of neurodegenerative disorders [73, 119]. Additionally, the analysis of another reversible PTM, protein phosphorylation, provides deeper insights into the diversity and crosstalk of reversible PTM-mediated signaling as a result of the short-term nitrosative stress in this neuronal in vitro system [106].

As a result, Cys-BOOST identified 2439 SNO peptides (1855 confidently quantified), representing 2158 unique SNO sites on 1443 proteins. 2151 SNO sites were identified in both,

control (basal) and SNAP-treated samples, covering a wide dynamic rage of the SH-SY5Y proteome (Figure 3.22).

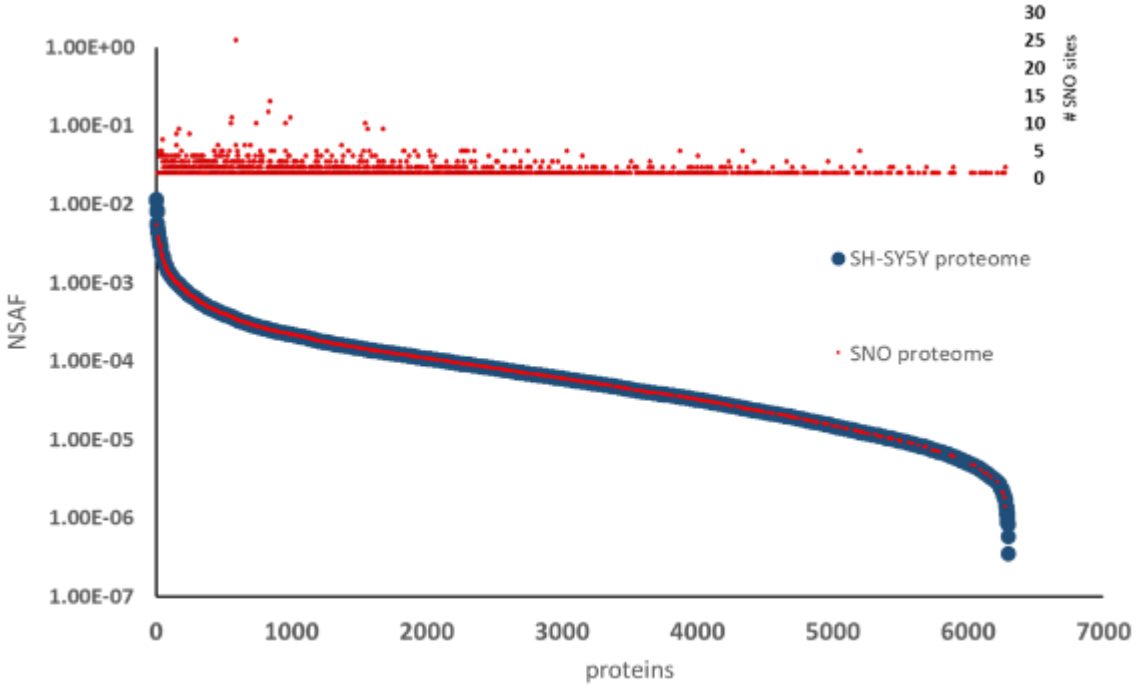

Figure 3.22 Good coverage of the SH-SY5Y SNO proteome. Proteome dynamic range represented by NSAF values (blue): Only proteins with at least 1 unique peptide (1% protein FDR) were considered and ordered in descending abundance, as represented by descending NSAF values of 6294 SH-SY5Y proteins. SNO proteome (red): The NSAF values for 1413 proteins with quantified high confidence SNO sites are shown as red dots [27]. Top: The number of SNO sites identified per protein demonstrates that even for proteins of low abundance multiple SNO sites could be detected [27].

Gene Ontology (GO) annotation analysis of SH-SY5Y SNO proteins showed enrichment of several molecular functions (Figure 3.23a) and biological processes (Figure 3.23b). 65 and 39 SNO sites were significantly upregulated (≥ 1.5-fold, ANOVA p-value ≤ 0.05) and downregulated (≥ 1.5-fold, ANOVA p-value ≤ 0.05), respectively (Figure 3.23c), with an enrichment of proteins involved in protein folding, translation, DNA-replication, NADH metabolic processes and cadherin binding (Figure 3.23d).

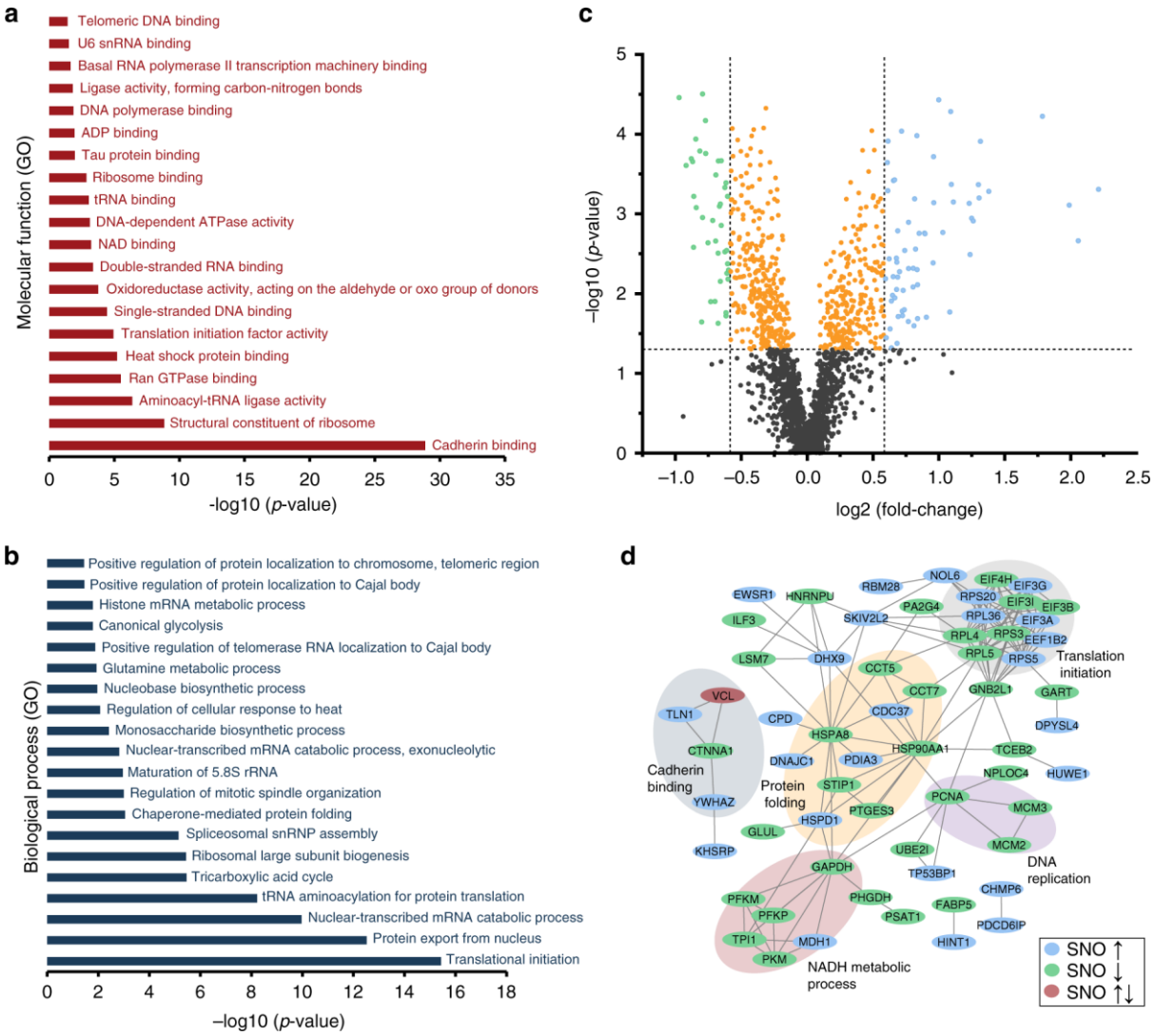

Figure 3.23 SNO analysis of SNAP-treated and non-treated (control) SH-SY5Y cells. (a-b) Top 20 enriched GO terms (PANTHER Overrepresentation Test (http://www.pantherdb.org/), p-values defined by Fisher's exact test) of the SH-SY5Y SNO proteome: (a) molecular function and (b) biological process. (c) Volcano plot of SNO peptides in SNAP-treated vs non-treated samples. Green dots (N=39) represent significantly downregulated (≥ 1.5-fold, ANOVA p-value ≤ 0.05) and blue dots (N=65) significantly upregulated (≥ 1.5-fold, ANOVA p-value ≤ 0.05) SNO peptides. (d) High confidence STRING network of proteins with significantly changed (≥ 1.5-fold, ANOVA p-value ≤ 0.05) SNO levels. Proteins with upregulated SNO sites are marked blue, with downregulated green and with both up- and down-regulated red. P-values derived from N=4 replicates [27].

Proteins involved in NADH metabolic processes and DNA-replication showed predominantly downregulated SNO. Several proteins involved in neurogenesis, axonogenesis and guidance were detected with significantly upregulated SNO sites (e.g. drebrin (DBN1) Cys 632, 2.5-fold;

Golgi SNAP receptor complex member 1 (GOSR1) Cys 34, 1.7-fold; dihydropyrimidinase-related protein 4 (DPYSL4) Cys 369, 1.6-fold; microtubule-associated protein 1B (MAP1B) Cys 2041, 1.6-fold, and Cys 963, 2.4-fold; dedicator of cytokinesis protein 7 (DOCK7) Cys 388, 1.6-fold; and PC4 and SFRS1-interacting protein (PSIP1) Cys 204 2.0-fold), whereas Cys 99 of glutamine synthetase (GLUL) involved in positive regulation of glutamatergic synaptic transmission was detected 0.6-fold downregulated. The decreased SNO of GLUL, an enzyme converting neurotoxic glutamate to harmless glutamine, might indicate its functional activation and the protective role of its Cys 99 under nitrosative stress. Additionally, novel candidates of neuroprotection modulated by SNO, such as DOCK7 were identified. It has been shown that DOCK7 is involved in neurogenesis and that the presence of *DOCK7* mutations directly impacts the manifestation of neurological diseases [120]. The data herein moreover indicates that proteins, such as GOSR1, with a known neuroprotective role against redox-based cytoxicity might be controlled by SNO, rather than only by protein expression [121]. Other examples are endoplasmic reticulum (ER)-stress proteins and unfolded protein response (UPR)-related proteins such as CDC37, HSPD1 and PDIA3. Uehara *et al.* have shown that SNO inhibits the ability of PDI to prevent neurotoxicity associated with ER-stress and protein misfolding [122]. Using Cys-BOOST we could identify two novel SNO-sites (Cys 85 and 92) in PDIA3. Hence, indicating that SNO of proteins involved in ER-stress and UPR might be a synergistic and synchronous pathobiochemical process in the etiology of neurological diseases, as has already been demonstrated for Alzheimer's disease [123]. The existence of a considerable number of downregulated SNO underlines the importance of the activation of protein de-nitrosylation pathways and might indicate the activation of these proteins in response to cellular stress, via liberation of active site Cys or allosteric Cys residues [124]. Reduced levels of SNO were detected in proteins with key functions in metabolic processes such as GAPDH (Cys 247), GLUL (Cys 99), PFKM (Cys 114), PFKP (Cys 123), PKM (Cys 49) and TPI1 (Cys 164). In contrast, MDH1, which produces NADH as a byproduct of its enzymatic activity, was detected with upregulated SNO at Cys 154. These findings once more point to the involvement of SNO in rerouting of glucose to the pentose phosphate pathway which generates NADH to support cellular antioxidant defense [125, 126]. Moreover, considering the regulated SNO sites on VCL and CTNNA1, the SNO-related control of the cadherin–catenin complex, which is crucial for dendrite and synapse morphogenesis [127], could be inferred.

After TiO_2 enrichment 2142 unique phosphorylated peptides on 1026 proteins were quantified, from which 144 were significantly changed (≥ 1.5-fold, ANOVA p-value ≤ 0.05) as a result of the SNAP treatment. The combined STRING network analysis of proteins with significantly

changed SNO and/or phosphorylation sites suggests that distinct biological process are preferentially controlled by one of the two PTMs (Figure 3.24).

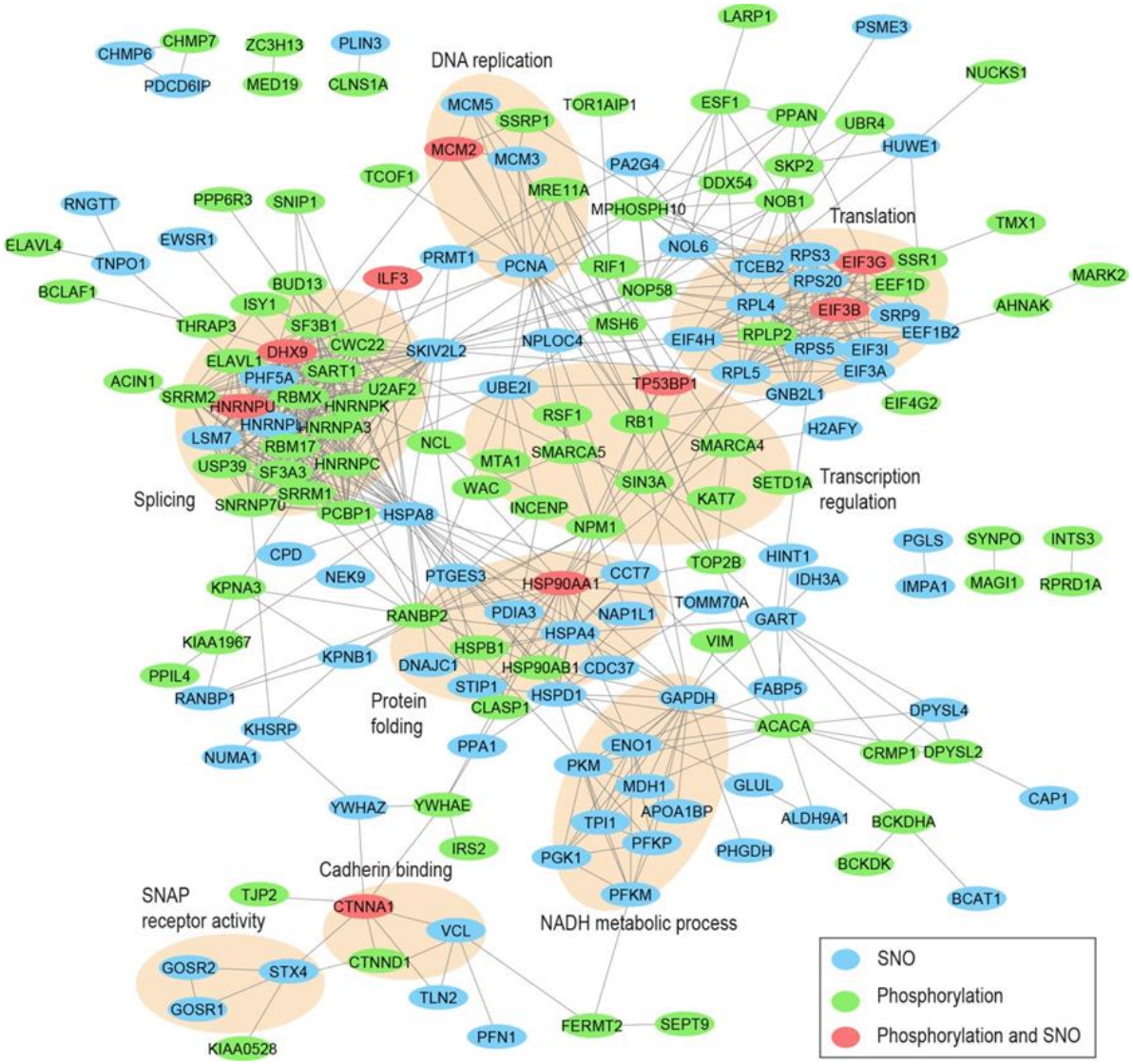

Figure 3.24 STRING network analysis of proteins with significantly changed (≥ 1.5-fold change, ANOVA p-value ≤ 0.05) SNO and/or phosphorylation sites.

Thus, proteins involved in splicing and transcription regulation (transcription cofactor activity and transcription factor binding) preferentially possessed significantly changed phosphorylation sites, whereas the proteins involved in translation, NADH metabolic process and Soluble N-ethylmaleimide-sensitive Attachment Protein (SNAP*) receptor activity preferentially possessed significantly changed SNO. In total, 10 proteins were found with both significantly regulated SNO and phosphorylation sites, nine of which are represented in the STRING network. Interestingly, both modifications could be detected neither simultaneously or separately in the same peptide sequence. Despite this absence of a more direct interaction

of both PTMs based on primary protein structure in the data, the general occurrence of this type of crosstalk cannot be excluded and more comprehensive analyses might be required in the future, for instance using larger amounts of starting material in order to further increase the depth of the two PTM-centric datasets. Nevertheless, the indication of the distinct biological process preferentially controlled by one of the two PTMs in the applied model system, aids to our understanding of cellular signaling and reversible PTM crosstalk, as both SNO and phosphorylation are key reversible PTMs involved in signaling [128, 129].

3.10 Outlook

The vast (patho)physiological relevance of SNO introduces immense possibilities for application of Cys-BOOST. The most tempting applications include, SNO analysis in the model systems and clinical samples of neurodegenerative diseases, ischemia-reperfusion and cardiovascular diseases. Importantly, the high sensitivity of Cys-BOOST enables the use of clinical samples of limited amount, such as biopsies. Indeed, aberrant SNO levels might also be present in cancer, however, SNO analysis of tumor samples might be extremely challenging if not impossible, given the high demands for sample preparation. One of the advantages of incorporation of TMT-based quantification in Cys-BOOST is the possibility to quantify up to 16 different (clinical) samples, which comes along with a concurrent increase in total sample amount, allowing the detection and quantification of SNO sites even from low individual sample amounts. Clinical applications of Cys-BOOST might also benefit from the use of a 'booster' TMT channel, where substantially more sample is labelled and added to the multiplexed total sample, in order to boost the general signal and enable the quantification of peptides/proteins that could not be detected otherwise [130]. Thus, as Cys-BOOST is well-compatible with TMT labeling and provides high specificity and sensitivity, it offers a ready-to-use analytical platform for SNO analysis in clinical samples. As demonstrated in this work the technical variation of the Cys-BOOST workflow --- even when done manually --- is low, so that theoretically large numbers of samples could be processed using liquid handling systems. This opens a vast possibility for biomarker discovery and for the investigation of disease mechanisms and targets.

Moreover, minor modulations of the Cys-BOOST workflow will enable the study of diverse Cys modifications using reducing agents or alkyne reagents specific for the PTM-of-interest. As reversible Cys PTMs exist in homeostasis, analysis of different forms of Cys PTMs is desirable to understand the redox regulation of biological processes via Cys.

Another interesting possibility is the multi-PTM analysis, as demonstrated for phosphorylation and SNO in this thesis. Similarly, the FT of the Cys-BOOST can be collected, desalted and used for enrichment or immunoprecipitation strategies enabling the analysis of diverse PTMs (e.g. Lys-acetylation, ubiquitylation, SUMOylation and others). The PTM crosstalk analysis will lead to a more comprehensive understanding of biological processes regulated on the PTM level. While in this work no evidence could be collected for the concurrent presence of phosphorylation and SNO on the very same peptide, the use of alternative enzymes, such as shown in our group for the broad-specificity protease Subtilisin [131] might shed more light onto this important topic. It has been demonstrated that certain parts of the proteome cannot

be covered by gold-standard trypsin, which is an even more important drawback for PTM research than for global proteomics. Also, the use of enzymes that enable ‘middle-down’ proteomics, i.e. the analysis of considerably longer peptide sequences, might be an important future application of Cys-BOOST.

Clearly, the here presented work might only be the beginning of a long journey to understand the relevance of SNO and other Cys PTMs as well as their crosstalk.

4. Conclusion

The work presented here introduces Cys-BOOST: a novel chemical proteomics strategy for SNO analysis using ST in combination with Cys enrichment by a Dde-biotin-azide bioorthogonal cleavable-linker, and amine-reactive TMT labeling for quantitative LC-MS^2 (MS^3)-based analysis.

The performance of Cys-BOOST was demonstrated by enrichment of the Cys peptides from tryptic HeLa digests with high specificity and sensitivity. The direct comparison between Cys-BOOST (N=3) and iodoTMT (N=3) shows superior performance of Cys-BOOST in terms of both the number of identified (25,019 vs 9966) Cys peptides, technical reproducibility (RSD of 9 % vs 36 %) and specificity (98 % vs 74 %).

Applying Cys-BOOST for SNO analysis in GSNO-treated and control HeLa cell extracts reveals thousands of novel SNO targets and allows the identification of proteome-wide GSNO-mediated SNO consensus motifs. These motifs demonstrate for the first time on a proteome-wide scale the contribution of acid-base catalysis and local hydrophobicity to the thus far elusive target-selectivity of SNO.

The impact of the early nitrosative stress on neuron-like cells was studied by applying Cys-BOOST for the combined quantitative analysis of SNO, protein phosphorylation and global protein expression in SH-SY5Y neuroblastoma cells, with and without short-term treatment with NO donor. The analysis reveals significant regulation of SNO levels in proteins involved in neurogenesis, axonogenesis, glutamatergic synaptic transmission, cadherin binding, NADH metabolic process, protein folding, translation initiation, and DNA replication. In contrast, proteins involved in splicing and transcription regulation were found with significantly altered phosphorylation levels.

Collectively, the current work establishes Cys-BOOST as highly sensitive, specific and reproducible analytical tool, enabling in-depth quantitative SNO analysis, both *in-vitro* and *in-vivo*. Cys-BOOST is also reinforced as a current method of choice for SNO analysis when compared to the existing SNO studies using diverse analytical strategies (Supplementary Table 2). The identification of thousands of SNO targets across protein classes validates SNO as a global regulator of protein function. The findings on SNO consensus motifs shed light on the nature of SNO formation and its exquisite specificity. Detection of the significantly altered SNO levels on key neuronal proteins suggests novel candidates of neuroprotection modulated by SNO.

5. Methods

5.1 Cell culture

HeLa S3 cells were cultured in 100 mm^2 tissue culture (TC) dishes to ~ 80 % confluency in Dulbecco's Modified Eagle Medium (DMEM) medium supplemented with 10 % fetal bovine serum (FBS), 1 % penicillin/streptomycin at 37 °C, 5 % CO_2. Medium was removed and cells were washed with phosphate buffered saline (PBS). Cells were harvested with 0.05 % Trypsin, 0.02 % ethylenediaminetetraacetic acid (EDTA) in PBS, incubated at 37 °C for 5 min. Trypsin was diluted with excess of fresh medium, cells were pelleted for 5 min at 300 × g, and the pellets were washed twice with PBS.

SH-SY5Y cells were cultured in N=8 100 mm^2 TC dishes to 60-80 % confluency in DMEM medium supplemented with 10 % fetal FBS, 1 % penicillin/streptomycin at 37 °C, 5 % CO_2. Medium was removed and cells were washed with PBS. Fresh DMEM medium with 1 % penicillin/streptomycin was added and the cells were starved for 45 min at 37 °C, 5 % CO_2, with the sterilization-UV light of the incubator switched off. Medium was removed and the cells were washed with PBS. 3 mL of 100 µM SNAP in PBS was added to four TC dishes, whereas 3 mL of PBS was added to the other four TC dishes. Cells were incubated for 5 min at 37 °C, 5 % CO_2 with the sterilization-UV light of the incubator switched off. The medium was removed, and cells were washed with PBS followed by lysis on the TC dishes.

5.2 Cell lysis

For total Cys analysis the HeLa cell pellet from 100 mm^2 TC dish was lysed in 500 µL of 1% (w/v) sodium dodecyl sulfate (SDS), 150 mM NaCl, 100 mM HEPES (pH 7.5) supplemented with protease inhibitor cocktail Complete Mini. For SNO analysis HeLa cell pellets from 100 mm^2 TC dishes were lysed each in 500 µL of HENS buffer (1 % (w/v) SDS, 1 mM EDTA, 100 µM neocuproin, 100 mM HEPES (pH 7.5)), supplemented with protease inhibitor cocktail Complete Mini. The lysates were incubated with 7 µL of benzonase nuclease (25 units/µL) and 2 mM $MgCl_2$ for 30 min at 37 °C, followed by centrifugation at 18,000 x g for 30 min at 4 °C. SH-SY5Y cells were lysed on TC dishes with 1 mL of lysis buffer containing 100 mM IAA in HENS supplemented with protease inhibitor cocktail Complete Mini. The lysates were ultrasonicated (15 s, amplitude 40).

5.3 BCA assay

BCA assay for protein amount determination in lysates was performed according to the manufacturer's instructions. Briefly, BSA standard dilutions 125 µg/mL, 250 µg/mL, 500 µg/mL, 750 µg/mL and 1000 µg/mL were made in water and used for calibration carve generation. Lysates were diluted 25, 50, 75 or 125 times (depending on the estimated concentration of the lysate) with water. 25 µL of each dilution of the sample and the BSA standard was added to each well of the 96 well plate (N=3 technical replicates for both the samples and the standard). Reagent A and Reagent B (50:1) from the BCA assay kit were mixed. 200 µL of A+B mixture was added to each well. The plate was covered and placed in the oven at 56 ˚C for 30 min, afterwards brought to RT and was finally scanned (Thermo Scientific MULTISCAN FC) at 562 nm.

5.4 Acetone precipitation

Acetone precipitation or double acetone precipitation was used for the removal of the excess of reagents on the protein level. Proteins were precipitated by addition of 5 volumes of ice-cold acetone followed by incubation for 20 min at -80 °C and centrifugation at 18,000 x g for 30 min at 4 °C; subsequently, the supernatant was carefully removed. If double acetone precipitation was necessary, the protein pellet was dissolved in a small volume of 1 % SDS and the precipitation was repeated with 10 volumes of ice-cold acetone. When necessary, the pellet was resolubilized by ultrasonication (15 s, amplitude 40).

5.5 Protein digestion

The protein pellet was resuspended in 1 % SDS to a final concentration of 2 mg/mL. Oxidized Cys were reduced with 5 mM TCEP for 1 h, at 56 °C, with agitation at 300 rpm. The pH was adjusted with 200 mM HEPES, pH 7.5. Cys were alkylated with 12 mM IAA for 1 h, at 25 °C, with shaking at 300 rpm in the dark. Proteins were digested using the filter-aided sample preparation (FASP) [132, 133] protocol with modifications or in-solution digestion. For FASP samples were diluted 5-fold with freshly prepared 8 M urea, 100 mM Tris-HCl at pH 8.5 and transferred to 30 kDa Molecular Weight Cut-off (MWCO) centrifugal filters. The liquid was passed through the filter at 13,800 x g, 25 °C and the same centrifugation conditions were applied for all the following FASP steps. The concentrates contained in the filter devices were washed 3 × with 200 µL of 8 M urea, 100 mM Tris-HCl, pH 8.5 and 3 × with 200 µL of 50 mM

triethylamonium bicarbonate (TEAB), pH 8.5. The concentrate was digested in 100 µL of 0.2 M guanidine hydrochloride (GuHCl), 50 mM TEAB pH 8.5, 1 mM $CaCl_2$ and trypsin in a ratio 20:1 (protein:enzyme) at 37 °C overnight. The digests were collected by centrifugation, and the filters were rinsed with 100 µL of 50 mM TEAB and centrifuged.

For in-solution digestion excess of the reagents was removed by acetone precipitation with 10 volumes of ice-cold acetone. The protein pellets were resuspended in 0.2 M GuHCl, 50 mM TEAB pH 8.5, 1 mM $CaCl_2$ and trypsin was added (20:1; protein:enzyme). Proteins were digested at 37 °C overnight with agitation at 300 rpm. The digest was stopped by addition of 1 % trifluoroacetic acid (TFA) or the peptides were labeled with TMT 10plex™ directly after the digest. The quality of the digest was ensured using a monolithic column HPLC-setup [134].

5.6 TMT-10plex labeling

The digests were labeled with TMT 10plex™ according to the manufacturer's instructions. Briefly, 41 µL of anhydrous ACN was added to each 0.8 mg TMT 10plex™ vial. Peptides (~ 100 µg protein digest) in 100 µL of 50-100 mM TEAB were mixed with 41 µL TMT 10plex™ reagent and reacted for 1 h at 25 °C with shaking at 300 rpm. The reaction was quenched with 8 µL of 5% hydroxylamine for 15 min. If not stated otherwise, the samples labeled with different TMT channels were pooled.

5.7 Solid phase extraction

SPE was applied for removal of the excess reagents and desalting of the samples on the peptide level. Samples in 200 µL of 0.1 % TFA were desalted with self-packed stage tips using C18 3M Empore SPE Extraction Disks. In brief, the 200 µL pipette tip was packed with 2 mm of C18 3M Empore SPE Extraction material and 500 µg of Oligo R3 reversed phase Resin in ACN. ACN was removed by centrifugation at 500 x g, 25 °C. The same centrifugation conditions were applied for all the following steps. The cartridge was equilibrated with 200 µL of 0.1 % TFA. The samples were loaded, washed with 100 µL of 0.1 % TFA and eluted with 100 µL of 70 % ACN, 0.1 % TFA. The samples were dried under vacuum.

5.8 Iodoacetamide alkyne labeling

A mix of synthetic Cys peptides (ETCVVVYTGYGNR, CSDIISYTFK, GEHGFIGCR, YLAADKDGNVTCER; 0.55 nmol each) in water or proteome digests in 1% SDS were reduced with 5 mM TCEP for 1 h, 56 ºC. The pH was adjusted with 200 mM HEPES (pH 7.5), and 12 mM IAA-alkyne was added and reacted for 1 h, 25 ºC in darkness. The samples were acidified and the peptides were measured by LC-MS/MS.

5.9 Copper(I)-catalyzed alkyne-azide cycloaddition

IAA-alkyne labeled samples (synthetic Cys peptides or protein digest) were dissolved in 100 mM potassium phosphate buffer (PPB), pH 7 (~ 25 µM peptide-alkyne). CuAAC was performed via stepwise addition of 150 µM biotin-azide linker (Diazo-biotin-azide, Diol-biotin-azide or DDE-biotin-azide), a premixed solution of CuSO4 (≥ 99%) and THPTA, sodium ascorbate or TCEP, and aminoguanidine hydrochloride (Table 5.1). The reaction was incubated for 1 h, at 25 °C.

Table 5.1 CuAAC protocols (P1, P2, P3 and P4).

Reagents	***P1***	***P2***	***P3***	***P4***
Peptide-alkyne	25 µM	25 µM	25 µM	25 µM
$CuSO_4$	0.25 mM	2 mM	1 mM	0.5 mM
THPTA	1.25 mM	0.1 mM	0.1 mM	1.25 mM
Ascorbate	5 mM	2 mM	x	5 mM
TCEP	x	x	1 mM	x
Aminoguanidine hydrochloride	5 mM	x	x	5 mM
Biotin-azide linker	150 µM	150 µM	150 µM	150 µM

5.10 Streptavidin binding and depletion of background peptides

Directly after CuAAC the samples were incubated with prewashed (with 1 mL PBS) High Capacity Streptavidin – Agarose Resin for 1 h, at 25 ºC, head over tail rotation. The beads were pelleted by centrifugation for 30 s at 500 x g, rested on ice for 5 min and the supernatant was removed. The same procedure was applied for removal of the supernatant in all the following steps of the enrichment. The beads were washed 4 × with 1.5 mL of 2 M urea in PBS, 2 × with 1.5 mL of PBS and 2 × with 1.5 mL of 100 mM Na_2PHO_4, pH 7.5. After each washing step the supernatant was removed.

5.11 Elution via chemical cleavage of the Diazo-biotin-azide linker

Diazo-biotin-azide linker was conjugated with ~ 25 µM of IAA-alkyne labeled synthetic Cys peptides via CuAAC. The samples were desalted using SPE, reconstituted in 50 mM Na dithionite in PPB, pH 7.0 and reacted for 30 min at 25 ºC. Fresh 50 mM Na dithionite in PPB was added and reacted for 30 min at 25 ºC two more times. Afterwards the samples were desalted. The pellets were resuspended in 0.1 % aqueous TFA and measured by LC-MS/MS.

5.12 Elution via chemical cleavage of the Diol-biotin-azide linker

~ 25 µM of IAA-alkyne labeled Cys synthetic peptides (heavy and light form of each peptide; Table 5.2) in PPB were conjugated with Diol-biotin-azide via CuAAC. The samples were incubated with 40 µL of prewashed High Capacity Streptavidin – Agarose Resin for 1 h, at 25 ºC, with head over tail rotation. The peptides were released by the oxidative cleavage of the vicinal diol with 1 mM $NaIO_4$ (light form of the peptide) or 10 mM $NaIO_4$ (heavy form of the peptide) in Na_2HPO_4, pH 7.4, at 25 ºC for 20 min, with head over tail rotation in darkness. The supernatant was collected, and the reaction was repeated 2 more times. All supernatants were combined. $NaIO_4$ was quenched by addition of 10 mM threitol and the samples were desalted using SPE. The peptides were reacted with 5% hydroxylamine in 0.1 % TFA or an equal volume of 0.1 % TFA as control for 1 h, at 56 ºC with shaking at 550 rpm before the LC-MS/MS measurement.

Table 5.2 List of the synthetic Cys peptides (R/K indicate the light form of the peptide, whereas r/k indicate the heavy form ($^{13}C_6{}^{15}N_2$ for Lys, $^{13}C_6{}^{15}N_4$ for Arg)).

Sequence
FECQPGYR
FECQPGYr
LCFDNSFSTISEK
LCFDNSFSTISEk
VNLSCGGVSHPIR
VNLSCGGVSHPIr

5.13 Elution via chemical cleavage of the Dde-biotin-azide linker

~ 25 μM of IAA-alkyne labeled Cys synthetic peptides in PPB were conjugated with Dde-biotin-azide via CuAAC in N=4 replicates (N=2 the light form and N=2 the heavy form of each peptide from Table 5.2). The samples were incubated with 40 μL of prewashed High Capacity Streptavidin – Agarose Resin for 1 h, at 25 ºC, with head over tail rotation. The peptides were released by incubation with 2% hydrazine in Na_2HPO_4 pH 7.4, for 1 h, at 25 ºC with head over tail rotation. The supernatant was collected, and was either adjusted to 1% TFA or 25 mM ammonium formate content followed by SPE. The pellets were resuspended in 0.1 % TFA and measured by LC-MS/MS.

5.14 Comparison of Dde-biotin-azide linker and Diol-biotin-azide linkers for the enrichment of total Cys peptides from HeLa lysate

Hela lysate was reduced with 5 mM TCEP, free Cys were labeled with 12 mM IAA-alkyne and proteins were digested with trypsin. The digest was divided to N=4 replicates (~ 100 μg each) and labeled with TMT, two of which N=were conjugated via CuAAC with Dde-biotin-azide and the other N=2 with Diol-biotin-azide linker. The samples were incubated with 160 μL of prewashed High Capacity Streptavidin – Agarose Resin for 1 h, at 25 ºC, with head over tail rotation. The background peptides were washed, followed by elution of Cys peptides. For Diol-biotin-azide linker labeled peptides the elution was done using 1 mM $NaIO_4$ in Na_2HPO_4, pH 7.4, at 25 ºC for 20 min, with head over tail rotation in darkness. The supernatant was collected, and the reaction was repeated 2 more times. All supernatants were combined,

$NaIO_4$ was quenched by addition of 10 mM threitol and the samples were desalted using SPE. The peptides were reacted with 5% hydroxylamine in 0.1 % TFA for 1 h, at 56 ºC with shaking at 550 rpm before the LC-MS/MS measurement. For Dde-biotin-azide linker the elution was done using 2% hydrazine in Na_2HPO_4 pH 7.4, for 1 h, at 25 ºC with head over tail rotation. The supernatant was collected, acidified to 1% TFA, and desalted with SPE. The pellets were resuspended in 0.1 % aqueous TFA and measured by LC-MS/MS.

5.15 On-tip pH 10 fractionation

On-tip pH 10 fractionation was performed using self-packed (as described above) desalting cartridges. The cartridges were equilibrated with 200 µL of 20 mM ammonium formate, pH 10.0. The samples were loaded and washed with 200 µL of 20 mM ammonium formate at pH 10.0. Stepwise fractionation was performed using 50 µL of 16 %, 20 %, 24 %, 28 % and 80 % ACN in 20 mM ammonium formate, pH 10.0. After each elution step the column was washed with 20 µL of 20 mM ammonium formate, pH 10.0 and this wash was combined with the preceding eluate. Fractions were dried under vacuum and resolubilized in 0.1 % aqueous TFA for LC−MS/MS or LC-SPS analysis.

5.16 LC-MS/MS and LC-SPS

Peptides were LC separated using Ultimate 3000 RSLCnano systems. All samples were preconcentrated with 0.1% TFA on a trap column (100 µm × 2 cm, C18 Acclaim Pepmap viper) for 5 min at a flow rate of 20 µL/min, followed by separation on the main column (75 µm × 50 cm, C18 Acclaim Pepmap viper) at 250 nL/min and 60 °C. Binary buffers (A, 0.1 % formic acid (FA); B, 84 % ACN, 0.1% FA) and linear gradients of 3-30 % B for 180 min and 3-35 % B for 90 or 120 min were applied for peptide separation. The LC system was online-connected to an Orbitrap Fusion Lumos or a Q Exactive HF mass spectrometer, both equipped with nano ESI sources. On the Orbitrap Fusion Lumos, MS/MS scans were acquired by setting MS survey scans from 300 to 1550 m/z at a resolution of 120,000, using an automatic gain control (AGC) target value of 2×10^5 and a maximum injection time (IT) of 50 ms. MS/MS scans were acquired in DDA mode in the Orbitrap at a resolution of 60,000. Precursor ions were selected using an IW of 0.8 m/z, an AGC target value of 5×10^4, an IT of 200 ms with TopS (3 s) option and a dynamic exclusion (DE) of 20 s. Isolated precursors were fragmented using HCD with a normalized collision energy (CE) of 40. SPS scans were acquired according to O'Connell *et al.* [60] with slight modifications. MS survey scans were acquired in the Orbitrap from 375 to

1550 m/z at a resolution of 120,000, using an AGC target value of 2×10^5 and an IT of 50 ms. The top speed option with a cycle time of 3 s was used to select precursors with an IW of 0.4 Da, followed by CID fragmentation. MS^2 scans were acquired in the ion trap in Turbo mode with an AGC target value of 2×10^4, an IT of 105 ms, a DE of 20 s and normalized CE of 35. From each MS^2 the top 10 fragment ions (SPS ions) were simultaneously selected with IWs of 0.4 Da for HCD with a CE of 65. MS^3 scans were acquired in the Orbitrap at a resolution of 50,000, with an AGC target value of 1.5×10^5 and an IT of 130 ms. On the Q Exactive HF MS, survey scans were acquired from 300 to 1750 m/z at a resolution of 60,000, using an AGC target value of 1×10^6 and an IT of 120 ms. MS/MS scans were acquired at a resolution of 60,000. For DDA (Top15) precursors were selected with an IW of 0.4 m/z, minimum AGC target value of 2×10^5 an IT of 200 ms and a DE of 30 s. Fragmentation was done using HCD with a CE of 33.

5.17 Cys-BOOST

Protein lysates containing IAA-alkyne labeled peptides (e.g. SNO specifically reduced with 20 mM sodium ascorbate labeled with 12 mM IAA-alkyne or total Cys reduced with 5 mM TCEP labeled with 3 mM IAA-alkyne) were digested with trypsin using FASP or in-solution digestion as described in 5.5. Peptides were labeled with TMT 10plex™, pooled and desalted as described in 5.6 and 5.7. CuAAC was used for conjugation of the Dde-biotin-azide linker to IAA-alkyne labeled peptides as described in 5.9 (P1 protocol). The reaction mixture was directly incubated with High Capacity Streptavidin – Agarose Resin and the background peptides were depleted as described in 5.10. Chemical elution of the target peptides was done with 2 % hydrazine as described in 5.13. On-tip pH 10 fractionation of the eluate was done as described in 5.15. Samples were resuspended in 0.1 % TFA and analyzed by LC-MS/MS or LC-SPS as described in 5.16.

5.18 iodoTMT-based enrichment

IodoTMT labeled protein lysates peptides (e.g. SNO specifically reduced with 20 mM sodium ascorbate labeled with 12 mM iodoTMTor total Cys reduced with 5 mM TCEP labeled with 3 mM iodoTMT) were digested with trypsin using FASP or in-solution digestion as described in 5.5. Peptides were incubated with 200 µL prewashed Immobilized Anti-TMT™ Antibody Resin for 2 h, at RT, head over tail rotation. The beads were pelleted by centrifugation for 30 sec at 500 x g, rested on ice for 5 min and the supernatant was removed. The same procedure was

applied for the removal of the supernatant in all the following steps. The beads were washed 3 × with 1.5 mL of 1 M urea in 100 mM Tris-HCl, pH 7.5, 2 × with 1.5 mL of 100 mM Tris-HCl at pH 7.5 and with 1 × 1.5 mL of water. After each washing step the supernatant was removed. The peptides were eluted with 100 µL of 50 % ACN, 1 % TFA. Eluates were dried under vacuum and resuspended in 100 µL of 20 mM ammonium formate, pH 10.0 for on-tip fractionation or resuspended in 0.1 % aqueous TFA and measured by LC-MS/MS.

5.19 Recovery of the Immobilized Anti-TMT Antibody Resin- based enrichment

50 nmol of each synthetic peptide in 100 µL of 100 mM TEAB was labeled with two different channels (TMT1 and TMT2) of TMT-10plex (0.8 µg in 40 µL of ACN) (Table 5.3). Thus, each peptide was labeled with one TMT group at its free N-terminus. The excess of TMT reagent was removed, the peptides were purified by LC (done by technical service bioanalytics) and the exact amount was determined by amino acid analysis (AAA) (done by technical service bioanalytics). For each peptide, 1 pmol of its TMT1- and TMT2-labeled version were mixed and measured on nano-LC-MS/MS to verify that identical amounts of TMT1 and TMT2 labeled peptides were used based on AAA results. 80 pmol from each of the three TMT1-labeled peptides (i.e. 240 pmol TMT peptides in total) were spiked to 20 µg HeLa or BSA digests, corresponding to the ~4 % TMT-labeled peptides in 96% background peptides to mimic the natural occurrence of Cys in the proteome. Samples were incubated with 60 ul of Immobilized Anti-TMT™ Antibody Resin overnight at 4 ºC, head over tail rotation. The experiment was performed in N=3 technical replicates. Afterwards, the beads were washed with 300 µL of 3 × 1 M urea in 100 mM Tris pH 7.5, 3 × 300 µL of 100 mM Tris pH 7.5, and 1× 300 µL of water. The peptides were eluted with 150 µL of 50 % ACN, 1% TFA in water and 80 pmol from each of the three TMT2-labed peptides were spiked to the eluates. The eluates were dried under the vacuum, resuspended in 0.1 % aqueous TFA and measured by LC-MS/MS. Recovery ($R_{\%}$) of anti-TMT enrichment was calculated based on the TMT reporter intensities ($R_{\%}$= Int_{TMT2} x 100/ Int_{TMT1}).

Table 5.3 NHS-TMT labeled peptides used for the anti-TMT recovery test.

Peptide	***TMT1***	***TMT2***
sVGLGAYLVR	126	130
dGNGFLSAAELR	129	130
sPGPGAQSALR	131	130

5.20 Total Cys analysis for comparison of Cys-BOOST and iodoTMT

HeLa cell lysate was precipitated by addition of 5 volumes of ice-cold acetone. The protein pellet was resuspended in 1 % SDS to a final concentration of 2 mg/mL. Cys were reduced with 5 mM TCEP for 1 h, at 56 °C, with agitation at 300 rpm. The lysate was divided in N=3 replicates for Cys-BOOST and N=3 replicates for iodoTMT based enrichment, 100 µg of total protein each. The pH was adjusted with 200 mM HEPES, pH 7.5. Cys were alkylated with 12 mM IAA-alkyne or 12 mM iodoTMT for Cys-BOOST and iodoTMT based enrichment, respectively, for 1 h, at 25 °C, with shaking at 300 rpm in the dark. Proteins were digested using FASP. The digests were acidified with 1 % TFA and were dried under vacuum. The quality of the digest was ensured using monolithic column HPLC-setup.

For Cys-BOOST, peptides were redissolved in 100 µL of 100 mM TEAB, pH 8.5 and labeled with TMT 10plex™. The samples were dried under vacuum and resuspended in 200 µL of 0.1 % TFA and desalted using SPE. The samples were dried under vacuum. The N=3 replicates labeled with 3 different TMT channels were kept separate. Dde-biotin-azide linker was conjugated to IAA-alkyne labeled peptides via CuAAC. The samples were dissolved in 100 µL of 100 mM PPB, pH 7.0. CuAAC was performed via stepwise addition of 150 µM Dde-biotin-azide linker, a premixed solution of 250 µM $CuSO_4$ and 1.25 mM THPTA, 5 mM sodium ascorbate and 5 mM aminoguanidine hydrochloride. The reaction was incubated for 1 h, at 25 °C. Directly after the CuAAC the samples were incubated with 250 µL of prewashed High Capacity Streptavidin – Agarose Resin for 1 h, at RT, head over tail rotation. The beads were pelleted by centrifugation for 30 s at 500 x g, rested on ice for 5 min and the supernatant was removed. The same procedure was applied for removal of the supernatant in all the following steps of the enrichment. The beads were washed 4 × with 1.5 mL of 2 M urea in PBS, 2 × with 1.5 mL of PBS and 2 × with 1.5 mL of 100 mM Na_2PHO_4, pH 7.5. After each washing step the supernatant was removed. The peptides were released by incubation with 125 µL of 2% hydrazine in 100 mM Na_2PHO_4, pH 7.5 for 1 h, at RT, head over tail rotation. Subsequently, the beads were rinsed with 125 µL of 50 mM ammonium formate and this wash was combined with the eluate. The replicates were pooled and fractionated using on-tip pH 10 fractionation. The pH 10 fractions were resuspended in 0.1 % aqueous TFA and measured by LC-MS/MS.

For iodoTMT based enrichment peptide pellets were dissolved in 100 µL of 100 mM Tris-HCl, pH 7.5. The N=3 replicates labeled with 3 different iodoTMT channels were kept separate. Each replicate was incubated with 200 µL prewashed Immobilized Anti-TMT™ Antibody Resin for 2 h, at RT, head over tail rotation. The beads were pelleted by centrifugation for 30 seconds at 500 x g, rested on ice for 5 min and the supernatant was removed. The same procedure

was applied for the removal of the supernatant in all the following steps. The beads were washed 3 × with 1.5 mL of 1 M urea in 100 mM Tris-HCl, pH 7.5, 2 × with 1.5 mL of 100 mM Tris-HCl at pH 7.5 and with 1 × 1.5 mL of water. After each washing step the supernatant was removed. The peptides were eluted with 100 µL of 50 % ACN, 1 % TFA. Eluates were dried under vacuum and resuspended in 100 µL of 20 mM ammonium formate, pH 10.0. The replicates were pooled and fractionated using on-tip pH 10 fractionation. The pH 10 fractions were resuspended in 0.1 % aqueous TFA and measured by LC-MS/MS.

5.21 Total free Cys labeling with increasing concentrations of IAA-alkyne

Total Cys of HeLa cell lysates (2 mg/mL) were reduced with 5 mM TCEP for 1 h at 56 °C, the pH of the samples was adjusted with 200 mM HEPES (pH 7.5), then the samples were labeled with 5 mM, 25 mM, 50 mM or 100 mM IAA-alkyne for 30 min at 25 °C. Excess of the reagents was removed by acetone precipitation and fluorescent 5-TAMRA-azide was introduced using CuAAC. 5 µg of each lysate were separated by SDS-PAGE, followed by fluorescence detection on Typhoon Trio imaging system at 580 nm. Afterwards, the gel was stained with Coomassie Brilliant Blue solution. Fluorescence signal intensities and protein abundance (based on Coomassie staining) were quantified using ImageJ. The fluorescence signal was normalized to protein abundance (Coomassie staining) in each lane.

5.22 S-nitrosylation reduction conditions

Analysis of SNO reduction conditions (20 mM sodium ascorbate (+asc), 10 min UV and control (– sodium ascorbate (–asc)) was performed in 200 µM GSNO-treated HeLa lysates. Free Cys were blocked with 100 mM IAA, excess of the reagent was removed by double acetone precipitation. SNO was switched with 3 mM IAA-alkyne in the presence (+asc) or absence (–asc) of 20 mM sodium ascorbate or after 10 min exposure to UV light. After tryptic digestion, TMT labeling, Cys-BOOST enrichment and on-tip pH 10 fractionation the pellets were resuspended in 0.1 % aqueous TFA were analyzed by LC-SPS. From enrichment FT 1 µg was measured by LC-SPS. The amount of switched SNO peptides was relatively quantified in each sample based on the TMT reporter ion intensities (S/N).

5.23 Analysis of the IAA blocking completeness in the initial step of the switch technique

The free Cys in SH-SY5Y cell lysates (2 mg/mL in HENS) were blocked with 25 mM, 50 mM or 100 mM IAA for 30 min at 25 °C. Excess of the reagents was removed by double acetone precipitation. The pellets were resolubilized and a second labeling step with 10 mM IAA-alkyne for 30 min at 25 °C was applied for blocking of the remaining free Cys. After tryptic digestion and TMT labeling the IAA-alk labeled peptides were enriched using Cys-BOOST. The eluate was desalted, the pellets were resuspended in 0.1 % aqueous TFA and analyzed by LC-SPS. From Cys-BOOST FT 1 µg was measured by LC-SPS. The amount of the remaining free Cys after IAA blocking was relatively quantified in each sample based on the TMT reporter ion intensities (S/N).

5.24 S-nitrosylation analysis in GSNO-treated HeLa lysates

The concentration of the lysates was adjusted to 2 mg/mL with lysis buffer. N=3 replicates, 300 µg of total protein each, were incubated with 200 µM GSNO in HENS, another N=3 replicates were incubated with the corresponding volume of HENS for 20 min, at 25 °C, with agitation at 300 rpm. Proteins were precipitated with 5 volumes of ice-cold acetone as described above. When necessary, the pellet was resolubilized by ultrasonication (15 s, amplitude 40). Samples were resuspended in 150 µL of HENS and incubated with 100 mM IAA for 30 min, at 25 °C with agitation at 300 rpm in the darkness. Excess of IAA was removed by double acetone precipitation, first with 5 volumes of ice-cold acetone. Afterwards the pellet was dissolved in 150 µL of HENS and precipitated with 10 volumes of ice-cold acetone. Next, samples were prepared for the SNO switch. Pellets were resolubulized in 300 µL of HENS. The SNO switch was performed by incubating the samples with 20 mM sodium ascorbate and 3 mM IAA-alkyne for 1 h, at 25 °C with agitation at 300 rpm in the darkness. Until this point the samples were protected from light or processed under a lamp only emitting wavelengths > 500 nm. Excess of the reagents was removed by double acetone precipitation first with 5 volumes, afterwards with 10 volumes of ice-cold acetone. The pellets were dissolved in 100 µL of 1 % SDS. The following steps of reduction with 5 mM TCEP, adjustment of pH with 200 mM HEPES pH 7.5, alkylation with 12 mM IAA, tryptic digestion, TMT 10plex™ labeling and desalting were conducted as described above in section 5.20 for total Cys analysis by Cys-BOOST. The samples (N=3 GSNO treated, N=3 controls) labeled with 6 channels of the TMT 10plex™ were pooled. Enrichment was performed as described above for total Cys analysis by Cys-BOOST with all steps scaled up 3 times. The pH 10 fractions were resuspended in 0.1

% aqueous TFA and measured by LC-MS/MS. Additionally, 1 µg from Cys-BOOST FT was measured by LC-MS/MS.

5.25 S-nitrosylation analysis in SNAP-treated SH-SY5Y cells

The free thiols of SH-SY5Y lysates were blocked with 100 mM IAA for 30 min, at 25 °C with agitation at 300 rpm. The excess of IAA was removed by double acetone precipitation, as described above. Pellets were resolubulized in 250 µL of HENS. Protein concentrations were determined by BCA. Protein concentration was adjusted to 1 mg/mL with HENS and the SNO switch was performed as above (see 5.24). Excess of the reagents was removed by double acetone precipitation. Afterward, protein pellets were dissolved in 1 % SDS to a final concentration of 2 mg/mL and incubated with 5 mM TCEP for 1 h, at 56 °C, with agitation at 300 rpm. The pH was adjusted to 7.5 with 200 mM HEPES. Cys were alkylated with 20 mM IAA for 1 h, at 25 °C, with agitation at 300 rpm in the dark. Excess of the reagents was removed by acetone precipitation with 10 volumes of ice-cold acetone. The protein pellets were resuspended in 125 µL of 50 mM TEAB pH 8.5, 1 mM $CaCl_2$, 0.2 M GuHCl and trypsin was added (20:1; protein:enzyme). Proteins were digested at 37 °C overnight with agitation at 300 rpm. The digests were labeled with TMT-10plex. Samples were dried under vacuum, resuspended in 200 µL of 0.1 % TFA, pooled and desalted. Enrichment was performed as described above for total Cys analysis by Cys-BOOST with all steps scaled up 3-fold. The eluate was acidified to 1% TFA and desalted. The sample was dried under vacuum and resolubilized in 0.1% TFA for LC-SPS analysis.

5.26 Phosphopeptide enrichment

The dry pellet of Cys-BOOST FT was dissolved in water and 25 % (max. 200 µg) was taken for phosphopeptide enrichment using titanium dioxide (TiO_2, Titansphere TiO, 5 µm particle size) according to Engholm-Keller et al. [135] with slight modifications. Briefly, the 25 % FT was dried under vacuum and resolubilized in 100 µL of buffer 1 (80% ACN, 5% TFA, and 1 M glycolic acid). TiO_2 beads (6:1, TiO2/peptide (w/w)) were added to the sample and incubated for 10 min on a shaker at 25 °C. The beads were pelleted by centrifugation at 500 rpm for 30 s. The incubation step was repeated 2 more times, first with 3:1 TiO_2 beads, then with 1.5:1 TiO_2 beads. The supernatant was discarded after the last incubation step. 100 µL of buffer 1 was used to combine TiO_2 beads from all 3 steps. The sample was centrifuged at 500 rpm for 30 s and the supernatant was discarded. Next, the beads were washed with 100 µL of 80%

ACN, 1% TFA, followed by another washing step with 10% ACN, 0.1% TFA. TiO_2 beads were dried under vacuum and phosphopeptides were eluted with 100 µL of 1% (v/v) ammonium hydroxide, pH 11.3 for 10 min on a shaker at 25 °C. Beads were pelleted at 500 rpm, the eluate was collected and acidified with 12 µL of 100% FA and 3 µL of 10% TFA. Another 50 µL of of 1% (v/v) ammonium hydroxide was added to the beads, mixed for 15 s, centrifuged as before and the eluates were pooled. The eluate was desalted with self-made stage tips as described above. The sample was dried under vacuum and resolubilized in 0.1% TFA for nano-LC−SPS analysis.

5.27 Global proteome analysis for SH-SY5Y cells

5 % (max. 40 µg total protein) of Cys-BOOST FT was dried under vacuum, resolubilized in 10 mM ammonium formate, fractionated by high pH RP chromatography at pH 8.0, using an UltiMate 3000 HPLC. Fractionation was performed on a Zorbax 300SB-C18 column, 0.5 x 150 mm, 5 µm particle size column using a binary buffer system; buffer A: 10 mM ammonium formate, pH 8.0 and buffer B: 84% ACN in 10 mM ammonium formate, pH 8.0. Peptides were loaded onto the column in buffer A at a flow rate of 12.5 µL/min and separated using the following gradient: 3 - 15 % B in 10 min, 15 - 55 % B in 55 min, 55 - 95 % B in 5 min, 95% B hold for 5 min. In total, 16 fractions were collected at 60 s intervals from min 5 to 75, in concatenation mode. The fractions were dried under vacuum and resolubilized in 0.1% TFA for LC-SPS analysis.

5.28 Data analysis

MS raw files were processed with Proteome Discoverer (PD) v 1.4 and v2.2, using Sequest HT and Mascot. For HeLa and SH-SY5Y experiments the human Uniprot database, (downloaded November 2016, 20,072 target entries) and a common contaminants database were used. MS^2 data were searched using mass tolerances of 10 ppm and 0.02 Da for precursor and product ions, respectively. SPS data was searched using mass tolerances of 10 ppm and 0.5 Da for precursors and MS^2 ions, respectively, and MS^3 spectra with 20 ppm integration tolerance were used for TMT reporter ion quantification. A maximum of 2 missed cleavages were allowed for trypsin. For iodoTMT analysis, iodoTMT6plex on Cys (+329.227 Da) and oxidation of methionine (Mox, +15.9949 Da) were set as dynamic modifications. For Cys-BOOST cl-DDE (cleaved form of the linker) on Cys (+195.112 Da) and Mox were set as dynamic modifications, TMT10plex (+229.163 Da) on N-termini and Lys were set as static

modifications. For Cys-BOOST based SNO analysis, CAM Cys (+57.021 Da) was set as an additional dynamic modification. For SH-SY5Y global proteome database search, TMT10plex, CAM and Mox were set as static and dynamic modifications, respectively. For protein phosphorylation analysis, phosphorylation (+79.966 Da) on Ser, Thr and Tyr was set as an additional dynamic modification. Percolator was used for PEP and FDR estimation and data was filtered at ≤ 1 % FDR on PSM and peptide levels. Site probabilities of Cys dynamic modifications and phosphorylation were determined using ptmRS [136]. Only unique peptides that passed the FDR criteria and had site localization probabilities ≥ 99 % were considered. Quantification was done based on the TMT reporter ion intensities, only spectra with an average reporter S/N threshold ≥ 10 were considered for quantification, for MS^2 analysis an additional co-Isolation threshold ≤ 20 was applied. For the total Cys analysis, normalization of the quantification data to total peptide amount was done using PD v2.2 and the data was scaled by dividing for each peptide the TMT reporter intensities of each channel by the corresponding average TMT reporter intensity of the 3 replicates. The SH-SY5Y SNO, protein phosphorylation, and global proteome data was likewise normalized to total peptide amount using PD v2.2. In contrast, the HeLa-SNO data was processed without normalization, owing to the significant fold changes present between GSNO-stimulated and untreated samples in majority of the quantified SNO peptides. In addition, low (< 5 %) RSD of reporter ion intensities were observed for background peptides present in the Cys-BOOST FT (1 µg measured by LC-MS/MS), showing that the protein amounts in all samples were equivalent. For the HeLa-SNO data, the low abundance resampling mode of the PD v2.2 was applied, which compensates for the missing values of the control TMT channels, by replacing them with random values sampled from the lower 5 % of the detected values. CAM or Mox peptides were not considered for quantification. P-values for all experiments were defined by one-way ANOVA (individual proteins) hypothesis test using PD v2.2.

5.28.1 S-nitrosylation motif analysis

The SNO motif analysis was performed using motif-x v1.2 [87, 137]. For all quantified Cys peptides the $R_{[GSNO]:[Control]}$ ratio was calculated and peptides were divided into three groups. SNO sites with $R \leq 1.5$, i.e. downregulated and non-significantly changed sites were considered as GSNO non-reactive sites. Next, SNO sites with $1.5 < R < 6$ (p-value ≤ 0.05) were considered as GSNO mild-reactive and $R \geq 6$ (p-value ≤ 0.05) as GSNO hyper-reactive sites. P-values defined by ANOVA. Each group was processed separately. The peptides were centered at the SNO residue, motif width was set to 15 amino acids, significance to $< 1 \times 10^{-6}$,

the foreground format to MS/MS and the human proteome was used as a reference database. All identified motifs were considered.

5.28.2 Protein network analysis

Protein interaction networks were generated using STRING v10.5. For HeLa-SNO analysis considering proteins with (i) significantly down-regulated ($R < 0.5$, p-value ≤ 0.05) SNO sites and (ii) the 500 unique proteins having the strongest up-regulated SNO sites ($R \geq 14.6$, p-value ≤ 0.05) using the highest confidence setting. For SH-SY5Y-SNO analysis considering proteins with significantly changed (≥ 1.5-fold, p-value ≤ 0.05) SNO levels using high confidence setting. P-values defined by ANOVA. The networks were visualized using Cytoscape (http://www.cytoscape.org/).

5.29 Data availability

The mass spectrometry proteomics data have been deposited to the ProteomeXchange Consortium via the PRIDE [138] partner repository with the dataset identifiers PXD011131 [http://dx.doi.org/10.6019/PXD011131], PXD012485 [http://dx.doi.org/10.6019/PXD012485].

5.30 Materials and equipment

5.30.1 Reagents and materials

5-TAMRA-azide	Carl Roth
Acetone for HPLC	Sigma Aldrich
Acetonitrile, LC-MS ChromaSolv	Sigma Aldrich
Aminoguanidine hydrochloride	Sigma Aldrich
Ammonium formate (≥ 99%)	Sigma Aldrich
Benzonase nuclease	Merck
Bicinchoninic acid assay	Thermo Scientific
C18 3M Empore SPE Extraction Disks	Sigma Aldrich

Calcium chloride	Sigma Aldrich
Coomassie Brilliant blue	Sigma Aldrich
Dde-biotin-azide linker	Jena Bioscience
Diazo-biotin-azide linker	Jena Bioscience
Diol-biotin-azide linker	Jena Bioscience
Disodium phosphate	Sigma Aldrich
DMEM medium	Sigma Aldrich
Ethylenediaminetetraacetic acid (EDTA)	Sigma Aldrich
Formic acid for HPLC	Sigma Aldrich
Guanidine hydrochloride (GuHCl)	Sigma Aldrich
HEPES	Sigma Aldrich
High Capacity Streptavidin – Agarose Resin	Thermo Scientific
Hydrazine (98%)	Sigma Aldrich
Immobilized Anti-TMT™ Antibody Resin	Thermo Scientific
Iodoacetamide (IAA)	Sigma Aldrich
Iodoacetamide alkyne (IAA-alkyne)	Setareh Biotech
IodoTMT	Thermo Scientific
Magnesium chloride	Sigma Aldrich
Neocuproin	Sigma Aldrich
Oligo R3 reversed – Phase Resin	Applied Biosystems
Protease inhibitor cocktail Complete Mini	Roche
S-nitrosoglutathione (GSNO)	Sigma Aldrich
S-Nitroso-N-Acetyl-D,L-Penicillamine (SNAP)	Sigma Aldrich
Sodium ascorbate (≥ 99%)	Carl Roth
Sodium chloride	Sigma Aldrich
sodium dodecyl sulfate (SDS)	Sigma Aldrich
Titansphere TiO, 5 µm particle size	GL Sciences Inc.

TMT 10plex™	Thermo Scientific
Tri(3 hydroxypropyltriazolylmethyl)amine (THPTA)	Sigma Aldrich
Triethylamonium bicarbonate (TEAB)	Thermo Scientific
Trifluoroacetic acid (TFA) for HPLC (≥99.0%)	Sigma Aldrich
Tris hydrochloride (Tris-HCl)	Sigma Aldrich
Tris(2-carboxyethyl)phosphine hydrochloride (TCEP)	Sigma Aldrich
Trypsin Sequencing grade	Promega
Urea	Sigma Aldrich

5.30.2 Synthetic peptides

CSDIISYTFK	ISAS, Dortmund
DGNGFLSAAELR	ISAS, Dortmund
ETCVVVYTGYGNR	ISAS, Dortmund
FECQPGYR	ISAS, Dortmund
FECQPGYr(13C(6)15N(4))	ISAS, Dortmund
GEHGFIGCR	ISAS, Dortmund
LCFDNSFSTISEK	ISAS, Dortmund
LCFDNSFSTISEk(13C(6)15N(2))	ISAS, Dortmund
SPGPGAQSALR	ISAS, Dortmund
SVGLGAYLVR	ISAS, Dortmund
VNLSCGGVSHPIR	ISAS, Dortmund
VNLSCGGVSHPIr(13C(6)15N(4))	ISAS, Dortmund
YLAADKDGNVTCER	ISAS, Dortmund

5.30.3 Cell lines

HeLa S3 cells (ACC 161)	DSMZ
SH-SY5Y cells (ACC 209)	DSMZ

5.30.4 LC-MS systems and LC columns

Main column Acclaim Pepmap (75 µm × 50 cm, C18)	Thermo Scientific
Main column Zorbax 300SB (0.5 x 150 mm, 5 µm particle size, C18)	Agilent Technologies
Orbitrap Fusion Lumos	Thermo Scientific
Q Exactive HF	Thermo Scientific
Trap column Acclaim Pepmap (100 µm × 2 cm, C18)	Thermo Scientific
Ultimate 3000 RSLCnano systems	Thermo Scientific

5.30.5 Other Instruments

Centrifuges	Eppendorf AG
Equipment for SDS-PAGE	Bio-Rad
Thermomixer	Eppendorf AG
Typhoon Trio imaging system	GE Healthcare
Vibra-Cell™ Ultrasonic Liquid Processor	Sonics & Materials

5.30.6 Software

Adobe Illustrator	Adobe

ChemDraw Pro	CambridgeSoft
Chromeleon Chromatogr aphy Data System	Thermo Scientific
Cytoscape	Cytoscape Consortium
EndNote	Thomson Reuters
Motif-x v1.2	Harvard Medical School
Origin Pro	Origin Lab Corporation
Proteome Discoverer v1.4 and v2.2	Thermo Scientific
STRING v10.5	String Consortium
Xcalibur	Thermo Scientific

6. Supplementary information

Supplementary Tables

Supplementary Table 1. SNO consensus motifs identified by motif-x v1.2 for (a) GSNO non-reactive ($R \leq 1.5$), (b) GSNO mild-reactive ($1.5 < R < 6$; p-value ≤0.05), (c) GSNO hyper-reactive ($R \geq 6$; p-value ≤0.05) SNO sites.

a

#	Motif	Motif Score	Foreground Matches	Foreground Size	Background Matches	Background Size	Fold Increase
1.	.......CL..L...	24.71	41	480	3831	315162	7.03
2.	...L...C.......	15.35	101	439	30548	311331	2.34
3.	...I...C.......	15.65	55	338	12652	280783	3.61
4.	...F...C.......	11.69	44	283	12323	268131	3.38
5.	...V...C.......	13.26	55	239	19105	255808	3.08
6.	.......CI......	9.82	29	184	9134	236703	4.08
7.	....L..C.......	7.32	37	155	20818	227569	2.61

b

#	Motif	Motif Score	Foreground Matches	Foreground Size	Background Matches	Background Size	Fold Increase
1.	.......C.....K.	10.53	156	1894	14849	315162	1.75
2.	.K.....C.......	6.48	127	1738	13781	300313	1.59

c

#	Motif	Motif Score	Foreground Matches	Foreground Size	Background Matches	Background Size	Fold Increase
1.	.......C...E...	16.00	372	3446	17478	315162	1.95
2.	....E..C.......	16.00	307	3074	15468	297684	1.92
3.	...D...C.....E.	23.09	35	2767	762	282216	4.68
4.	....D..C..E....	22.12	33	2732	691	281454	4.92
5.	.......CE......	16.00	251	2699	14481	280763	1.80
6.	....D..C.......	16.00	200	2448	9916	266282	2.19
7.	.......C..E....	15.65	204	2248	12638	256366	1.84
8.	.......CD......	15.95	172	2044	10396	243728	1.97
9.	...E...C.......	12.61	182	1872	12850	233332	1.77
10.	...D...C.......	13.72	137	1690	8820	220482	2.03
11.	......DC.......	10.26	121	1553	8742	211662	1.89
12.	.......C..D....	10.51	118	1432	8709	202920	1.92
13.	.......C.....E.	9.75	125	1314	10139	194211	1.82
14.	.....E.C.......	10.28	119	1189	9752	184072	1.89
15.	.......C...D...	9.94	88	1070	6809	174320	2.11
16.	.......C.D.....	9.15	86	982	7181	167511	2.04
17.	.......CT......	6.45	86	896	8700	160330	1.77
18.	.......C.....D.	6.91	66	810	6160	151630	2.01
19.	E......C.......	6.12	69	744	7222	145470	1.87
20.	D......C.......	6.59	55	675	5324	138248	2.12

Supplementary Table 2. Table of comparison of SNO studies.

Method	Model system	Number of SNO proteins/peptides/ sites	Amount of starting material/ condition [mg]	Quantification	Year	Reference
RAC	CysNO treated HEK293 cells	398 peptides	1	iTRAQ; MS2	2009	[71]
SNO-RAC	GSNO-treated mouse heart homogenates	951 proteins, ~2000 sites	1	Label-free; MS1	2011	[139]
SNO-RAC	GSNO-treated mouse skeletal muscle homogenates	488 sites	0.5	iTRAQ; MS2	2013	[140]
SNO-RAC	Cys-NO treated nuclear extracts of rat cortical neurons	614 proteins	0.4	N/a	2018	[93]
SNO ICAT	SNO-Trx1-treated SH-SY5Y cell lysate	50-76 sites	0.3	Light and heavy ICAT; MS1	2011	[141]
SNO ICAT	normoxic mouse heart	907 sites	N/a	Light and heavy ICAT; MS1	2017	[35]
iodoTMT	CysNO-treated BV-2 cells; LPS-stimulated BV-2 cells	134 sites; 101 sites	0.4	TMT; MS2	2014	[76]
iodoTMT	rat cardiomyocyte under hypoxia	169 proteins, 266 sites	0.3	TMT; MS2	2014	[70]
HPDP-biotin	CysNO-treated NPrEC cells	81 sites	1	N/a	2010	[142]
HPDP-biotin	LPS and IFN- γ-treated RAW264.7 cells	156 proteins	1	SILAC; MS1	2012	[143]
CysPAT	GSNO treated RAW 264.7 cell extracts	795 proteins, 1450 peptides	0.4	N/a	2018	[144]
Cys-BOOST	GSNO-treated HeLa cell extracts	3632 proteins, 8304 sites	0.3	TMT; MS2	2019	current study
Cys-BOOST	SNAP-treated SH-SY5Y cells	1443 proteins, 2158 sites	0.25	TMT; MS3	2019	current study

Supplementary figures

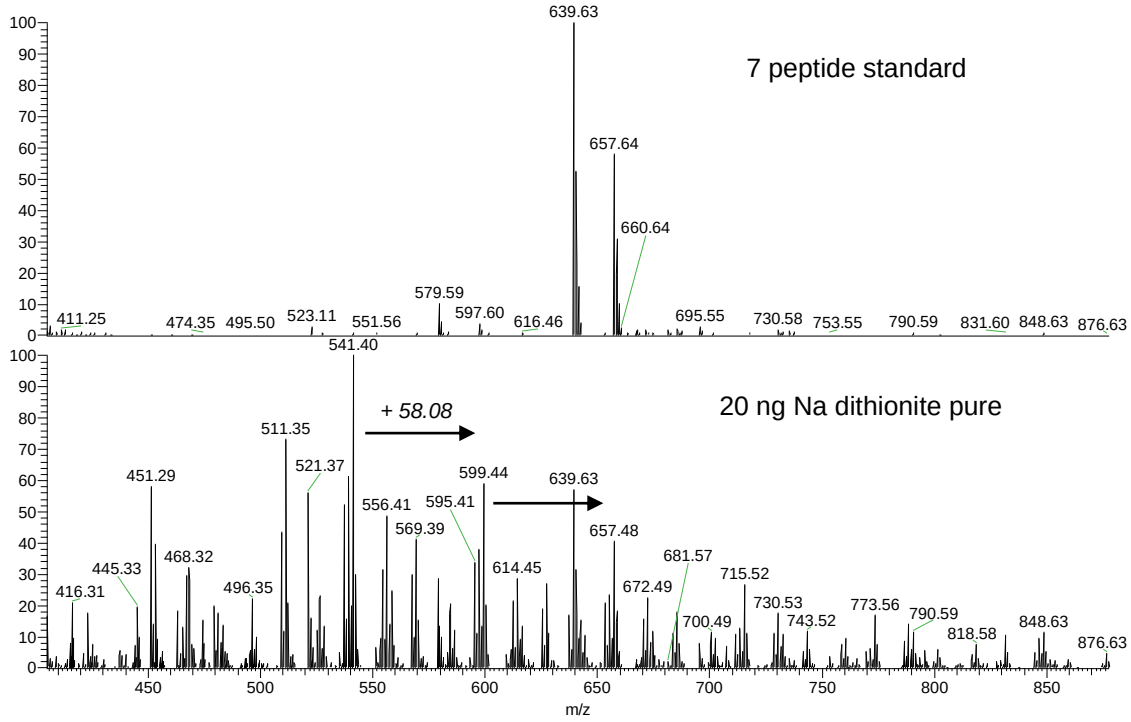

Supplementary Figure 1 PPG (+ 58.08 polymer increments) contamination in the stock of the Na dithionite detected by LC-MS compared to the previous run (7 peptide standard).

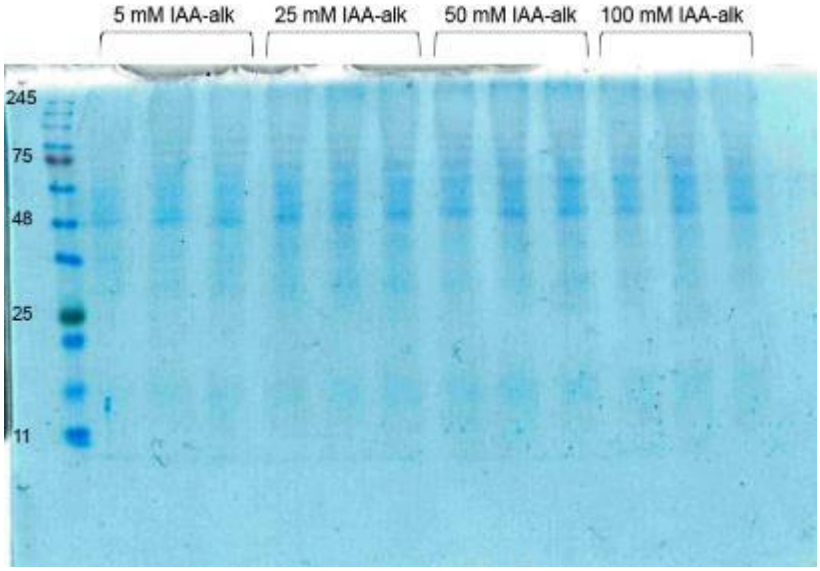

Supplementary Figure 2 Total free Cys labeling with increasing concentrations of IAA-alk. Coomassie detection of the HeLa lysates separated by SDS-PAGE.

7. Table of figures

8. Table of tables

References

1. Ezkurdia, I., et al., *Multiple evidence strands suggest that there may be as few as 19,000 human protein-coding genes.* Hum Mol Genet, 2014. **23**(22): p. 5866-78.
2. Jeremy M Berg, J.L.T., and Lubert Stryer, *Biochemistry*. 2002: New York: W H Freeman.
3. Mnatsakanyan, R., et al., *Detecting post-translational modification signatures as potential biomarkers in clinical mass spectrometry.* Expert Rev Proteomics, 2018. **15**(6): p. 515-535.
4. Gould, N., et al., *Regulation of protein function and signaling by reversible cysteine S-nitrosylation.* J Biol Chem, 2013. **288**(37): p. 26473-9.
5. Chung, H.S., et al., *Cysteine oxidative posttranslational modifications: emerging regulation in the cardiovascular system.* Circ Res, 2013. **112**(2): p. 382-92.
6. Kim, H.J., et al., *ROSics: chemistry and proteomics of cysteine modifications in redox biology.* Mass Spectrom Rev, 2015. **34**(2): p. 184-208.
7. Waszczak, C., et al., *Oxidative post-translational modifications of cysteine residues in plant signal transduction.* J Exp Bot, 2015. **66**(10): p. 2923-34.
8. Nietzel, T., et al., *Redox regulation of mitochondrial proteins and proteomes by cysteine thiol switches.* Mitochondrion, 2016.
9. Sun, J. and E. Murphy, *Protein S-nitrosylation and cardioprotection.* Circ Res, 2010. **106**(2): p. 285-96.
10. Mongin, A.A., P. Dohare, and D. Jourd'heuil, *Selective vulnerability of synaptic signaling and metabolism to nitrosative stress.* Antioxid Redox Signal, 2012. **17**(7): p. 992-1012.
11. Huang, H., et al., *Simultaneous Enrichment of Cysteine-containing Peptides and Phosphopeptides Using a Cysteine-specific Phosphonate Adaptable Tag (CysPAT) in Combination with titanium dioxide (TiO2) Chromatography.* Mol Cell Proteomics, 2016. **15**(10): p. 3282-3296.
12. Watanabe, Y., R.A. Cohen, and R. Matsui, *Redox Regulation of Ischemic Angiogenesis-Another Aspect of Reactive Oxygen Species.* Circ J, 2016. **80**(6): p. 1278-84.
13. Wang, S.B., et al., *Redox regulation of mitochondrial ATP synthase: implications for cardiac resynchronization therapy.* Circ Res, 2011. **109**(7): p. 750-7.
14. Murad, F., *Cyclic guanosine monophosphate as a mediator of vasodilation.* J Clin Invest, 1986. **78**(1): p. 1-5.
15. Stamler, J.S., et al., *S-nitrosylation of proteins with nitric oxide: synthesis and characterization of biologically active compounds.* Proc Natl Acad Sci U S A, 1992. **89**(1): p. 444-8.
16. Stamler, J.S., et al., *(S)NO signals: translocation, regulation, and a consensus motif.* Neuron, 1997. **18**(5): p. 691-6.
17. Lane, P., G. Hao, and S.S. Gross, *S-nitrosylation is emerging as a specific and fundamental posttranslational protein modification: head-to-head comparison with O-phosphorylation.* Sci STKE, 2001. **2001**(86): p. re1.
18. Hess, D.T., et al., *Protein S-nitrosylation: purview and parameters.* Nat Rev Mol Cell Biol, 2005. **6**(2): p. 150-66.
19. Di Giacomo, G., et al., *Established Principles and Emerging Concepts on the Interplay between Mitochondrial Physiology and S-(De)nitrosylation: Implications in Cancer and Neurodegeneration.* Int J Cell Biol, 2012. **2012**: p. 361872.
20. Bechtold, E. and S.B. King, *Chemical methods for the direct detection and labeling of S-nitrosothiols.* Antioxid Redox Signal, 2012. **17**(7): p. 981-91.
21. Nakamura, T. and S.A. Lipton, *Emerging role of protein-protein transnitrosylation in cell signaling pathways.* Antioxid Redox Signal, 2013. **18**(3): p. 239-49.
22. Anand, P. and J.S. Stamler, *Enzymatic mechanisms regulating protein S-nitrosylation: implications in health and disease.* J Mol Med (Berl), 2012. **90**(3): p. 233-44.

23. Gow, A., et al., *S-Nitrosothiol measurements in biological systems.* J Chromatogr B Analyt Technol Biomed Life Sci, 2007. **851**(1-2): p. 140-51.
24. Saville, B., *A scheme for the colorimetric determination of microgram amounts of thiols.* Analyst, 1958(993).
25. Stomberski, C.T., D.T. Hess, and J.S. Stamler, *Protein S-Nitrosylation: Determinants of Specificity and Enzymatic Regulation of S-Nitrosothiol-Based Signaling.* Antioxid Redox Signal, 2019. **30**(10): p. 1331-1351.
26. Jia, J., et al., *Target-selective protein S-nitrosylation by sequence motif recognition.* Cell, 2014. **159**(3): p. 623-34.
27. Mnatsakanyan, R., et al., *Proteome-wide detection of S-nitrosylation targets and motifs using bioorthogonal cleavable-linker-based enrichment and switch technique.* Nature Communications, 2019. **10**(1): p. 2195.
28. Chen, Y.J., et al., *dbSNO 2.0: a resource for exploring structural environment, functional and disease association and regulatory network of protein S-nitrosylation.* Nucleic Acids Res, 2015. **43**(Database issue): p. D503-11.
29. Oh, C.K., et al., *S-Nitrosylation of PINK1 Attenuates PINK1/Parkin-Dependent Mitophagy in hiPSC-Based Parkinson's Disease Models.* Cell Rep, 2017. **21**(8): p. 2171-2182.
30. Yao, D., et al., *Nitrosative stress linked to sporadic Parkinson's disease: S-nitrosylation of parkin regulates its E3 ubiquitin ligase activity.* Proc Natl Acad Sci U S A, 2004. **101**(29): p. 10810-4.
31. Raju, K., et al., *Regulation of brain glutamate metabolism by nitric oxide and S-nitrosylation.* Sci Signal, 2015. **8**(384): p. ra68.
32. Chouchani, E.T., et al., *Cardioprotection by S-nitrosation of a cysteine switch on mitochondrial complex I.* Nat Med, 2013. **19**(6): p. 753-9.
33. Yasinska, I.M. and V.V. Sumbayev, *S-nitrosation of Cys-800 of HIF-1alpha protein activates its interaction with p300 and stimulates its transcriptional activity.* FEBS Lett, 2003. **549**(1-3): p. 105-9.
34. Okamoto, S., et al., *S-nitrosylation-mediated redox transcriptional switch modulates neurogenesis and neuronal cell death.* Cell Rep, 2014. **8**(1): p. 217-28.
35. Chouchani, E.T., et al., *Identification and quantification of protein S-nitrosation by nitrite in the mouse heart during ischemia.* J Biol Chem, 2017. **292**(35): p. 14486-14495.
36. Okamoto, S. and S.A. Lipton, *S-Nitrosylation in neurogenesis and neuronal development.* Biochim Biophys Acta, 2015. **1850**(8): p. 1588-93.
37. Forrester, M.T., et al., *Detection of protein S-nitrosylation with the biotin-switch technique.* Free Radic Biol Med, 2009. **46**(2): p. 119-26.
38. Qu, Z., C.M. Greenlief, and Z. Gu, *Quantitative Proteomic Approaches for Analysis of Protein S-Nitrosylation.* J Proteome Res, 2016. **15**(1): p. 1-14.
39. Stamler, J.S., et al., *Nitric oxide circulates in mammalian plasma primarily as an S-nitroso adduct of serum albumin.* Proc Natl Acad Sci U S A, 1992. **89**(16): p. 7674-7.
40. Giustarini, D., et al., *Nitrite and nitrate measurement by Griess reagent in human plasma: evaluation of interferences and standardization.* Methods Enzymol, 2008. **440**: p. 361-80.
41. Agurla, S., G. Gayatri, and A.S. Raghavendra, *Nitric Oxide (NO) Measurements in Stomatal Guard Cells.* Methods Mol Biol, 2016. **1424**: p. 49-56.
42. Gow, A.J., et al., *Immunohistochemical detection of S-nitrosylated proteins.* Methods Mol Biol, 2004. **279**: p. 167-72.
43. Hoffmann, E.d., Stroobant, V., *Mass spectrometry: Principles and applications (2nd ed.)*. Wiley. 2001.
44. Mora, J.F., et al., *Electrochemical processes in electrospray ionization mass spectrometry.* J Mass Spectrom, 2000. **35**(8): p. 939-52.
45. Cech, N.B. and C.G. Enke, *Practical implications of some recent studies in electrospray ionization fundamentals.* Mass Spectrom Rev, 2001. **20**(6): p. 362-87.

46. Hillenkamp, F., et al., *Matrix-assisted laser desorption/ionization mass spectrometry of biopolymers.* Anal Chem, 1991. **63**(24): p. 1193A-1203A.
47. N.Gushue, J., *Chapter 11 - Principles and Applications of Gas Chromatography Quadrupole Time-of-Flight Mass Spectrometry*. Comprehensive Analytical Chemistry. Vol. Volume 61. 2013. 255-270.
48. Makarov, A., *Electrostatic axially harmonic orbital trapping: a high-performance technique of mass analysis.* Anal Chem, 2000. **72**(6): p. 1156-62.
49. Buddhadeb Mallik, B.C., Deb N. Chakravarti, *Overview of Chromatography*. Current Protocols. 2008: Wiley.
50. Regnier, F.E., *High-performance liquid chromatography of biopolymers.* Science, 1983. **222**(4621): p. 245-52.
51. Hagan, R.L., *High-performance liquid chromatography for small-scale studies of drug stability.* Am J Hosp Pharm, 1994. **51**(17): p. 2162-75.
52. Wilkins, M.R., et al., *Progress with proteome projects: why all proteins expressed by a genome should be identified and how to do it.* Biotechnol Genet Eng Rev, 1996. **13**: p. 19-50.
53. Aebersold, R. and M. Mann, *Mass-spectrometric exploration of proteome structure and function.* Nature, 2016. **537**(7620): p. 347-55.
54. Altelaar, A.F.M., J. Munoz, and A.J.R. Heck, *Next-generation proteomics: towards an integrative view of proteome dynamics.* Nature Reviews Genetics, 2012. **14**(1): p. 35-48.
55. Zhang, Y., et al., *Protein analysis by shotgun/bottom-up proteomics.* Chem Rev, 2013. **113**(4): p. 2343-94.
56. Eng, J.K., A.L. McCormack, and J.R. Yates, *An approach to correlate tandem mass spectral data of peptides with amino acid sequences in a protein database.* J Am Soc Mass Spectrom, 1994. **5**(11): p. 976-89.
57. Perkins, D.N., et al., *Probability-based protein identification by searching sequence databases using mass spectrometry data.* Electrophoresis, 1999. **20**(18): p. 3551-67.
58. Cox, J., et al., *Andromeda: a peptide search engine integrated into the MaxQuant environment.* J Proteome Res, 2011. **10**(4): p. 1794-805.
59. Cox, J. and M. Mann, *MaxQuant enables high peptide identification rates, individualized p.p.b.-range mass accuracies and proteome-wide protein quantification.* Nat Biotechnol, 2008. **26**(12): p. 1367-72.
60. O'Connell, J.D., et al., *Proteome-Wide Evaluation of Two Common Protein Quantification Methods.* J Proteome Res, 2018. **17**(5): p. 1934-1942.
61. Rauniyar, N. and J.R. Yates, *Isobaric Labeling-Based Relative Quantification in Shotgun Proteomics.* Journal of Proteome Research, 2014. **13**(12): p. 5293-5309.
62. Savitski, M.M., et al., *Measuring and managing ratio compression for accurate iTRAQ/TMT quantification.* J Proteome Res, 2013. **12**(8): p. 3586-98.
63. Jaffrey, S.R., et al., *Protein S-nitrosylation: a physiological signal for neuronal nitric oxide.* Nat Cell Biol, 2001. **3**(2): p. 193-7.
64. Doulias, P.T., et al., *Nitric oxide regulates mitochondrial fatty acid metabolism through reversible protein S-nitrosylation.* Sci Signal, 2013. **6**(256): p. rs1.
65. Zhang, J., et al., *Reductive ligation mediated one-step disulfide formation of S-nitrosothiols.* Org Lett, 2010. **12**(18): p. 4208-11.
66. García-Santamarina, S., et al., *Monitoring in vivo reversible cysteine oxidation in proteins using ICAT and mass spectrometry.* Nature Protocols, 2014. **9**(5): p. 1131-1145.
67. Wojdyla, K., et al., *The SNO/SOH TMT strategy for combinatorial analysis of reversible cysteine oxidations.* J Proteomics, 2015. **113**: p. 415-34.
68. Guo, J., et al., *Resin-assisted enrichment of thiols as a general strategy for proteomic profiling of cysteine-based reversible modifications.* Nat Protoc, 2014. **9**(1): p. 64-75.
69. Shiio, Y. and R. Aebersold, *Quantitative proteome analysis using isotope-coded affinity tags and mass spectrometry.* Nat Protoc, 2006. **1**(1): p. 139-45.

70. Pan, K.T., et al., *Mass spectrometry-based quantitative proteomics for dissecting multiplexed redox cysteine modifications in nitric oxide-protected cardiomyocyte under hypoxia.* Antioxid Redox Signal, 2014. **20**(9): p. 1365-81.
71. Forrester, M.T., et al., *Proteomic analysis of S-nitrosylation and denitrosylation by resin-assisted capture.* Nat Biotechnol, 2009. **27**(6): p. 557-9.
72. Choi, Y.B., et al., *Molecular basis of NMDA receptor-coupled ion channel modulation by S-nitrosylation.* Nat Neurosci, 2000. **3**(1): p. 15-21.
73. Nakamura, T. and S.A. Lipton, *Redox modulation by S-nitrosylation contributes to protein misfolding, mitochondrial dynamics, and neuronal synaptic damage in neurodegenerative diseases.* Cell Death Differ, 2011. **18**(9): p. 1478-86.
74. Foster, M.W., T.J. McMahon, and J.S. Stamler, *S-nitrosylation in health and disease.* Trends Mol Med, 2003. **9**(4): p. 160-8.
75. Lopez-Sanchez, L.M., C. Lopez-Pedrera, and A. Rodriguez-Ariza, *Proteomic approaches to evaluate protein S-nitrosylation in disease.* Mass Spectrom Rev, 2014. **33**(1): p. 7-20.
76. Qu, Z., et al., *Proteomic Quantification and Site-Mapping ofS-Nitrosylated Proteins Using Isobaric iodoTMT Reagents.* Journal of Proteome Research, 2014. **13**(7): p. 3200-3211.
77. Verhelst, S.H.L., M. Fonović, and M. Bogyo, *A Mild Chemically Cleavable Linker System for Functional Proteomic Applications.* Angewandte Chemie, 2007. **119**(8): p. 1306-1308.
78. Yang, Y. and S.H. Verhelst, *Cleavable trifunctional biotin reagents for protein labelling, capture and release.* Chem Commun (Camb), 2013. **49**(47): p. 5366-8.
79. Presolski, S.I., V.P. Hong, and M.G. Finn, *Copper-Catalyzed Azide-Alkyne Click Chemistry for Bioconjugation.* Curr Protoc Chem Biol, 2011. **3**(4): p. 153-162.
80. Martell, J. and E. Weerapana, *Applications of copper-catalyzed click chemistry in activity-based protein profiling.* Molecules, 2014. **19**(2): p. 1378-93.
81. Chen, W., et al., *Simple and Integrated Spintip-Based Technology Applied for Deep Proteome Profiling.* Anal Chem, 2016. **88**(9): p. 4864-71.
82. Keshishian, H., et al., *Multiplexed, Quantitative Workflow for Sensitive Biomarker Discovery in Plasma Yields Novel Candidates for Early Myocardial Injury.* Mol Cell Proteomics, 2015. **14**(9): p. 2375-93.
83. Hogrebe, A., et al., *Benchmarking common quantification strategies for large-scale phosphoproteomics.* Nature Communications, 2018. **9**(1): p. 1045.
84. Forrester, M.T., M.W. Foster, and J.S. Stamler, *Assessment and application of the biotin switch technique for examining protein S-nitrosylation under conditions of pharmacologically induced oxidative stress.* J Biol Chem, 2007. **282**(19): p. 13977-83.
85. Murphy, E., et al., *Signaling by S-nitrosylation in the heart.* J Mol Cell Cardiol, 2014. **73**: p. 18-25.
86. Paoletti, A.C., et al., *Quantitative proteomic analysis of distinct mammalian Mediator complexes using normalized spectral abundance factors.* Proc Natl Acad Sci U S A, 2006. **103**(50): p. 18928-33.
87. Schwartz, D., M.F. Chou, and G.M. Church, *Predicting protein post-translational modifications using meta-analysis of proteome scale data sets.* Mol Cell Proteomics, 2009. **8**(2): p. 365-79.
88. Greco, T.M., et al., *Identification of S-nitrosylation motifs by site-specific mapping of the S-nitrosocysteine proteome in human vascular smooth muscle cells.* Proc Natl Acad Sci U S A, 2006. **103**(19): p. 7420-5.
89. Doulias, P.T., et al., *Structural profiling of endogenous S-nitrosocysteine residues reveals unique features that accommodate diverse mechanisms for protein S-nitrosylation.* Proc Natl Acad Sci U S A, 2010. **107**(39): p. 16958-63.
90. Perez-Mato, I., et al., *Methionine adenosyltransferase S-nitrosylation is regulated by the basic and acidic amino acids surrounding the target thiol.* J Biol Chem, 1999. **274**(24): p. 17075-9.

91. Lim, J.C., et al., *A low pKa cysteine at the active site of mouse methionine sulfoxide reductase A.* J Biol Chem, 2012. **287**(30): p. 25596-601.
92. Witt, A.C., et al., *Cysteine pKa depression by a protonated glutamic acid in human DJ-1.* Biochemistry, 2008. **47**(28): p. 7430-40.
93. Smith, J.G., et al., *Proteomic analysis of S-nitrosylated nuclear proteins in rat cortical neurons.* Sci Signal, 2018. **11**(537).
94. Gow, A.J., D.G. Buerk, and H. Ischiropoulos, *A novel reaction mechanism for the formation of S-nitrosothiol in vivo.* J Biol Chem, 1997. **272**(5): p. 2841-5.
95. Eu, J.P., et al., *The skeletal muscle calcium release channel: coupled O2 sensor and NO signaling functions.* Cell, 2000. **102**(4): p. 499-509.
96. Broillet, M.C., *A single intracellular cysteine residue is responsible for the activation of the olfactory cyclic nucleotide-gated channel by NO.* J Biol Chem, 2000. **275**(20): p. 15135-41.
97. Martinez-Ruiz, A., et al., *S-nitrosylation of Hsp90 promotes the inhibition of its ATPase and endothelial nitric oxide synthase regulatory activities.* Proc Natl Acad Sci U S A, 2005. **102**(24): p. 8525-30.
98. Retzlaff, M., et al., *Hsp90 is regulated by a switch point in the C-terminal domain.* EMBO Rep, 2009. **10**(10): p. 1147-53.
99. Morrell, C.N., et al., *Regulation of platelet granule exocytosis by S-nitrosylation.* Proc Natl Acad Sci U S A, 2005. **102**(10): p. 3782-7.
100. Matsushita, K., et al., *Nitric oxide regulates exocytosis by S-nitrosylation of N-ethylmaleimide-sensitive factor.* Cell, 2003. **115**(2): p. 139-50.
101. Weichsel, A., J.L. Brailey, and W.R. Montfort, *Buried S-nitrosocysteine revealed in crystal structures of human thioredoxin.* Biochemistry, 2007. **46**(5): p. 1219-27.
102. Yasinska, I.M. and V.V. Sumbayev, *S-nitrosation of Cys-800 of HIF-1α protein activates its interaction with p300 and stimulates its transcriptional activity.* FEBS Letters, 2003. **549**(1-3): p. 105-109.
103. Kim, J., et al., *STAT3 regulation by S-nitrosylation: implication for inflammatory disease.* Antioxid Redox Signal, 2014. **20**(16): p. 2514-27.
104. Nakato, R., et al., *Regulation of the unfolded protein response via S-nitrosylation of sensors of endoplasmic reticulum stress.* Sci Rep, 2015. **5**: p. 14812.
105. Umbrello, M., et al., *The key role of nitric oxide in hypoxia: hypoxic vasodilation and energy supply-demand matching.* Antioxid Redox Signal, 2013. **19**(14): p. 1690-710.
106. Venne, A.S., L. Kollipara, and R.P. Zahedi, *The next level of complexity: crosstalk of posttranslational modifications.* Proteomics, 2014. **14**(4-5): p. 513-24.
107. Spriggs, K.A., M. Bushell, and A.E. Willis, *Translational regulation of gene expression during conditions of cell stress.* Mol Cell, 2010. **40**(2): p. 228-37.
108. Kung, A.L., et al., *Suppression of tumor growth through disruption of hypoxia-inducible transcription.* Nat Med, 2000. **6**(12): p. 1335-40.
109. Freedman, S.J., et al., *Structural basis for recruitment of CBP/p300 by hypoxia-inducible factor-1 alpha.* Proc Natl Acad Sci U S A, 2002. **99**(8): p. 5367-72.
110. Fox, S.B., et al., *CITED4 inhibits hypoxia-activated transcription in cancer cells, and its cytoplasmic location in breast cancer is associated with elevated expression of tumor cell hypoxia-inducible factor 1alpha.* Cancer Res, 2004. **64**(17): p. 6075-81.
111. Liu, X., et al., *The structural basis of protein acetylation by the p300/CBP transcriptional coactivator.* Nature, 2008. **451**(7180): p. 846-50.
112. Hsu, M.F., et al., *S-nitrosylation of endogenous protein tyrosine phosphatases in endothelial insulin signaling.* Free Radic Biol Med, 2016. **99**: p. 199-213.
113. Fowler, N.J., et al., *Features of reactive cysteines discovered through computation: from kinase inhibition to enrichment around protein degrons.* Sci Rep, 2017. **7**(1): p. 16338.
114. Zhou, H.L., C.T. Stomberski, and J.S. Stamler, *Cross Talk Between S-Nitrosylation and Phosphorylation Involving Kinases and Nitrosylases.* Circ Res, 2018. **122**(11): p. 1485-1487.

115. Chen, Y.Y., et al., *Cysteine S-nitrosylation protects protein-tyrosine phosphatase 1B against oxidation-induced permanent inactivation.* J Biol Chem, 2008. **283**(50): p. 35265-72.
116. Gupta, A., et al., *PARK2 loss promotes cancer progression via redox-mediated inactivation of PTEN.* Mol Cell Oncol, 2017. **4**(6): p. e1329692.
117. Kovalevich, J. and D. Langford, *Considerations for the use of SH-SY5Y neuroblastoma cells in neurobiology.* Methods Mol Biol, 2013. **1078**: p. 9-21.
118. Chen, Y.J., et al., *Nitrite Protects Neurons Against Hypoxic Damage Through S-nitrosylation of Caspase-6.* Antioxid Redox Signal, 2018.
119. Nakamura, T., et al., *Aberrant protein s-nitrosylation in neurodegenerative diseases.* Neuron, 2013. **78**(4): p. 596-614.
120. Perrault, I., et al., *Mutations in DOCK7 in individuals with epileptic encephalopathy and cortical blindness.* Am J Hum Genet, 2014. **94**(6): p. 891-7.
121. Lee, H.O., et al., *GS28 Protects Neuronal Cell Death Induced by Hydrogen Peroxide under Glutathione-Depleted Condition.* Korean J Physiol Pharmacol, 2011. **15**(3): p. 149-56.
122. Uehara, T., et al., *S-nitrosylated protein-disulphide isomerase links protein misfolding to neurodegeneration.* Nature, 2006. **441**(7092): p. 513-7.
123. Wang, J., et al., *Neohesperidin Prevents Abeta25-35-Induced Apoptosis in Primary Cultured Hippocampal Neurons by Blocking the S-Nitrosylation of Protein-Disulphide Isomerase.* Neurochem Res, 2018. **43**(9): p. 1736-1744.
124. Foley, T.D., et al., *Potential widespread denitrosylation of brain proteins following prolonged restraint: proposed links between stress and central nervous system disease.* Metab Brain Dis, 2019. **34**(1): p. 183-189.
125. Bolanos, J.P. and A. Almeida, *The pentose-phosphate pathway in neuronal survival against nitrosative stress.* IUBMB Life, 2010. **62**(1): p. 14-8.
126. Zhou, H.L., et al., *Metabolic reprogramming by the S-nitroso-CoA reductase system protects against kidney injury.* Nature, 2019. **565**(7737): p. 96-100.
127. Seong, E., L. Yuan, and J. Arikkath, *Cadherins and catenins in dendrite and synapse morphogenesis.* Cell Adh Migr, 2015. **9**(3): p. 202-13.
128. Hess, D.T. and J.S. Stamler, *Regulation by S-nitrosylation of protein post-translational modification.* J Biol Chem, 2012. **287**(7): p. 4411-8.
129. Fischer, E.H., *Cell signaling by protein tyrosine phosphorylation.* Adv Enzyme Regul, 1999. **39**: p. 359-69.
130. Budnik, B., et al., *SCoPE-MS: mass spectrometry of single mammalian cells quantifies proteome heterogeneity during cell differentiation.* Genome Biol, 2018. **19**(1): p. 161.
131. Gonczarowska-Jorge, H., et al., *Quantifying Missing (Phospho)Proteome Regions with the Broad-Specificity Protease Subtilisin.* Anal Chem, 2017. **89**(24): p. 13137-13145.
132. Wisniewski, J.R., et al., *Universal sample preparation method for proteome analysis.* Nat Methods, 2009. **6**(5): p. 359-62.
133. Manza, L.L., et al., *Sample preparation and digestion for proteomic analyses using spin filters.* Proteomics, 2005. **5**(7): p. 1742-5.
134. Burkhart, J.M., et al., *Systematic and quantitative comparison of digest efficiency and specificity reveals the impact of trypsin quality on MS-based proteomics.* J Proteomics, 2012. **75**(4): p. 1454-62.
135. Engholm-Keller, K., et al., *TiSH--a robust and sensitive global phosphoproteomics strategy employing a combination of TiO2, SIMAC, and HILIC.* J Proteomics, 2012. **75**(18): p. 5749-61.
136. Taus, T., et al., *Universal and confident phosphorylation site localization using phosphoRS.* J Proteome Res, 2011. **10**(12): p. 5354-62.
137. Schwartz, D. and S.P. Gygi, *An iterative statistical approach to the identification of protein phosphorylation motifs from large-scale data sets.* Nat Biotechnol, 2005. **23**(11): p. 1391-8.
138. Vizcaino, J.A., et al., *2016 update of the PRIDE database and its related tools.* Nucleic Acids Res, 2016. **44**(D1): p. D447-56.

139. Kohr, M.J., et al., *Characterization of potential S-nitrosylation sites in the myocardium.* Am J Physiol Heart Circ Physiol, 2011. **300**(4): p. H1327-35.
140. Su, D., et al., *Quantitative site-specific reactivity profiling of S-nitrosylation in mouse skeletal muscle using cysteinyl peptide enrichment coupled with mass spectrometry.* Free Radic Biol Med, 2013. **57**: p. 68-78.
141. Wu, C., et al., *Distinction of thioredoxin transnitrosylation and denitrosylation target proteins by the ICAT quantitative approach.* J Proteomics, 2011. **74**(11): p. 2498-509.
142. Lam, Y.W., et al., *Comprehensive identification and modified-site mapping of S-nitrosylated targets in prostate epithelial cells.* PLoS One, 2010. **5**(2): p. e9075.
143. Torta, F. and A. Bachi, *Quantitative analysis of S-nitrosylated proteins.* Methods Mol Biol, 2012. **893**: p. 405-16.
144. Ibanez-Vea, M., et al., *Characterization of Macrophage Endogenous S-Nitrosoproteome Using a Cysteine-Specific Phosphonate Adaptable Tag in Combination with TiO2 Chromatography.* J Proteome Res, 2018. **17**(3): p. 1172-1182.